6.5 TSPA-LA MODEL FOR THE IGNEOUS SCENARIO CLASS

Igneous activity can lead to disruptive events that can affect the long-term performance of the Yucca Mountain repository. Yucca Mountain is in a region that has had volcanic activity in the geologic past, and, although there is a very low probability of recurrence of igneous activity affecting the repository, the mean probability is greater than 1 in 10,000 in 10,000 years (BSC 2004 [DIRS 169989], Table 7-1). Accordingly, igneous activity is examined with the TSPA-LA Model because it is not excluded under the probability criterion at 10 CFR 63.642 (a) [DIRS 178394]). The framework for this examination is the Igneous Scenario Class. The Igneous Scenario Class includes all screened-in features, events, and processes (FEPs) related to igneous activity (SNL 2007 [DIRS 179476]). Analysis of igneous activity in the Yucca Mountain region has led to a focus on post-Miocene activity as a basis for the TSPA-LA Model (BSC 2004 [DIRS 169989], Section 6.1.1.1). Figure 6.5-1 is a Yucca Mountain region map that shows the locations and ages of post-Miocene (less than 5.3 million years) igneous activity, represented by multiple volcanic centers.

A probabilistic volcanic hazard analysis (PVHA) was performed to assess the volcanic hazard at Yucca Mountain. For the PVHA, an expert panel was convened in the year 1995 to review pertinent data relating to volcanism at Yucca Mountain and, based on these data, to quantify both the annual probability and associated uncertainty of a volcanic event intersecting a proposed repository sited at Yucca Mountain (BSC 2004 [DIRS 169989], Section 6.1).

Disruption of the repository in the Igneous Scenario Class is addressed by two modeling cases: the Igneous Intrusion Modeling Case and the Volcanic Eruption Modeling Case. Figure 6.5-2 shows the theoretical relationship between an igneous intrusion and volcanic eruption at Yucca Mountain. Information about natural volcanic systems and parameters used to model their behavior is provided in *Characterize Eruptive Processes at Yucca Mountain, Nevada* (SNL 2007 [DIRS 174260]. In both modeling cases, magma propagates upward through the Earth's crust in fluid-driven cracks (dikes). The Igneous Intrusion Modeling Case considers only the intersection of repository drifts by one or more dikes. The Igneous Eruption Modeling Case considers an eruptive conduit that forms when a portion of the erupting dike begins to widen, creating a conduit to focus magma flow to the surface.

In the Igneous Intrusion Modeling Case, magma from dikes that intersect the repository footprint engulfs all DSs and WPs in the repository, rendering them incapable of protecting their contents. The CDSP WP and CSNF WP inner and outer barriers, the cladding in the case of CSNF, and the waste form itself including high-level radioactive waste (HLW) (Section 5.3.1) are instantly degraded during an igneous intrusion. The magnitude of radionuclide transport to the unsaturated zone (UZ) is controlled by the amount of seepage and the radionuclide solubilities. The radionuclides may be transported by groundwater downward through the UZ to the water table, then to the accessible environment by the water that flows in the SZ.

In the Volcanic Eruption Modeling Case, magma erupts at the Earth's surface. The eruptive conduit(s) intersects the repository and damages the WPs located within the conduit cross-sectional area. The rising magma entrains radionuclide waste particles and a portion of the erupting stream becomes a buoyant, convecting column that is ejected into the atmosphere. The contaminated tephra plume is transported downwind and the particles in the plume are dispersed

and eventually deposited on the land surface. The contaminated tephra is then subject to redistribution by hillslope and fluvial processes. The conceptual and mathematical model of contaminated tephra transport implemented by the TSPA-LA Model is described in *Atmospheric Dispersal and Deposition of Tephra from a Potential Volcanic Eruption at Yucca Mountain, Nevada* (SNL 2007 [177431]). The conceptual and mathematical model of redistribution processes implemented by the TSPA-LA Model is described in *Redistribution of Tephra and Waste by Geomorphic Processes Following a Potential Volcanic Eruption at Yucca Mountain, Nevada* (SNL 2007 [DIRS 179347]).

Both of these modeling cases are represented separately in the TSPA-LA Model analyses. Section 6.5.1 discusses the Igneous Intrusion Modeling Case and Section 6.5.2 discusses the Volcanic Eruption Modeling Case.

6.5.1 Igneous Intrusion Modeling Case

The implementation of the Igneous Intrusion Modeling Case includes the definition of submodels for the processes affecting release of radionuclides associated with igneous intrusion, and the implementation of submodels in the integrated TSPA-LA Model for the calculation of mean annual dose. The following sections address these two different aspects of the implementation.

6.5.1.1 TSPA-LA Submodels for the Igneous Intrusion Modeling Case

The Igneous Intrusion Modeling Case considers an igneous event in which a dike intersects the repository, and magma flows into and fills the drifts. This modeling case accounts for the effects of an intrusion on the subsurface characteristics and performance of the repository, and may or may not be accompanied by an eruptive conduit that intersects an emplacement drift and ejects material onto the surface or into the atmosphere. The flow characteristics of the intruding magma cause it to fill every drift within the repository. Contact with magma damages all WPs, DSs, and fuel cladding so that they no longer have waste isolation capability (DTN: LA0702PADE01EG.002_R0 [DIRS 179496], parmameters Fraction_DS_Failed_Ign_Input and Fraction_WP_Failed_Ign_Input). Magma intrusion, however, does not damage the invert. Because an intruded drift will fill with magma within 15 to 25 minutes (depending on the size of the aperture) (SNL 2007 [DIRS 177430], Sections 6.3.3.5.6), the igneous event is treated as an instantaneous event in the TSPA-LA Model. The magma then cools and solidifies in the emplacement drifts. Radionuclides dissolved in water moving through the basalt may be transported by the groundwater downward through the invert and into the UZ to the water table, and then to the accessible environment by flow and transport processes in the SZ, just as is simulated by the Nominal Modeling Case.

The TSPA-LA Model selects parameter values from the appropriate distributions for each of the model components and submodels for each realization of the Igneous Intrusion Modeling Case. The radionuclides in the CSNF and U.S. Department of Energy spent nuclear fuel (DSNF), including the HLW, are considered immediately available for dissolution and transport. Using these inputs, the fate of the radionuclides mobilized by the igneous intrusion is evaluated using the Nominal Scenario Class TSPA-LA Model components and submodels for flow and transport of the released radionuclides in the invert of the EBS, UZ, and SZ. The TSPA-LA Model

components needed to estimate mean annual dose in the Igneous Intrusion Modeling Case are shown on Figure 6.5-3. Modifications to the Nominal Scenario Class are indicated by the bulleted items on the figure.

- The probability of an igneous event is the annual frequency, expressed as a cumulative distribution function (CDF), of an intersection of the repository by a volcanic dike. The CDF is calculated in *Characterize Framework for Igneous Activity at Yucca Mountain, Nevada* (BSC 2004 [DIRS 169989], Section 6.5 and Table 7-1; DTN: LA0307BY831811.001_R0 [DIRS 164713], file PVHA-4PA.DST). The annual frequency of an intersection by an igneous event ranges from approximately 7.4×10^{-10} to 5.5×10^{-8} for the 5th and 95th percentiles, respectively, with a mean annual frequency of 1.7×10^{-8}. This mean annual frequency, which is independent of the characteristics of the event (i.e., size, duration, power) is applied to both the Igneous Intrusion and Volcanic Eruption Modeling Cases to determine mean annual dose.

- Because nominal processes do not progress sufficiently in 20,000 years to result in the release of any radionuclides, the Igneous Intrusion Modeling Case for 20,000 years does not evaluate any pre-intrusion degradation of the WPs, DSs, or CSNF cladding. Degradation of these EBS components is accounted for in the Nominal Scenario Class for 20,000 years (Section 6.1.3). However, for the 1,000,000-year Igneous Intrusion Modeling Case, the nominal processes of degradation of the WPs, DSs, and CSNF cladding do occur up until the time of the igneous intrusion. The inclusion of nominal processes before the igneous intrusion prevents over counting of any radionuclides released by nominal processes prior to the igneous intrusion.

- The intruded drifts have a seepage flux equal to the local percolation flux (SNL 2007 [DIRS 181244], Section 6.7.1.1) (i.e., capillary effects at the drift wall are neglected). The volumetric seepage rate is, therefore, obtained by applying the percolation flux at the base of the Paintbrush nonwelded hydrologic unit (PTn), provided by the EBS Thermal-Hydrologic (TH) Environment Submodel for the appropriate percolation flux subregion, to the projected area of the emplacement drift. In particular, the volumetric seepage rate for a single WP is set equal to that obtained by applying the flux at the base of the PTn to the 5.1-m-long by 5.5-m-wide drift segment representing one WP footprint.

- The DSs and WPs provide no hindrance to flow because they were damaged at the time of the igneous intrusion. Likewise, the basalt that has filled the drift is considered to be fractured so as to not hinder the flow of seepage (SNL 2007 [DIRS 177430], Section 8.1.2).

- No credit is taken for the CSNF cladding because it is considered entirely degraded at the time of the igneous intrusion (SNL 2007 [DIRS 177430], Section 8.1.2).

- All EBS and in-package chemistry-related submodels and parameters are the same as in the Nominal Scenario Class Modeling Case, with the exception of the uranium solubility submodel. As indicated in Section 6.3.7.5.2, Method 2 for uranium solubility is used for the Igneous Intrusion Modeling Case. Method 2 is based on the presence of silica in the

aqueous environment. In particular, the presence of basalt in the drifts implies that Na-boltwoodite needs to be included as a uranium solubility-controlling phase (SNL 2007 [DIRS 177418], Section 6.7.3). More specifically, two additional base solubility look-up tables are defined for this case, which include schoepite, Na-boltwoodite, and $Na_4UO_2(CO_3)_3$, depending on the pH and Pco_2.

Figure 6.5-4 shows information flow within the TSPA-LA Model for the Igneous Intrusion Modeling Case. Figure 6.5-5 indicates major inputs and outputs for each TSPA-LA Model realization, and describes the basis for confidence in the TSPA-LA Model analysis. Figures 6.5-3 and 6.5-4 indicate that the TSPA-LA Model framework for the Igneous Intrusion Modeling Case is similar to that of the Nominal Scenario Class. The principal model components and submodels used in the Igneous Intrusion Modeling Case are the same as those included in the Nominal Scenario Class. They are described in Sections 6.3.1 to 6.3.11. However, Sections 6.5.1.1.1 and 6.5.1.1.2 describe some model components and submodels that are modified to account for igneous intrusion. The following describes other changes to the Nominal Scenario Class that apply to the Igneous Intrusion Modeling Case.

6.5.1.1.1 Igneous Intrusion Engineered Barrier System Damage Submodel

Conceptual Model—The Igneous Intrusion Modeling Case describes the consequences of magma that intrudes into repository emplacement drifts, damages CSNF WPs and CDSP WPs in the intruded drifts, and solidifies. Since the flow characteristics of the magma cause it to intrude into every drift within the repository, every WP (and CSNF cladding) and DS is rendered incapable of protecting its contents. Conceptually, the CDSP and CSNF WP inner and outer barriers, the cladding in the case of CSNF, and the waste form itself are instantly degraded, leaving radionuclides available for transport through normal dissolution processes when seepage re-enters the drift. While the entire inventory is available for transport following an igneous intrusion, the magnitude of radionuclide transport to the UZ is controlled by the amount of seepage and the radionuclide solubilities. WP and DS degradation processes associated with normal conditions are considered in the Igneous Intrusion Modeling Case for 1,000,000 years up until the time of the event, but are not considered in the Igneous Intrusion Modeling Case for 20,000 years.

The geologic feature associated with an igneous intrusion entering the repository is a dike. Dikes are subvertical, elongated, tabular bodies of magma that can extend for many kilometers from a magma source. In the Yucca Mountain region, and for the Igneous Intrusion Modeling Case, the dikes are generally vertically oriented (SNL 2007 [DIRS 177432], Section 6.3.1). A grouping of more than one dike related to the same source of magma is a dike swarm. It is possible for one or more dikes in a swarm to intersect the repository and damage WPs. Figure 6.5-6 is a schematic diagram of the intersection of an igneous dike and a repository drift containing WPs.

TSPA-LA Model Abstraction—The TSPA-LA Model analysis of the Igneous Intrusion Modeling Case considers the assessment of the consequences of an igneous intrusion intersecting the repository. *Number of Waste Packages Hit by Igneous Events* (SNL 2007 [DIRS 177432]) describes the analysis conducted to estimate the number of WPs that would be damaged by an igneous intrusion.

6.5.1.1.2 Engineered Barrier System Environment Submodels in the Igneous Intrusion Modeling Case

The EBS TH Environment Submodel for the Igneous Intrusion Modeling Case differs from that used for the Nominal Scenario Class Modeling Case (Sections 6.3.2), in that it accounts for the temperature increase within and around the drift due to the intrusion of magma that fills the drift.

Conceptual Model—The heat from magma intruding into repository emplacement drifts will affect the EBS TH environment. Temperatures of the WPs, DSs, and the invert, spike to a maximum temperature at the time of the intrusion, and then cool back to ambient conditions (i.e., pre-igneous intrusion) over a 100-year time period. The associated temperature increases are described in *Dike/Drift Interactions* (SNL 2007 [DIRS 177430], Section 6.4.6 and Table 6-13). The in-drift relative humidity, invert liquid saturation, and invert liquid flux are similarly affected. The EBS chemical environment conditions are simulated just as they are for the Nominal Modeling Case since the ranges of pH and ionic strength of seepage water that has interacted with basalt is bounded by the ranges used by the Nominal Modeling Case (SNL 2007 [DIRS 177430], Section 6.7.6). EBS flow and transport processes are also simulated just as they are for the Nominal Modeling Case. Relevant EBS chemical, and flow and transport processes are turned "off" while boiling conditions exist within the drift.

TSPA-LA Model Abstraction—The EBS TH Environment Submodel (Sections 6.3.2) for the Igneous Intrusion Modeling Case accounts for the temperature of the intrusive body and its effect on the EBS temperatures at the time of intrusion. This temperature is derived as described in *Dike/Drift Interactions* (SNL 2007 [DIRS 177430], Section 6.4.6 and DTN: LA0702PADE01EG.001_R0 [DIRS 179495]). The Igneous Intrusion Modeling Case uses an initial temperature of the intrusive body of 1,150°C, and uses a cylindrical one-dimensional, transient heat conduction model to describe the cooling of the intrusive body and the surrounding rock mass. The effects of latent heat were considered and were found to have no impact on the results provided to the TSPA (SNL 2007 [DIRS 177430], Section 7.3.2.1.1.2). Temperatures return to ambient conditions (i.e., temperatures just before the event occurred) in approximately 100 years. Temperatures resulting from this abstraction are shown in Table 6.5-1. The five main columns of the table, labeled "For an Intrusion into a Repository at 25, 50, 100, 150, or 200°C," represent different 100-year temperature history shifts on the WP and drift wall depending on the temperatures of the WP and the drift wall at the time of the event.

The relative humidity within the intruded drifts is modeled as equal to zero when the magma temperature is at or greater than 100°C. Water saturation in the waste form and in corrosion product cells is set to zero for temperatures greater than 100°C, and set to one for temperatures less than 100°C.

All EBS and in-package chemistry-related submodels and parameters are the same as in the Nominal Scenario Class Modeling Case, with the exception of the uranium solubility submodel. As indicated in Section 6.3.7.5.2, Method two for uranium solubility is used for the Igneous Intrusion Modeling Case. Method two is based on the presence of silica in the aqueous environment. In particular, the presence of basalt in the drifts implies that Na-boltwoodite needs to be included as a uranium solubility-controlling phase (SNL 2007 [DIRS 177418],

Section 6.7.3). More specifically, two additional base solubility look up tables are defined for this case, which include schoepite, Na-boltwoodite, and $Na_4UO_2(CO_3)_3$, depending on the pH and Pco_2.

6.5.1.2 Mean Annual Dose Submodel for the Igneous Intrusion Modeling Case (Integration of Submodels)

The TSPA-LA Model calculates the mean annual dose for the Igneous Intrusion Modeling Case using a three-step process. First, a latin hypercube sample (LHS) of uncertain TSPA-LA Model parameters is generated. Each element of the LHS is a vector, specifying a value for each uncertain parameter. For each element in the LHS, a number of annual dose histories are computed using GoldSim. Each annual dose history is associated with a single igneous intrusion occurring at a specified time. For the 20,000-year intrusion case, the LHS size is 300 with event times at 10, 100, 600, 1000, 2000, 4000, 6000, 10,000, 14,000, and 18,000 years. For the 1,000,000-year intrusion case, the LHS sample size is 300 with event times at 250, 600, 1000, 4000, 10,000, 40,000, 100,000, 200,000, 400,000, and 800,000 years. The adequacy of the LHS sample size and the number of event times is discussed in Section 7.3.1 and 7.3.2.4, respectively. The in-package chemistry and temperature specific to the Igneous Intrusion Modeling Case are used to calculate radionuclide mobilization. Using these inputs, the fate of the mobilized radionuclides is evaluated using the Nominal Scenario Class submodels for radionuclide transport in the EBS, UZ, and SZ.

Second, for each element in the LHS, the expected annual dose history is calculated by Equation 6.1.2-16, using the annual dose histories computed for that realization. The integral in Equation 6.1.2-16 accounts for the uncertainty in the time of an igneous intrusion, and for the uncertainty in the frequency of igneous events, and is evaluated numerically by EXDOC (Section 6.1.5). The frequency of igneous events is sampled from the probability distribution described by Table 6.5-2. Finally, the mean annual dose history is calculated as the average of the expected annual dose histories from the set of realizations. Therefore, the analysis performed in the TSPA-LA Model for the Igneous Intrusion Modeling Case relies on: (1) inputs to assess consequences of an igneous intrusion within the repository and (2) inputs associated with the probability of the intrusive event.

6.5.1.3 Implementation in the TSPA-LA Model

Several inputs and feeds to the Igneous Intrusion Modeling Case originate from other TSPA-LA Models and are used in Igneous Intrusion Modeling Case calculations. Feeds from other model components and submodels to the Igneous Intrusion Modeling Case include the number of CSNF WPs and CDSP WPs in the intruded drifts and the log of the carbon dioxide fugacity. The Igneous Intrusion Modeling Case inputs are: (1) time-dependent temperature look-up tables and (2) parameters for the timing and probability of an igneous intrusion. Igneous Intrusion Modeling Case inputs are described in more detail in the following paragraphs.

For the temperature perturbation associated with an igneous intrusion, a two-dimensional look-up table based on Table 6.5-1 is implemented, which defines the shift in WP temperature for times up to 100 years after magma intrusion into the drift(s). A similar two-dimensional look-up table is implemented for drift-wall and invert temperatures as magma enters the drift(s).

Temperature values are interpolated from the tables based on: (1) the temperatures of the WP, drift wall, and invert when the igneous intrusion occurs and (2) the elapsed time since the igneous intrusive event occurred (SNL 2007 [DIRS 177430], Table 8-2), where $T_{r=0m}$ and $T_{r=3m}$ refer to the temperatures at a radius of 0 m (i.e., centerline of the WP) and 3 m (i.e., drift wall and invert) from the drift center, respectively.

Inputs also include: (1) the mean annual frequency of a dike intersecting the repository (BSC 2004 [DIRS 169989]), Section 6.5.3); and (2) the minimum and maximum times during the simulation at which the igneous intrusion can occur.

6.5.1.4 Model Component Consistency and Conservatism in Assumptions and Parameters

There are differences in assumptions and parameter sets used in the TSPA-LA Model that have arisen in the development of the abstractions and process models. Most of these differences are due to the use of conservative assumptions in the process model or analysis when uncertainty is difficult to quantify. Understanding and evaluating potential impacts from these assumptions with respect to the mean annual dose is conducted through a series of processes described in Section 7.4 (Uncertainty Characterization Reviews), Section 7.7 (Corroboration of Results with Auxiliary Analyses), and Section 8.4 (Validity and Defensibility of Performance Demonstration). To enhance understanding of the complex interactions within the TSPA-LA Model, a discussion of consistency among model components and submodels and identification of conservative assumptions in abstractions, process models, and parameter sets supporting the Igneous Intrusion Modeling Case are discussed below.

6.5.1.4.1 Consistency of Assumptions

In-Package Chemistry and the Instantaneous Degradation of CSNF—The In-Package Chemistry Abstraction (SNL 2007 [DIRS 180506]) does not consider instantaneous degradation of CSNF in the range of conditions analyzed with the process model and in the development of the subsequent abstraction. Very fast degradation rates were considered but did not approach instantaneous degradation of CSNF. However, within the TSPA-LA Model, instantaneous degradation of the CSNF occurs in the Igneous Intrusion Modeling Case.

Effect on the TSPA-LA Model—The instantaneous degradation of the CSNF waste form is recommended during an igneous intrusion. Because the in-package pH conditions are controlled by the buffering capacity of the degradation products of CSNF (SNL 2007 [DIRS 180506], Section 6.3.4.1[a]), instantaneous degradation of CSNF means that the maximum pH buffering capacity will be achieved almost immediately, at which time the pH conditions will be well constrained. Well-buffered chemical solutions are part of the in-package chemistry abstraction, therefore, the implemented pH abstraction is sufficient to cover this instantaneous CSNF degradation condition. Similarly, the ionic strength abstraction is sufficient to cover the condition following the instantaneous degradation of CSNF inside a failed WP.

6.5.1.4.2 Identification of Conservatisms in Submodels and Abstractions

WPs and DSs are Completely Damaged— Because there will be no backfill in the drifts, there are no credible mechanisms to block or mitigate the resulting effects from a dike intrusion into a

drift or the effects of the magma on the WPs and DSs (SNL 2007 [DIRS 177432], Section 5.1). Hence, in the Igneous Intrusion Modeling Case, all WPs and DSs located in magma-intruded drifts are assumed to be sufficiently damaged that they provide no hindrance to flow, or protection of their radionuclide inventories to dissolution processes. In addition, no credit is taken for entombment of the waste by the solidified magma. Rather, when in-drift conditions are favorable for the re-entry of seepage, the mobilization of the CDSP and CSNF inventories is controlled only by the radionuclide solubilities.

In addition, since the waste form is conservatively assumed to be entirely degraded during an igneous intrusion, any contribution to its degradation that could have occurred by seepage through fracturing of the basalt is already accounted for. This conservative assumption increases the release of radionuclides from the EBS above the release that would occur if some credit were taken for WPs, DSs, and the solidified magma, all of which would provide some hindrance to flow through the waste form.

Drift Seepage Equal to Percolation after Intrusion—In the Igneous Intrusion Modeling Case, the seepage is set equal to 100 percent of the local percolation flux at the base of the PTn (Section 6.3.3) for magma-intruded drifts. The intruded basalt in the drift is assumed to provide no resistance to water flow. Because all of the WPs and DSs are failed, the entire seepage flux enters the WP and is available for advective transport of radionuclides from the EBS (SNL 2007 [DIRS 181244], Section 6.7.1.1).

This is a conservative abstraction for implementation in the TSPA-LA Model that results in an increase in the release of radionuclides from the EBS over that which would occur if some credit were taken for the cooled magma diverting some of the seepage away from the waste form.

Drift and Dike Interactions—Several conservative assumptions are made for the dike and drift interactions as follows:

1. The filling of the drifts with magma does not consider the presence of the EBS component (e.g., DSs), rubble filled drift, or other features, nor the effects of cooling and temperature-dependent viscosity during magma flow, that could impede the flow of magma and therefore contact fewer WPs than the total inventory (SNL 2007 [DIRS 177430], Section 5.2).

2. WPs engulfed by magma are instantaneously failed and provide no further protection of their contents (SNL 2007 [DIRS 177430], Section 8.1.2).

3. Upon cooling, the basalt is highly fractured and does not provide any hindrance to seepage. The thermal properties of the basalt-filled drift are assumed to be the same as the surrounding host rock (SNL 2007 [DIRS 177430], Section 5.3.1).

These conservative assumptions result in an overestimation of the amount and mobilization of radionuclide inventory for transport through the EBS, UZ and SZ, and hence contribute to higher than expected doses.

6.5.1.5 Alternative Conceptual Model(s) for Igneous Intrusion Modeling Case

An important reason for considering alternative conceptual models (ACMs) is to help build confidence that plausible changes in modeling assumptions or simplifications will not change conclusions regarding subsystem and total system performance. Section 6.2 outlines the general consideration and treatment of ACMs used to support the TSPA-LA Model. Conservatism at the subsystem level has been used to select the best ACM to use rather than quantitatively propagate multiple ACMs to the TSPA-LA Model. Generally, additional uncertainty is incorporated into the selected conceptual model if more than one ACM is deemed appropriate for use rather than considering multiple ACMs in the TSPA-LA Model. If an ACM appears to be significant at the subsystem level, then an appropriate abstraction is developed for that ACM for consideration within the TSPA-LA Model. The result of the process is documented within the individual analysis model reports. It is important to note that treatment of ACMs within the individual analysis model reports may differ significantly to be consistent with available data and current scientific understanding. Therefore, the Igneous Intrusion Modeling Case ACMs are summarized below.

ACM for Estimating the Igneous Event Rates in the Probabilistic Volcanic Hazard Analysis—The PVHA model uses the number of identified post-Miocene era volcanic events observable at the surface plus some buried in the Yucca Mountain region. *Characterize Framework for Igneous Activity at Yucca Mountain, Nevada* (BSC 2004 [DIRS 169989], Sections 6.3.1.6 through 6.3.1.7 and Table 6-4) identifies an ACM for the PVHA in which a significant number of buried (i.e., unidentified) volcanic centers would be included in the estimation of the igneous event rates. The basis for the ACM is that aeromagnetic anomalies suggest that a significant number of unidentified volcanic events were unaccounted for in the PVHA, thus underestimating the volcanic hazard. However, this ACM was not considered because its effects on the probability of an igneous event could not be quantified without further data collection. A drilling and sampling program is underway to determine if any of these anomalies represent Quaternary buried volcanic centers. In addition, an update to the PVHA is underway to reassess the probability of intersection and the probability of a volcanic center being located on Yucca Mountain. Total mean annual dose from the Igneous Scenario Class can reasonably be expected to vary linearly with frequency.

ACMs for Estimating the Intersection Annual Probability in the Probabilistic Volcanic Hazard Analysis—*Characterize Framework for Igneous Activity at Yucca Mountain, Nevada* (BSC 2004 [DIRS 169989], Section 6.3.1.8 and Table 6-5) identifies several ACMs for estimating the intersection probability (i.e., the annual probability of a volcanic event intersecting the repository footprint). The ACM probabilities are captured by the probability used in the PVHA, which indicates that any impacts on the TSPA-LA from using one of these ACMs would be negligible.

ACMs for Dike Propagation—*Dike/Drift Interactions* (SNL 2007 [DIRS 177430], Section 6.3.3.5), identifies ACMs for dike propagation that use hydraulic-fracture models. The *Dike/Drift Interactions* report (SNL 2007 [DIRS 177430], Section 6.3.8) concluded that none of these models were appropriate for the dike propagation in the vicinity of an underground repository, as none of the models has a free surface that can model the changing behavior of the

dike as the surface is approached. Thus, the ACMs were used for validation comparisons only and were not appropriate for use in the TSPA-LA.

ACMs for Effusive Magma Flow into Drifts—*Dike/Drift Interactions* (SNL 2007 [DIRS 177430], Section 6.3.3.5) identifies ACMs for effusive or pyroclastic flow from a dike into a drift. Simulation of these flows and their interactions with WPs is computationally intensive and, therefore, not practical for implementation within the TSPA-LA Model. Instead, the abstractions included in *Number of Waste Packages Hit by Igneous Events* (SNL 2007 [DIRS 177432]), accounts for the effects of these flows within the TSPA framework.

ACMs for TH Effects on Magma Filled and Neighboring Non-Magma Filled Drifts Drifts—*Dike/Drift Interaction* (SNL 2007 [DIRS 177430], Section 6.4.7) identifies ACMs for the TH behavior of magma-filled drifts and its effects on neighboring drifts when an igneous intrusion into the repository affects a limited number of drifts rather than all the drifts. These ACMs involve an evaluation of additional physics, including latent heat of crystallization, host-rock saturation, and enhanced vapor diffusion, and an alternative model for heat conduction around affected emplacement drifts. Inclusion of the latent heat of crystallization and host-rock saturation in the heat transfer analyses was evaluated and is shown to have a negligible effect on the results, producing elevated temperature histories (i.e., above boiling) no more than two to five years longer than without these ACMs included in the analysis (SNL 2007 [DIRS 177430], Section 6.4.7).

With respect to the TH implementation of igneous intrusion in the TSPA-LA, these ACMs do not produce elevated temperature histories (i.e., above boiling) significantly longer than those already in use. Hence, the impact to the TSPA-LA of using any of these TH ACMs is negligible.

No ACMs were recommended for inclusion in the TSPA-LA Model.

6.5.2 Volcanic Eruption Modeling Case

The Volcanic Eruption Modeling Case in the TSPA-LA Model considers the possibility of a volcanic eruptive conduit intersecting the repository footprint resulting in the dispersal of waste-contaminated tephra in the atmosphere with eventual deposition on the ground surface. This modeling case evaluates only the post-eruption consequences due to waste deposited at the location of the reasonably maximally exposed individual (RMEI) directly or redistributed from upstream in the Fortymile Wash watershed. It does not include an evaluation of annual dose received during the active volcanic eruption phase when the waste is transported and dispersed in the atmosphere. The active eruption phase is evaluated separately in Section 6.5.2.4 to show that the mean annual dose during the active eruption phase is small compared to the mean annual dose during the post-eruption time period.

Implementation of the Volcanic Eruption Modeling Case for the TSPA-LA Model includes the determination of both the probability of the event and its consequences. The probability of an eruptive event is determined by two factors. The first is the probability of an eruption penetrating the repository sampled from the probability distribution for the annual frequency of an intersection of the repository by a dike, as provided in *Characterize Framework for Igneous Activity at Yucca Mountain, Nevad*a (BSC 2004 [DIRS 169989], Table 6-8, Section 6.5.3.1;

DTN: LA0307BY831811.001_R0 [DIRS 164713]) and shown in Table 6.5-2. The second factor is the probability of an eruption that intersects the repository footprint, given that a dike intersection of the repository occurs; this value is 0.28 (parameter Eruptive_Center_Probability_a in *Number of Waste Packages Hit by Igneous Events* (SNL 2007 [DIRS 177432], Section 7.2). Note that all igneous events with dikes that intersect the repository are assumed to also have eruptive conduits, but only a fraction of these conduits intersect the repository footprint (other conduits might form along a dike where it extends outside the repository footprint). The annual frequency of an eruption through the repository is estimated by multiplying the two probability factors described above.

The Volcanic Eruption Modeling Case in the TSPA-LA Model includes submodels for the processes affecting the release, transport, and redistribution of radionuclides associated with the volcanic eruption, and implements the submodels for the calculation of mean annual dose. The following sections (Sections 6.5.2.1 to 6.5.2.2) address these submodels and their implementation for the Volcanic Eruption Modeling Case. In addition, the model evaluation, model conservatism, and ACMs are discussed in Sections 6.5.2.3 and 6.5.2.4.

6.5.2.1 TSPA-LA Submodels for the Volcanic Eruption Modeling Case

The submodels for evaluating the consequences of the Volcanic Eruption Modeling Case are shown on Figure 6.5-7, which does not contain as many model components and submodels as the Igneous Intrusion Modeling Case (Figure 6.5-3). Figure 6.5-8 illustrates the flow of information in the TSPA-LA Volcanic Eruption Modeling Case and the relationship between the submodels for the Volcanic Eruption Modeling Case. Figure 6.5-9 indicates the major inputs and outputs of the Volcanic Eruption Modeling Case, the features included in the TSPA-LA Model, and the foundation for confidence in the Volcanic Eruption Modeling Case.

Four submodels are considered in the Volcanic Eruption Modeling Case. Volcanic Interaction with the Repository Submodel (Section 6.5.2.1.1) describes the number of WPs that may be destroyed by, and entrained in, a volcanic eruption and the amount of waste available for atmospheric transport. The Atmospheric Transport Submodel (Section 6.5.2.1.2) describes the atmospheric transport of this erupted tephra/waste mixture and eventual deposition on the land surface. The Tephra Redistribution Submodel (Section 6.5.2.1.3) describes the redistribution of the contaminated tephra to the location of the RMEI. The Volcanic Ash Exposure Submodel (Section 6.5.2.1.4) uses the volcanic ash biosphere dose conversion factors (BDCFs) to estimate mean annual dose to the RMEI, which was previously presented in the Biosphere Model Component (Section 6.3.11.2). The following subsections describe these four components of the Volcanic Eruption Modeling Case.

6.5.2.1.1 Volcanic Interaction with the Repository Submodel

Conceptual Model—Eruptive events involving the intersection of an eruptive conduit with the repository could result in the atmospheric release of volcanic tephra and mobilized waste from the repository and subsequent deposition on the ground surface. Figure 6.5-10 is a schematic diagram of the intersection of an igneous dike and eruptive conduit with the repository. The quantity of waste erupted into the atmosphere is conceptualized in the Volcanic Eruption Modeling Case as depending on the distribution of WPs in the emplacement drifts, the number

and size of eruptive conduits intersecting the drifts, the degree of damage to those WPs, the amount of waste from the WPs that is entrained into the erupting material, and the fraction of magma that is erupted into the ash cloud (tephra). The size and number of dikes associated with an eruptive event considered credible for the Yucca Mountain region are described in *Characterize Eruptive Processes at Yucca Mountain, Nevada* (SNL 2007 [DIRS 174260], Table 7-1). The conduit diameter is given as a normal distribution with a mean diameter of 15 m. Data and output from *Characterize Eruptive Processes at Yucca Mountain, Nevada* (SNL 2007 [DIRS 174260], Table 7-1) allow for up to three conduits to form along the thickest dike (referred to as the master dike) in a dike swarm. The number of WPs intersected by conduits is a function of conduit area, the number of conduits, and the conduit location within the repository. Only WPs located partially or entirely within a conduit are assumed to be destroyed, making all of the waste in these WPs available for entrainment in the erupting pyroclastic material. The potential for WPs located outside the conduit diameter to be mobilized by magma and moved toward the conduit is analyzed in *Dike/Drift Interactions* (SNL 2007 [DIRS 177430], Section 6.4.8.3.2). The analysis concludes that WP movement outside of a conduit profile is not expected considering expected magma velocities, pressures, and viscosities, as well as WP dimensions and densities. Estimates of the number of WPs that might be intersected during an eruptive sequence are based on the probability distribution described in *Number of Waste Packages Hit by Igneous Events* (SNL 2007 [DIRS 177432], Section 7.1).

TSPA-LA Model Abstraction—The mass of waste incorporated in the tephra plume from an eruptive event depends on the waste inventory, the number of WPs intersected, and the fraction of waste-containing magma that is erupted in a tephra plume instead of lava flows and scoria cone. The CDF for the number of WPs intersected by conduits is shown in Table 6.5-3. Figure 6.5-11 graphically illustrates the CDF and probability for the number of WPs that could be potentially intersected by an eruptive conduit(s) from igneous activity culminating in a volcanic eruption within the repository footprint (SNL 2007 [DIRS 177432], Section 7.1). As seen on the figure, the Waste Packages Hit analysis indicates that there is approximately a 70 percent probability that no WPs will be hit by a volcanic eruption intersecting the repository. The small conduit diameters relative to drift spacing mean that 70 percent of the conduits intersecting the repository footprint would form between drifts and therefore not intersect any WPs. In the 30 percent of cases in which one or more packages are hit, the most likely number hit is four and the maximum number hit is seven.

The Volcanic Eruption Modeling Case includes the mass of waste in both the CSNF WPs and CDSP WPs that are hit, and the proportions of each kind of waste released from the repository in the erupting material. The mass of waste hit is multiplied by the magma partitioning factor to account for the partitioning of magma into surface lava flows, scoria cone, and tephra plume (SNL 2007 [DIRS 177431], Section 6.5.2.9). The magma partitioning factor is specified as a uniform distribution from 0.1 to 0.5 and represents the fraction of magma that is erupted into the tephra plume to be considered in the Volcanic Eruption Modeling Case. Waste potentially deposited with surface lava flows and scoria cone is not part of the contaminated tephra that is ejected into the atmosphere, and is therefore, not considered in the TSPA-LA analysis which models only aerial dispersal and subsequent redistribution of contaminated tephra.

6.5.2.1.2 Atmospheric Transport Submodel

Conceptual Model—The conceptual model for the Atmospheric Transport Submodel is a vertical column of heated tephra and waste particles, resulting in a buoyant plume that reaches neutral buoyancy at some level in the atmosphere. The plume is then transported downwind and, because of dispersive processes, spreads out laterally as it is transported. Solids fall from the plume as it travels depending on the wind speed, particle density, and settling velocity. The pyroclastic material ejected into the atmosphere from a volcanic eruption eventually falls to the ground surface and forms a contaminated tephra sheet of varying thickness extending and thinning, generally, downwind from the volcanic vent (SNL 2007 [DIRS 177431], Section 6.3).

Figure 6.5-12 is a schematic illustration of a volcanic eruption intersecting the repository at Yucca Mountain. The figure shows the transport of radioactive waste in the tephra plume from the repository to the location of the RMEI under the condition of a southerly directed wind.

TSPA-LA Model Abstraction—Atmospheric transport and deposition of erupted waste is evaluated using the ASHPLUME code (ASHPLUME_DLL_LA V2.1, STN: 11117-2.1-00 [DIRS 181035]) described in *Atmospheric Dispersal and Deposition of Tephra from a Potential Volcanic Eruption at Yucca Mountain, Nevada* (SNL 2007 [DIRS 177431], Section 6.5). The ASHPLUME code is implemented directly in the TSPA-LA Volcanic Eruption Model, using the ASHPLUME computer code as a dynamically linked library (DLL).

The ASHPLUME code simulates a violent Strombolian eruption with entrainment of radioactive waste in the erupted plume as waste particles attached to the pyroclastic fragments in the plume. The waste-contaminated tephra particles ejected into the atmosphere form a contaminated deposit on the land surface. The parameter "incorporation ratio" is a cutoff ratio for the minimum size of a tephra particle that can carry a waste particle of a given size. Expressed as the Log_{10} of the ratio, an incorporation ratio of 0 is used in the TSPA implementation, meaning the maximum waste particle size is equal to the tephra particle size. The mathematical formulation of this incorporation ratio and the approach to determining the mass fraction of waste that is incorporated in an eruption is discussed in *Atmospheric Dispersal and Deposition of Tephra from a Potential Volcanic Eruption at Yucca Mountain, Nevada* (SNL 2007 [DIRS 177431], Section 6.5.2.6). The wind speed and direction that result in atmospheric transport of the erupted material are represented in the ASHPLUME code in terms of CDFs (DTN: MO0408SPADRWSD.002_R0 [DIRS 171751]). These CDFs are specified for 1-km height increments between 0 km and 13 km above the mountain. Wind speed and direction for a given model realization are selected from the height bin appropriate to the eruption column height for that realization. Once selected, the wind speed and direction are assumed to be constant throughout the eruption duration in the ASHPLUME model. The impact of this simplification is considered to be negligible based on the analysis in *Atmospheric Dispersal and Deposition of Tephra from a Potential Volcanic Eruption at Yucca Mountain, Nevada* (SNL 2007 [DIRS 177431], Section 7.6). The ASHPLUME mathematical model for atmospheric dispersion and deposition of the particles in the plume is based on the theoretical model by Suzuki in "A Theoretical Model for Dispersion of Tephra" (Suzuki 1983 [DIRS 100489], pp. 95 to 113). The movement of air mass in the atmosphere is random within the scale of eddy motions in wind currents. Therefore, the dispersion of the contaminated tephra particles in the atmosphere is also random. Particles disperse in the atmosphere in both vertical

and horizontal directions. The scale of horizontal turbulence is much greater than the scale of vertical turbulence. Therefore, particle diffusion is considered to be two-dimensional in the horizontal "x-y" plane. Particle movement in the vertical "z" direction is accounted for by the particle settling velocity. The ASHPLUME mathematical model and its solution are described in *Atmospheric Dispersal and Deposition of Tephra from a Potential Volcanic Eruption at Yucca Mountain, Nevada* (SNL 2007 [DIRS 177431], Section 6.5). The Atmospheric Transport Submodel predicts the ground-level concentrations (areal density, g/cm^2) of tephra and waste directly deposited at the location of the RMEI and the spatial distribution of tephra and waste in the Fortymile Wash watershed for a simulated volcanic event. The tephra concentration in the Fortymile Wash watershed is converted into volcanic ash thickness by the Tephra Redistribution Submodel and redistributed to the RMEI location along with incorporated waste.

The uncertain ASHPLUME code input parameters that may significantly affect the outcome of TSPA-LA Model calculations are expressed as probability distributions to be used in the TSPA-LA Model. Table 6.5-4 shows key ASHPLUME code input parameters, and indicates those that are represented by probability distributions and those that use fixed values.

6.5.2.1.3 Tephra Redistribution Submodel

Conceptual Model—Waste-contaminated tephra deposited on the ground surface in Fortymile Wash by the Atmospheric Transport Submodel could be redistributed to the RMEI location due to hillslope and fluvial processes. Therefore, the waste concentration used in the Biosphere Submodel to determine dose consists of contributions from both waste-contaminated tephra at the RMEI location deposited directly when atmospheric conditions move the eruptive plume toward that location, and any waste-contaminated tephra redistributed from upstream that may have been deposited in the Fortymile Wash Watershed. Three major processes are considered in the tephra redistribution conceptual model: (1) mobilization from hillslopes; (2) mixing and dilution with uncontaminated sediments during channel transport; and (3) diffusion into the soil column at the RMEI location. A detailed description of the tephra redistribution conceptual model can be found in *Redistribution of Tephra and Waste by Geomorphic Processes Following a Potential Volcanic Eruption at Yucca Mountain, Nevada* (SNL 2007 [DIRS 179347], Section 6.2).

The conceptual tephra redistribution model divides the Fortymile Wash drainage area into two domains: the drainage basin and the alluvial fan. The drainage basin includes the vent location and the tephra and waste deposited on the landscape in the event of a volcanic eruption through the repository (Figure 6.5-13). The RMEI location is considered to be on the Fortymile Wash alluvial fan south of the fan apex. The drainage basin and the alluvial fan are divided at the fan apex. The location of the RMEI is specified in the same area for the igneous eruption case as for all other modeling cases so that estimates of the dose are calculated at a consistent location for the nominal, intrusive, and eruptive modeling cases. This means that model realizations with wind blowing away from this location and away from the Fortymile Wash do not contribute to dose calculations.

The tephra redistribution model uses a spatially distributed analysis of hillslopes and channels in the drainage basin upstream of the fan apex to provide an estimate of the mass of tephra and waste that could be transported from the upper drainage basin to the RMEI location by hillslope

and fluvial processes. The model mobilizes and transports tephra and waste deposited on the landscape toward the RMEI location if it falls on steep slopes or on active channels. Before the mobilized tephra and waste are deposited at the RMEI location, they are transported through the alluvial channel system where mixing with uncontaminated channel sediments leads to dilution. Mixing occurs during flood events as sediment and tephra are entrained from the bed, mixed by turbulent flow, and redeposited on the bed. The depth to which tephra and channel sediment are mixed is the scour depth. The ratio of the tephra thickness to the scour depth at the fan apex, just upstream from the RMEI location, is used as the fraction of channel-bed material composed of tephra when the redistributed tephra and waste reach the RMEI location.

The tephra and waste transported from the upper drainage basin, and primary tephra and waste deposited at the RMEI location, provide the initial conditions for redistribution of radionuclides into the soil column at the RMEI location. The Tephra Redistribution Submodel considers the migration of radionuclides within the soil as a diffusion process due to suspension and redeposition of fine particles by infiltration, and physical mixing of soil particles by freeze-thaw cycles and bioturbation. The diffusion coefficients used in the model were calibrated using measured ^{137}Cs profiles on channels and inter-channel divides of the upper Fortymile Wash alluvial fan and therefore incorporate all of the potential diffusion processes (SNL 2007 [DIRS 179347], Sections 6.3.3 and 6.5.9). The time-dependent concentration resulting from the diffusion process is used by the Volcanic Ash Exposure Submodel to calculate dose to the RMEI.

TSPA-LA Model Abstraction–The Tephra Redistribution Submodel is implemented in the TSPA-LA Volcanic Eruption Model using the computer code FAR V1.2 (STN: 11190-1.2-00 [DIRS 182225]). The FAR V1.2 code is implemented as a DLL and is incorporated directly within the TSPA-LA Volcanic Eruption Model. The mathematical description of the FAR V1.2 code is provided in *Redistribution of Tephra and Waste by Geomorphic Processes Following a Potential Volcanic Eruption at Yucca Mountain, Nevada* (SNL 2007 [DIRS 179347], Section 6.3).

Gridded values of tephra and waste concentration computed by the ASHPLUME code are passed to the FAR code for redistribution calculations. FAR V1.2 maps the tephra and waste concentration to a 30-m resolution digital elevation model grid covering the Fortymile Wash drainage basin. The calculation of time-dependent waste concentration at the RMEI location proceeds in six steps (SNL 2007 [DIRS 179347], Section 6.3.3).

Step 1: Because ASHPLUME calculations are carried out on a relatively coarse polar grid, a bilinear interpolation is performed on the ASHPLUME-generated grid values of tephra and waste concentration to rectify the concentration values to the much higher resolution digital elevation model grid.

Step 2: The digital elevation model file is processed to fill any artificial “holes” in topography due to imperfections in the digital elevation model data. The file is scanned recursively to slightly raise any “pits” or “flats” where the downstream direction is not well defined.

Step 3: A set of spatial analyses are performed on the input digital elevation model to determine slopes, contributing area, and scour depths for the drainage basin. The waste-contaminated tephra is mobilized from slopes greater than a specified critical slope.

Step 4: The mobilized tephra is routed through the channel system to model the dilution effect. Routing of mobilized tephra and uncontaminated channel-bed sediments is performed using a bifurcation routing algorithm. The resulting grid of tephra thickness routed through each digital elevation model pixel is divided by the grid of scour depth routed through each pixel to yield a dilution factor at each channel grid cell in the basin. The dilution factor at the apex of the alluvial fan (one particular cell in the grid) is used in subsequent steps.

Step 5: Initial concentrations of waste in channels and on interchannel divides at the RMEI location are determined. This step represents the transfer of waste from the upper drainage basin to the RMEI location on the alluvial fan. In channels, the mass of waste is the sum of the direct deposition of waste and waste transported from the upper basin by fluvial processes. On interchannel divides, the concentration of waste is determined solely from direct deposition of waste-contaminated tephra.

Step 6: Time-dependent diffusion of radionuclides within a finite depth of permeable soil is calculated using the initial concentrations determined in **Step 5**. Inputs to this step include the permeable depths on divides, L_d, and in channels, L_c, and diffusivity values for divides, D_d, and channels, D_c.

The mixing/dilution processes implemented in Steps 1 to 5 are assumed to occur instantaneously after the potentially contaminated tephra is deposited on the ground surface after a volcanic eruption. To simplify the model conceptualization, the diffusion process in Step 6 is the only process considered to be time-dependent in the Tephra Redistribution Submodel. This is a reasonable simplification, given the expected relatively short time scale of the mixing processes.

Descriptions of the key input parameters to the Tephra Redistribution Submodel are shown in Table 6.5-5. The results of the Tephra Redistribution Submodel calculations are passed to the Volcanic Ash Exposure Submodel for dose calculations. The results consist of four time series of mass concentration: (1) concentration on divides averaged over the tillage depth; (2) concentration on divides averaged over the resuspendable surface layer; (3) concentration in channels averaged over the tillage depth; and (4) concentration in channels averaged over the resuspendable surface layer. The concentrations on divides and channels are combined using the weighting factor, *F,* for the fraction of the alluvial fan composed of channels (and 1-*F* for the fraction of the alluvial fan composed of divides) to yield one concentration for the resuspendable surface layer and one concentration for the tillage depth for use by the Volcanic Ash Exposure Submodel in dose calculations.

6.5.2.1.4 Volcanic Ash Exposure Submodel

The Volcanic Ash Exposure Submodel provides the calculation of annual dose for the Volcanic Eruption Modeling Case. Details of the dose calculation are provided with the Biosphere Model

Component description in Section 6.3.11. Implementation of the Volcanic Eruption Modeling Case for the TSPA-LA Model includes the determination of both the probability of the event and its consequences.

During the atmospheric transport and redistribution on the ground surface, radionuclide concentrations in the waste are proportional to those in the waste inventory that combine each type of WP hit, with consideration of radionuclide decay. The calculated radionuclide concentrations in volcanic tephra or in a soil/tephra mixture using the redistribution submodel provide the radioactive source term for calculating annual dose to the RMEI. A set of the BDCFs appropriate to the Volcanic Eruption Modeling Case is developed according to the Biosphere Model Component described in Section 6.3.11. The annual dose associated with the radioactive source is calculated by multiplying radionuclide concentrations by the volcanic ash BDCFs.

6.5.2.2 Implementation in the TSPA-LA Model

This subsection describes the inputs, feeds, software, and model calculations required for the Volcanic Eruption Modeling Case. The Volcanic Eruption component of the TSPA-LA Model is implemented as a separate, stand-alone GoldSim model file.

The determination of atmospheric dispersal and deposition of ash and waste fuel particles from a hypothetical volcanic eruption that intersects the repository is accomplished using the ASHPLUME_DLL_LA V.2.1 code, which is dynamically coupled to the TSPA-LA Model. The ASHPLUME DLL requires input parameters that define the characteristics of the eruptive event, the environmental conditions, and the mass of the waste to be included in the event. The key ASHPLUME input parameters are shown in Table 6.5-4. The mass of waste to be included in the eruptive event is calculated based on the proportion of CSNF WPs to CDSP WPs in the repository, a sampled parameter that selects the number of WPs affected by the eruptive event, and a factor that accounts for the proportion of waste-contaminated magma that is erupted into the tephra column. Note that this is the total mass of waste that the ASHPLUME code uses, and not a mass vector by radionuclide species. These inputs to the ASHPLUME code are located in the ASHPLUME_DLL input container in the TSPA-LA Model. GoldSim (GoldSim V.9.60.100, STN: 10344-9.60-01 [DIRS 181903]) first samples the input parameters that are probability distributions, and then passes all parameters to the ASHPLUME code. The ASHPLUME code then calculates the waste and ash deposition results (g/cm^2) at the RMEI location, followed by an additional calculation (using the same input parameters) at many grid points covering the Fortymile Wash watershed.

The TSPA-LA Model then performs calculations for the Tephra Redistribution Submodel. The consequences of a volcanic eruption include the potential increase in dose at the location of the RMEI from the transport of radioactive waste-contaminated ash through hillslope and fluvial transport mechanisms. The Tephra Redistribution Submodel accounts for this effect at the location of the RMEI for both interchannel divides and distributary channels. The volcanic ash redistribution calculations are performed using the computer code FAR V1.2 (STN: 11190-1.2-00 [DIRS 182225]). Inputs to this DLL define such parameters as directly deposited ash and waste concentrations at the RMEI location and at grid points covering the Fortymile Wash watershed; critical gradient and drainage density for tephra mobilization; scour

depth; diffusion parameters; and Biosphere Model Component inputs. GoldSim samples those inputs that are probability distributions and then passes all inputs to FAR V1.2, which uses these inputs to calculate the time-dependent waste concentration on interchannel divides and distributary channels. The TSPA-LA Model takes these ash redistribution results and, using the areal weighting factor, F (Table 6.5-5), for interchannel divides and distributary channels, determines the source terms for:

- Ingestion and radon exposure for the interchannel divides and distributary channels
- Long-term inhalation exposure for interchannel divides and distributary channels
- Short-term inhalation exposure for interchannel divides and distributary channels.

The TSPA-LA Model then converts the source terms back into the masses of the individual radionuclide species based on total repository inventory and accounts for radioactive decay. As described in Section 6.3.11, these source terms are then multiplied by the corresponding BDCFs to determine dose.

Section 6.1.2.4.3 describes the calculation of annual dose histories for the TSPA-LA Model for the Volcanic Eruption Modeling Case. The TSPA-LA Model calculates the mean annual dose for the Volcanic Eruption Modeling Case using a three-step process. First, an LHS of epistemically uncertain TSPA-LA Model parameters is generated. Each element $\mathbf{e}_i$ in the LHS defines values for the epistemic parameters listed in Table 6.5-4. For each element in the LHS, a number of annual dose histories are computed using GoldSim. The characteristics of each eruption (e.g., eruptive power and eruptive height) and the wind conditions at the time of the eruption are specified by elements of a separate LHS, $\mathbf{u}$, for the aleatory parameters listed in Table 6.5-4. Using these inputs, the amount of waste entrained in the eruptive plume, its deposition and redistribution are evaluated using the models described above, to produce a single annual dose history, $D_{IE}(\tau \mid [1, t, 1, \mathbf{u}_l], \mathbf{e}_i)$. Each annual dose history D_{IE} is associated with a single volcanic eruption occurring at a specified time t, which affects one WP, and with specified eruptive characteristics and specified wind conditions.

Second, for each element of the LHS of epistemic parameters, the expected annual dose history is calculated by Equation 6.1.2-18 (Section 6.1.2.4.3), using the annual dose histories computed for that realization. The integral in Equation 6.1.2-18 (Section 6.1.2.4.3) accounts for the aleatory uncertainty in the time and characteristics of the eruption and the wind conditions, as well as the uncertainty in the frequency of igneous events, and is evaluated numerically by EXDOC (Section 6.1.5). The frequency of igneous events is sampled from the probability distribution described in Table 6.5-2. Finally, the mean annual dose history is calculated as the average of the expected annual dose histories from the set of realizations.

The total expected annual dose result for the Volcanic Eruptive Modeling Case presented in Section 8.2.3.2 was calculated using GoldSim to implement the dose histories, and EXDOC to implement Equation 6.1.2-18 (Section 6.1.2.4.3). To implement the calculation of the contribution of individual radionuclides to the mean annual dose histories presented in Section 8.2.3.2, an alternative technique was used. In addition to implementing the single annual dose history calculation, the GoldSim model file for the Volcanic Eruption Modeling Case also implements a calculation of the mean dose history for individual radionuclides by considering a "blended" sampling of all epistemic and aleatory parameters as follows:

$$\overline{\overline{D}}_i(\tau) = \frac{pE}{M}\sum_{j=1}^{M}\lambda_{I,j}N_{IE,j}F_j\int_0^{\tau} D_{IE,i}(\tau \mid t,1,\mathbf{u}_j,\mathbf{e}_j)dt \qquad \text{Eq. 6.5.2-1}$$

where

$\overline{\overline{D}}_i(\tau)$ = mean annual dose history for radionuclide i

M = the number of samples of "blended" aleatory **u** and epistemic **e** parameters used to compute the mean

λ_I = frequency of igneous events (Table 6.5-2) **e**

pE = probability that an igneous event includes a conduit that intersects waste, or 0.083 (This is the probability that one or more waste packages are intersected by a conduit (i.e. 1.0 minus 0.703 from Table 6.5-3) times the probability that a conduit forms inside the repository footprint on a dike that intersects the repository (0.28 from SNL 2007 [DIRS 177432], Section 7.2))

N_{IE} = the number of WPs affected by an eruptive conduit (sampled from the non-zero portion of Table 6.5-3) **u**

F = the fraction of WP contents ejected into the atmosphere (Magma_Partitioning_a in Table 6.5-4) **u**, and

$D_{IE,i}(\tau|t,1,\mathbf{u}_j,\mathbf{e}_j)$ = annual dose history for radionuclide i conditional on an eruption at time t, which affects one repository average WP for "blended" sample j of all aleatory and epistemic parameters.

The total mean annual dose for the Volcanic Eruption Modeling Case is the sum of the contributions from the individual radionuclides. Equation 6.5.2-1 was used to calculate the contribution of individual radionuclides to the mean annual dose histories presented in Section 8.2.3.2. It should be noted that the mean of the expected dose calculated using EXDOC as presented in Section 6.1.2.4.3, and the mean calculated with Equation 6.5.2-1 are mathematically equivalent, however, slight numerical differences will be observed in the results of the two methods due to different parameter sampling and the different numerical solution techniques employed by the two methods. Equation 6.5.2-1 was used to produce the individual radionuclide contribution results for the Volcanic Eruption Modeling Case because it is less computationally intensive when only the mean value is required.

6.5.2.3 Model Component Consistency and Conservatism in Assumptions and Parameters

To enhance understanding of the complex interactions within the TSPA-LA Model, a discussion of consistency among model components and submodels, and identification of TSPA-LA Model conservatisms in submodels and abstractions specific to the Volcanic Eruption Modeling Case, are discussed below.

6.5.2.3.1 Consistency of Assumptions

Volcanic Ash Particle Size—The size distribution of ash particles transported by the ASHPLUME code is generally much larger than the particle size used to calculate the inhalation BDCFs. The ASHPLUME model is appropriate for particles of mean diameter greater than 15 to 30 μm (Jarzemba et al. 1997 [DIRS 100987], p. 2-2). The dose coefficients for inhalation are for particles with activity median aerodynamic diameter of 1 μm (BSC 2005 [DIRS 172827], Section 6.5.3.1).

Effect on the TSPA-LA Model—An analysis was conducted in *Characteristics of the Receptor for the Biosphere Model* (BSC 2005 [DIRS 172827], Section 6.5.5.2) regarding the effects of the size distribution of ash particles transported by the ASHPLUME code being generally much larger than the particle size used to calculate the inhalation BDCFs. It was concluded from that analysis that the application of dose coefficients for particles with activity median aerodynamic diameter of 1 μm will not underestimate the doses from inhalation of resuspended material and that the dose coefficients are adequate for use in the biosphere model.

6.5.2.3.2 Identification of Conservatisms in Submodels and Abstractions

Radionuclide Waste Form Completely Destroyed—As described in *Atmospheric Dispersal and Deposition of Tephra from a Potential Volcanic Eruption at Yucca Mountain, Nevada*, (SNL 2007 [DIRS 177431], Section 5.1.2), WP failure and entrainment of fragmented waste within rising magma is assumed to occur due to the intersection of an eruptive conduit with WPs. In the TSPA-LA Model implementation, the WPs hit are assumed to be completely destroyed and all of the waste contained in the WPs is available to be erupted. This conservative assumption tends to maximize the release of radionuclides from the EBS.

6.5.2.4 Alternative Conceptual Model(s) for the Volcanic Eruption Modeling Case

Secondary Dike Propagation ACM—Woods et al. (2002 [DIRS 163662]) describe an eruptive ACM in which magma could potentially flow horizontally in a drift to a secondary vent opening at some point along the drift, sometimes referred to as the "dogleg" scenario. In this ACM, after an intersected dike fills with magma, the pressurization generates a new opening at some distance down the drift that becomes the main vent to the surface. This ACM could potentially affect a larger number of waste packages than is considered in the Volcanic Eruption Modeling Case in which the eruptive conduit propagates vertically through a drift. However, modeling of magma flow in drifts described in *Dike/Drift Interactions* (SNL 2007 [DIRS 177430], Sections 6.3.3.5.6, 6.5, and 8.1.3), indicates that this secondary breakout condition is not expected to occur because of heat loss and stoppage due to solidification of the magma in the secondary fracture. Based on the results of this analysis (SNL 2007 [DIRS 177430]), the Secondary Dike Propagation ACM was not included in the Volcanic Eruption Modeling Case in the TSPA-LA Model.

Volcanic Eruption Phase Dose ACM—This subsection describes an ACM for the volcanic eruption phase dose received by a receptor that does not leave the region during a volcanic eruption. The result of this calculation, showing that the mean eruption phase dose is insignificant compared to the mean post eruption phase dose, is used as the basis for excluding

this ACM from the Volcanic Eruption Modeling Case in the TSPA-LA Model. Because a high concentration of airborne radioactive particulates is expected during this phase, inhalation of airborne-contaminated ash particles is the only pathway considered, as described in *Biosphere Model Report* (SNL 2007 [DIRS 177399], Section 6.15.2). The receptor has the same inhalation characteristics as those for the RMEI discussed in Section 6.3.11.

The eruption phase of a volcanic event refers to the conditions that exist during the volcanic eruption before the deposition of volcanic ash on the ground is completed. The dose factors for determining inhalation dose during a volcanic eruption are different from the BDCFs used for the time period after the deposition of volcanic ash on the ground. These dose factors are provided for use in the TSPA-LA Model in DTN: MO0702PAINHALA.001_R0 [DIRS 179329]. To calculate the daily dose from inhaling a specific radionuclide during a volcanic eruption, the activity concentration of that radionuclide in air is multiplied by the appropriate dose factor. The total inhalation dose from concentrations of primary radionuclides in air is then calculated as (SNL 2007 [DIRS 177399], Section 6.15.2.2, Equation 6.15-9):

$$D_{inh} = \sum_i D_{inh,i} = \sum_i DF_i \times Ca_i \qquad \text{(Eq. 6.5.2-2)}$$

where

D_{inh} = total inhalation dose rate for all radionuclides (Sv/day)

$D_{inh,\,i}$ = inhalation dose rate for a primary radionuclide i (Sv/day)

DF_i = dose factor for a primary radionuclide i (Sv/day per Bq/m^3)

Ca_i = activity concentration of a primary radionuclide i in air (Bq/m^3) (Equation 6.5.2-5).

The total inhalation dose during a volcanic eruption can then be calculated by multiplying the inhalation dose rate by the duration of the volcanic eruption:

$$D = D_{inh} \times t_{vol} \qquad \text{(Eq. 6.5.2-3)}$$

where

D = total inhalation dose during volcanic eruption (Sv)

t_{vol} = duration of volcanic eruption, or volcanic eruption time (day).

The activity concentration of a radionuclide in air, Ca_i, is proportional to the volcanic ash concentration in air, which can vary with time during the eruption phase. To estimate the activity concentration in air, it is assumed that the ratio of waste to ash in volcanic ash does not change between the time it was in the air and the time it was deposited on the ground:

$$Ca_{waste\_air} = Ca_{ash\_air} \times \frac{C_{waste\_dep}}{C_{ash\_dep}} \qquad \text{(Eq. 6.5.2-4)}$$

where

Ca_{waste_air} = mass concentration of waste in air (g/m^3)

Ca_{ash_air} = mass concentration of volcanic ash in air (g/m^3) (Equation 6.5.2-7)

C_{waste_dep} = mass concentration of waste deposited on the ground (g/m^2)

C_{ash_dep} = mass concentration of volcanic ash deposited on the ground (g/m^2).

Both mass concentrations of waste and volcanic ash deposited at the location of the RMEI on the ground can be obtained from the results of the TSPA-LA Model for the Igneous Scenario Class. By using the mass concentration of waste in air, activity concentrations of individual radionuclides can be calculated as:

$$Ca_i = Ca_{waste\_air} \times f_i \times SA_i \quad \text{(Eq. 6.5.2-5)}$$

where

f_i = fraction of an individual radionuclide, i, among the total waste mass, dimensionless (Equation 6.5.2-6)

SA_i = specific activity for the individual radionuclide, i, (pCi/g).

The fraction of an individual radionuclide should be weighted by the number of CSNF and CDSP WPs hit, as follows:

$$f_i = \frac{N_{CSNF} \times m_{CSNF,i} + N_{CDSP} \times (m_{HLW,i} + m_{DSNF,i})}{\sum_i [N_{CSNF} \times m_{CSNF,i} + N_{CDSP} \times (m_{HLW,i} + m_{DSNF,i})]} \quad \text{(Eq. 6.5.2-6)}$$

where

N_{CSNF} = number of CSNF WPs hit by volcanic eruption

N_{CDSP} = number of CDSP WPs hit by volcanic eruption

$m_{CSNF,\,i}$ = mass of radionuclide, i, per CSNF WP (g)

$m_{HLW,\,i}$ = mass of radionuclide, i, for HLW per CDSP WP (g)

$m_{DSNF,\,i}$ = mass of radionuclide, i, for DSNF per CDSP WP (g).

As mentioned before, the mass concentration of volcanic ash may vary with time during the eruption phase. However, the average mass concentration of volcanic ash in air, Ca_{ash_air}, can be calculated using the amount of ash deposited on the ground, ash settling velocity, and volcanic eruption time:

$$Ca_{ash\_air} = \frac{C_{ash\_dep}}{0.01 \times V_0 \times 86{,}400 \times t_{vol}} \quad \text{(Eq. 6.5.2-7)}$$

where

V_0 = settling velocity for volcanic ash (cm/sec) (Equation 6.5.2-8)

t_{vol} = eruption duration (days)

0.01 = unit conversion (m/cm)

86,400 = unit conversion (sec/day).

The settling velocity of volcanic ash can be calculated, and its equation and inputs are given in *Atmospheric Dispersal and Deposition of Tephra from a Potential Volcanic Eruption at Yucca Mountain, Nevada,* (SNL 2007 [DIRS 177431], Section 6.5.1 Equation 6-4 and Table 8-2):

$$V_0 = \frac{\psi_p g d^2}{9\eta_a F^{-0.32} + \sqrt{81\eta_a^2 F^{-0.64} + \frac{3}{2}\psi_p \psi_a g d^3 \sqrt{1.07 - F}}} \quad \text{(Eq. 6.5.2-8)}$$

where

Ψ_a = density of air (0.001734 g/cm^3 used in TSPA-LA Model)

Ψ_p = density of particles, dependent on particle size (g/cm^3) (Equation 6.5.2-9)

g = gravitational acceleration constant (980 cm/s^2)

η_a = viscosity of air (0.000185 g/cm-s used in TSPA-LA Model)

F = shape factor for particles (0.5 used in TSPA-LA Model)

d = mean particle diameter (cm).

The particle density, Ψ_p, depends on the particle size, and larger particles are less dense because of the incorporation of more gas bubbles. Particle density is a function of the particle log-diameter, ρ_a in cm, as follows (SNL 2007 [DIRS 177431], Section 6.5.1, Equation 6-5):

$$\begin{aligned} &\Psi_p = \Psi_p^{high} && \text{for } \rho_a < \rho_a^{low} \\ &\Psi_p = \Psi_p^{low} + (\Psi_p^{high} - \Psi_p^{low})(\rho_a^{high} - \rho_a)/(\rho_a^{high} - \rho_a^{low}) && \text{for } \rho_a^{low} < \rho_a < \rho_a^{high} \\ &\Psi_p = \Psi_p^{low} && \text{for } \rho_a > \rho_a^{high} \end{aligned} \quad \text{(Eq. 6.5.2-9)}$$

where

Ψ_p^{high} = ash particle density at minimum particle size (2.08 g/cm^3 used in TSPA-LA Model)

Ψ_p^{low} = ash particle density at maximum particle size (1.04 g/cm^3 used in TSPA Model)

ρ_a^{low} = log ash particle size in cm at maximum ash density (-3 used in TSPA-LA Model)

ρ_a^{high} = log ash particle size in cm at minimum ash density (0 used in TSPA-LA Model)

ρ_a = log(d), log particle diameter in cm.

The mass of radionuclides in CSNF, DSNF, and HLW ($m_{CSNF,\,i}$, $m_{DSNF,\,i}$ and $m_{DSNF,\,i}$), changes with time due to decay and ingrowth in the radioactive waste. This causes the annual dose during the eruption phase to decrease with time if a volcano occurs at a later time, T. Because some parameters that define an eruptive event are uncertain as shown in Table 6.5-4, the calculation of Equations 6.5.2-2 to 6.5.2-9 was carried out using the GoldSim software. The input values for these equations were taken directly from the Volcanic Eruption Modeling Case of the Igneous Scenario Class in the TSPA-LA Model. The mean annual dose for eruptions that occur at times $T = \tau$ due to M realizations of the volcanic eruption phase parameters are calculated with GoldSim as

$$\overline{\overline{D}}(\tau) \cong \frac{pE}{M} \sum_{j=1}^{M} D(\tau, \mathbf{a}_j, \mathbf{e}_j)\, \lambda_{I,j} \qquad \text{Eq. 6.5.2-10}$$

where

$\overline{\overline{D}}(\tau)$ = mean total annual eruption phase inhalation dose at time τ due to volcanic eruptions that occur at times $T = \tau$ (Sv/yr)

$D(\tau,\mathbf{a}_j,\mathbf{e}_j)$ = total annual eruption phase inhalation dose (Eq. 6.5.2-3) for eruptions that occur at times $T = \tau$ and with aleatory parameters $\mathbf{a}_j$ and epistemic parameters $\mathbf{e}_j$ (Table 6.5-4) (Sv)

$\lambda_{I,j}$ = annual frequency of intersection of the repository by a volcanic dike (1/yr)

pE = probability of one or more eruptive centers intersecting the repository given the intersection of a dike (0.28).

The detailed calculations and the output of eruption phase dose are in output DTN: MO0708TSPAGENT.000 [DIRS 183000]. The calculation results of 1,000 realizations of Equation 6.5.2-10 using the GoldSim software are shown on Figure 6.5-14, which includes a comparison between the mean annual doses to the RMEI during the volcanic eruptive phase and post-eruption processes (Volcanic Eruption Modeling Case, Equation 6.5.2-1). The mean annual dose from the volcanic eruption phase is small compared to the mean annual dose caused by volcanic ash deposited on the ground calculated in the TSPA-LA Model. Because of its relative insignificance to the annual dose, the contribution from this eruptive phase dose ACM is not included in the TSPA-LA Model.

Table 6.5-1. Waste Form Temperatures Inside Intrusive Body

Time Since Igneous Event	For an Intrusion into a Repository at 25°C		For an Intrusion into a Repository at 50°C		For an Intrusion into a Repository at 100°C		For an Intrusion into a Repository at 150°C		For an Intrusion into a Repository at 200°C	
Years	WP	Drift Wall	WP	Drift Wall	WP	Drift Wall	WP	Drift Wall	WP	Drift Wall
0	1,150	1,150	1,150	1,150	1,150	1,150	1,150	1,150	1,150	1,150
0.1	977	592	1,006	620	1,012	644	1,019	668	1,026	692
0.2	702	462	749	494	768	524	786	553	804	583
0.3	530	382	577	416	603	449	629	483	655	516
0.4	422	326	467	360	498	396	529	432	560	468
0.5	351	284	394	318	428	356	462	394	497	431
0.6	301	252	341	286	378	325	415	364	452	403
0.7	264	226	303	260	341	300	380	341	418	381
0.8	236	206	273	239	313	281	353	322	392	363
0.9	213	189	249	222	290	264	331	306	372	349
1	195	175	230	208	272	251	314	293	356	336
2	111	106	142	136	187	182	233	228	279	274
3	82.8	80.4	111	109	158	156	206	203	253	251
4	68.4	67.0	96.0	94.5	144	142	192	190	240	238
5	59.7	58.9	86.8	85.8	135	134	183	183	232	231
6	54.0	53.4	80.7	80.0	129	129	178	177	227	226
7	49.8	49.4	76.3	75.8	125	125	174	173	223	222
8	46.7	46.4	73.0	72.6	122	122	171	171	220	220
9	44.3	44.0	70.5	70.2	120	119	169	168	218	217
10	42.4	42.2	68.4	68.2	118	117	167	167	216	216
20	33.7	33.6	59.2	59.2	109	109	158	158	208	208
30	30.8	30.8	56.1	56.1	106	106	156	156	205	205
40	29.3	29.3	54.6	54.6	104	104	154	154	204	204
50	28.5	28.5	53.7	53.7	104	104	153	153	203	203
60	27.9	27.9	53.1	53.1	103	103	153	153	203	203
70	27.5	27.5	52.6	52.6	103	103	152	152	202	202
80	27.2	27.2	52.3	52.3	102	102	152	152	202	202
90	26.9	26.9	52.0	52.0	102	102	152	153	202	202
100	26.7	26.7	51.8	51.8	102	102	152	152	202	202

Sources: DTN: LA0702PADE01EG.001_R0 [DIRS 179495].
Modified from Table 6-13 in *Dike/Drift Interactions* (SNL 2007 [DIRS 177430], Section 6.4.6).

Table 6.5-2. Annual Frequencies of Intersection of Repository by a Dike for the License Application Footprint

Hazard Level (%)	Annual Frequency of Intersection of Repository by a Dike
Mean	1.69×10^{-8}
5	7.41×10^{-10}
10	1.48×10^{-9}
15	2.29×10^{-9}
20	3.02×10^{-9}
30	4.57×10^{-9}
40	6.92×10^{-9}
50	1.00×10^{-8}
60	1.45×10^{-8}
70	2.04×10^{-8}
80	2.69×10^{-8}
85	3.31×10^{-8}
90	4.07×10^{-8}
95	5.50×10^{-8}

Sources: DTN: LA0307BY831811.001_R0 [DIRS 164713].
Composite frequency results from full enumeration of the expert elicitation, excerpted from Table 6-8 in *Characterize Framework for Igneous Activity at Yucca Mountain, Nevada* (BSC 2004 [DIRS 169989], Section 6.5.3.1).

Table 6.5-3. Cumulative Distribution Function for the Number of Waste Packages Hit by Conduits

Number of WPs Hit	CDF Value
0	0.703
1	0.710
2	0.748
3	0.806
4	0.942
5	0.981
6	0.994
7	1.000

Source: DTN: SN0701PAWPHIT1.001_R2 [DIRS 182961].

Table 6.5-4. Key Parameters for the ASHPLUME Code

TSPA-LA Model Parameter Name	Description	Distribution Type	Uncertainty Type	Value(s)
C	Constant relating eddy diffusivity and particle fall time ($cm^2/s^{5/2}$)	Point value	Fixed value	400
Erupt_Power_a	Eruptive power (W)	Log uniform	Aleatory	Min = 1.0×10^9 Max = 1.0×10^{12}
Beta_Dist_a	Column diffusion constant	Uniform	Epistemic	Min = 0.01 Max = 0.5
Erupt_Velocity_a	Initial rise velocity (cm/s)	Uniform	Aleatory	Min = 1 Max = 1.0×10^4
AirDen	Density of air (g/cm^3)	Point value	Fixed value	0.001734
AirVis	Viscosity of air (g/cm-s)	Point value	Fixed value	0.000185
Fshape	Ash particle shape factor	Point value	Fixed value	0.5
Dash_Mean_a	Mean ash particle diameter (cm)	Log triangular	Epistemic	Min = 0.001 Mode = 0.01 Max = 0.1
Dash_sigma_a	Ash particle diameter standard deviation (log cm)	Uniform	Epistemic	Min = 0.301 Max = 0.903
Dmax_trans	Maximum particle diameter for transport (cm)	Point value	Fixed value	10
AshDen_maxD	Ash particle density at minimum particle size (g/cm^3)	Point value	Fixed value	2.08
AshDen_MinD	Ash particle density at maximum particle size (g/cm^3)	Point value	Fixed value	1.04
LogD_minDen	Log ash particle size at minimum ash density (log(cm))	Point value	Fixed value	0
LogD_maxDen	Log ash particle size at maximum ash density (log(cm))	Point value	Fixed value	–3
D_min	Minimum waste particle diameter (cm)	Point value	Fixed value	0.0001
D_mode	Mode of waste particle diameter (cm)	Point value	Fixed value	0.0013
D_max	Maximum waste particle diameter (cm)	Point value	Fixed value	0.2

Table 6.5-4. Key Parameters for the ASHPLUME Code (Continued)

TSPA-LA Model Parameter Name	Description	Distribution Type	Uncertainty Type	Value(s)
Rhocut	Waste incorporation ratio	Point value	Fixed value	0.0
Erupt_Time_a	Eruption duration (seconds)	Log uniform	Aleatory	DTN: LA0702PADE03GK.002_R1 [DIRS 179980]
Wind_Direction	Wind direction (degrees)	Empirical	Aleatory	DTN: MO0408SPADRWSD.002_R0 [DIRS 171751]
Wind_Speed	Wind speed (cm/s)	Empirical	Aleatory	DTN: MO0408SPADRWSD.002_R0 [DIRS 171751]
A_cutoff	Threshold limit on ash accumulation (g/cm^2)	Point value	Fixed value	1×10^{-10}
Magma_Partitioning_a	Fractional multiplier on waste mass to account for waste-containing magma erupted in scoria cone and lava flows	Uniform	Aleatory	Min = 0.1 Max = 0.5

Source: DTN: LA0702PADE03GK.002_R1 [DIRS 179980].

Table 6.5-5. Key Input Parameters to the Tephra Redistribution Submodel

TSPA Parameter Name	Parameter Description	Distribution type	Uncertainty Type	Value (s)
Critical_Slope_a	Critical gradient for tephra mobilization from hillslopes	Uniform	Epistemic	0.21 – 0.47
Drainage_Density_a	Average drainage density for the Fortymile Wash drainage basin	Uniform	Epistemic	20 – 33 km^{-1}
Scour_Depth_a	Scour depth in Fortymile Wash at the fan apex	Uniform	Epistemic	73 – 122 cm
RMEI_Area	Area of the Fortymile Wash fan	Constant	fixed value	33 km^2
Fraction_Channel_a	Fraction, *F*, of the Fortymile Wash fan subject to fluvial activity	Uniform	Epistemic	0.09 – 0.54
L_Channels_a	Depth of permeable soil on channels, L_c, of the Fortymile Wash fan (RMEI location)	Constant	fixed value	200 cm
L_Divides_a	Depth of permeable soil on divides, L_d. of the Fortymile Wash fan (RMEI location)	Uniform	Epistemic	102 – 140 cm
D_Channels_a	Diffusivity of waste in channels, D_c, of the Fortymile Wash fan (RMEI location)	Uniform	Epistemic	0.035 – 0.266 cm^2/yr
D_Divides_a	Diffusivity of waste in divides, D_d, of the Fortymile Wash fan (RMEI location)	Uniform	Epistemic	0.001 – 0.095 cm^2/yr
Ash_Density_a	Tephra settled density	Truncated normal	Epistemic	300 – 1,500 kg/m^3 mean = 1,000 kg/m^3 std. dev. = 100 kg/m^3
b_Tillage	Tillage depth	Uniform	Epistemic	0.05 – 0.30 m

Source: DTNs: MO0702PAFARDAT.001_R3 [DIRS 182578];
LA0612DK831811.001_R1 [DIRS 179987] (Tephra density);
MO0702PAVBPDCF.000_R0 [DIRS 179330] (Tillage depth);
MO0704PASCOURD.000_R1 [DIRS 182149] (Scour depth).

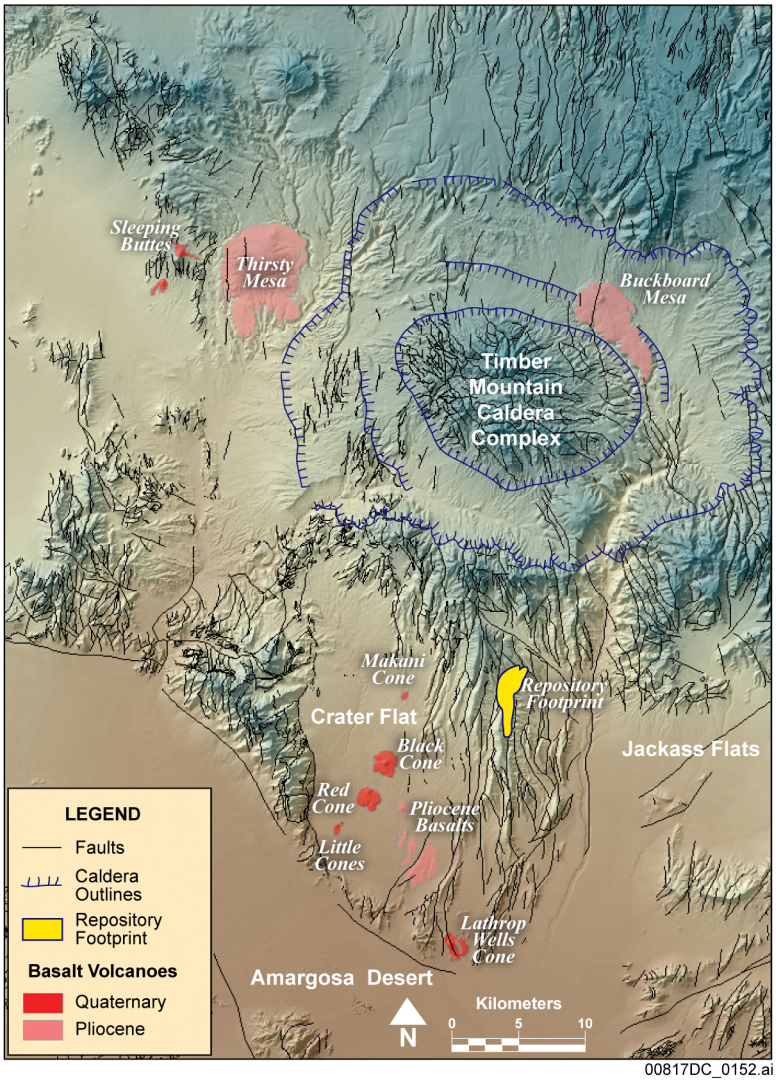

Source: Modified from CRWMS M&O 1998 [DIRS 123196], Figure 2.1.

NOTE: Only volcanoes exposed on the surface are shown.

Figure 6.5-1. Location and Age of Post-Miocene (less than 5.3 million years) Volcanoes (or clusters where multiple volcanoes have indistinguishable ages) in the Yucca Mountain Region

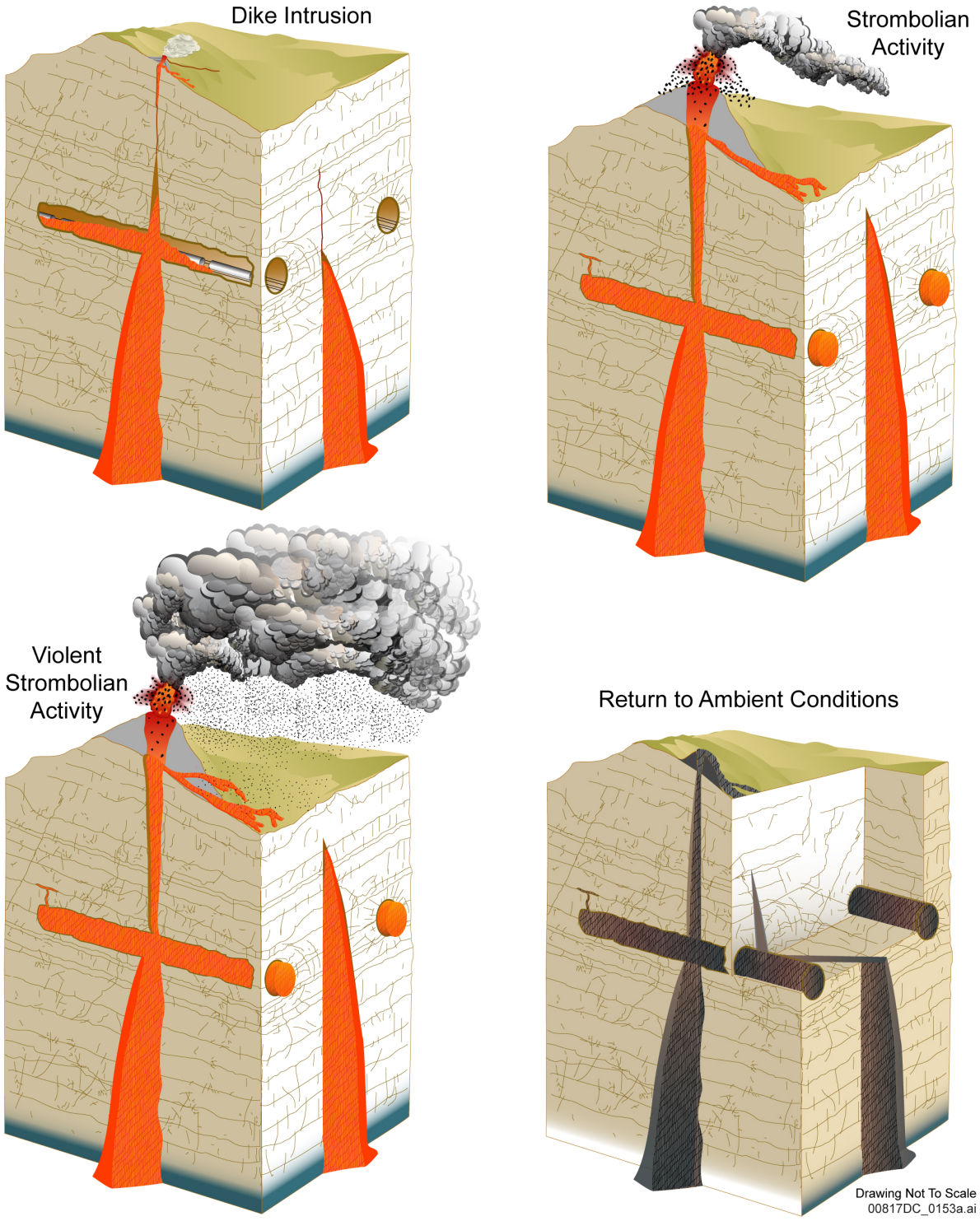

Source: Modified from SNL 2007 [DIRS 177430], Figure 1-1.

Figure 6.5-2. Schematic Drawing of the Processes Associated with a Dike Intrusion or Eruption through the Repository

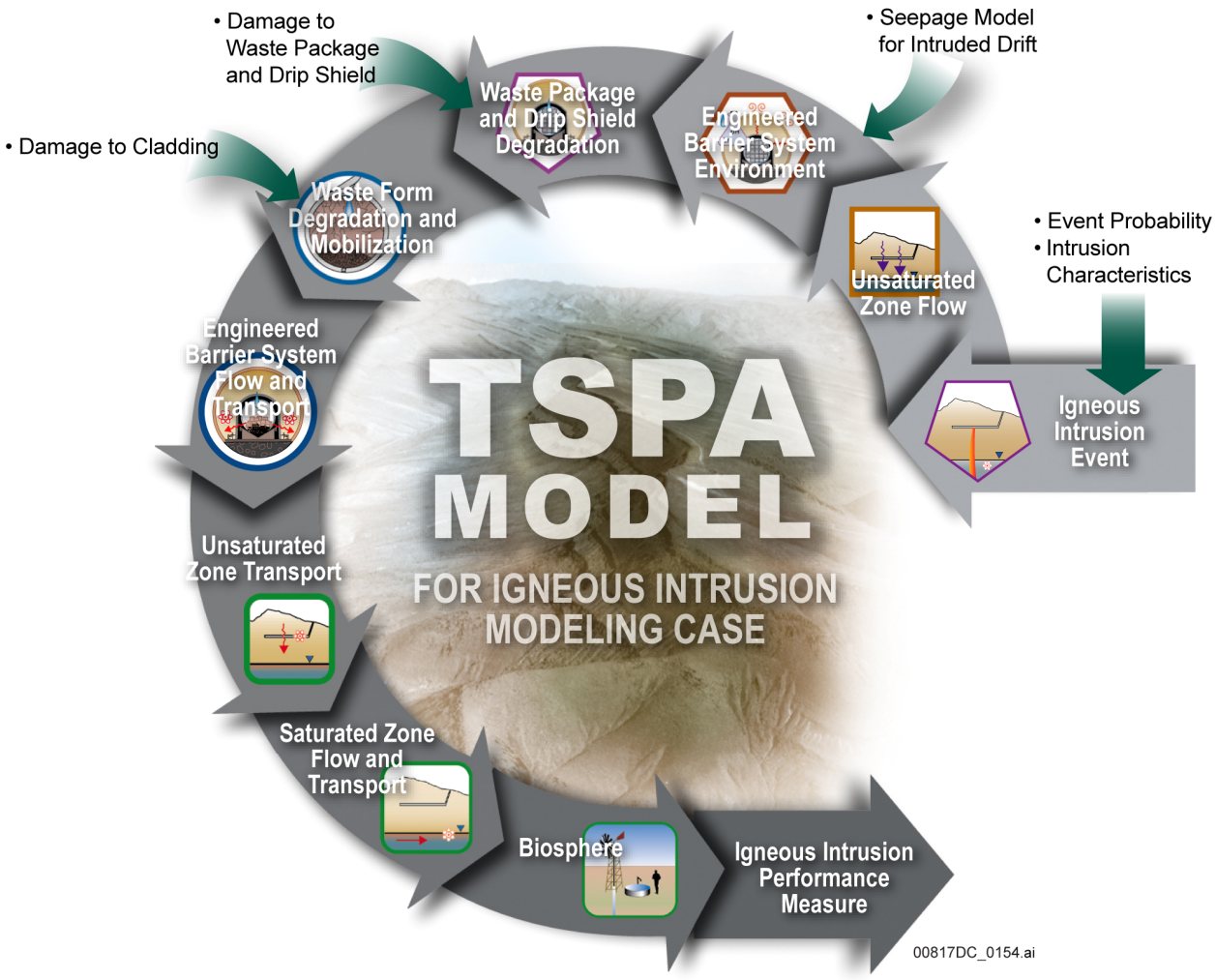

Figure 6.5-3. TSPA-LA Model Components for the Igneous Intrusion Modeling Case

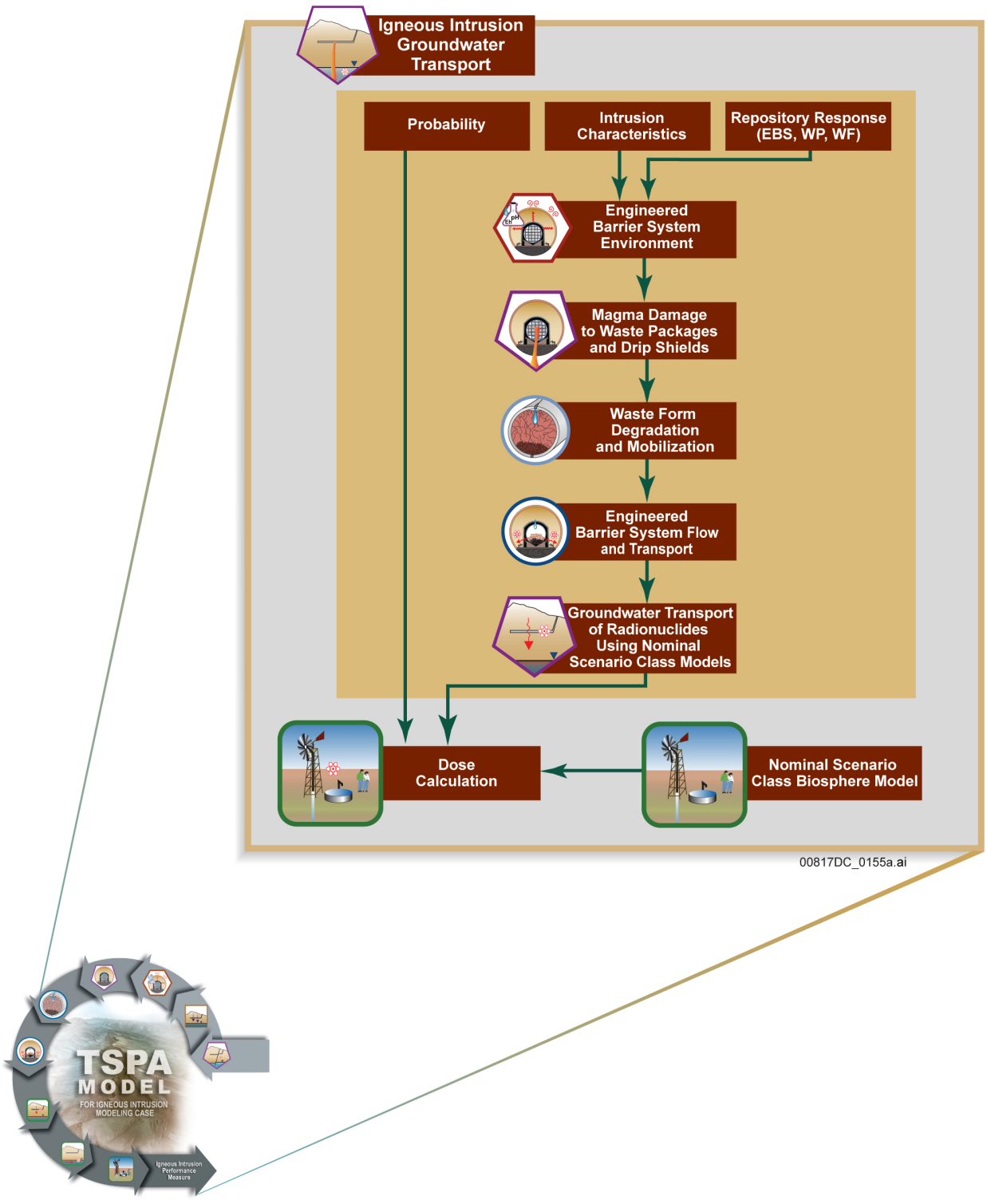

Figure 6.5-4. Information Flow Diagram for the TSPA-LA Igneous Intrusion Modeling Case

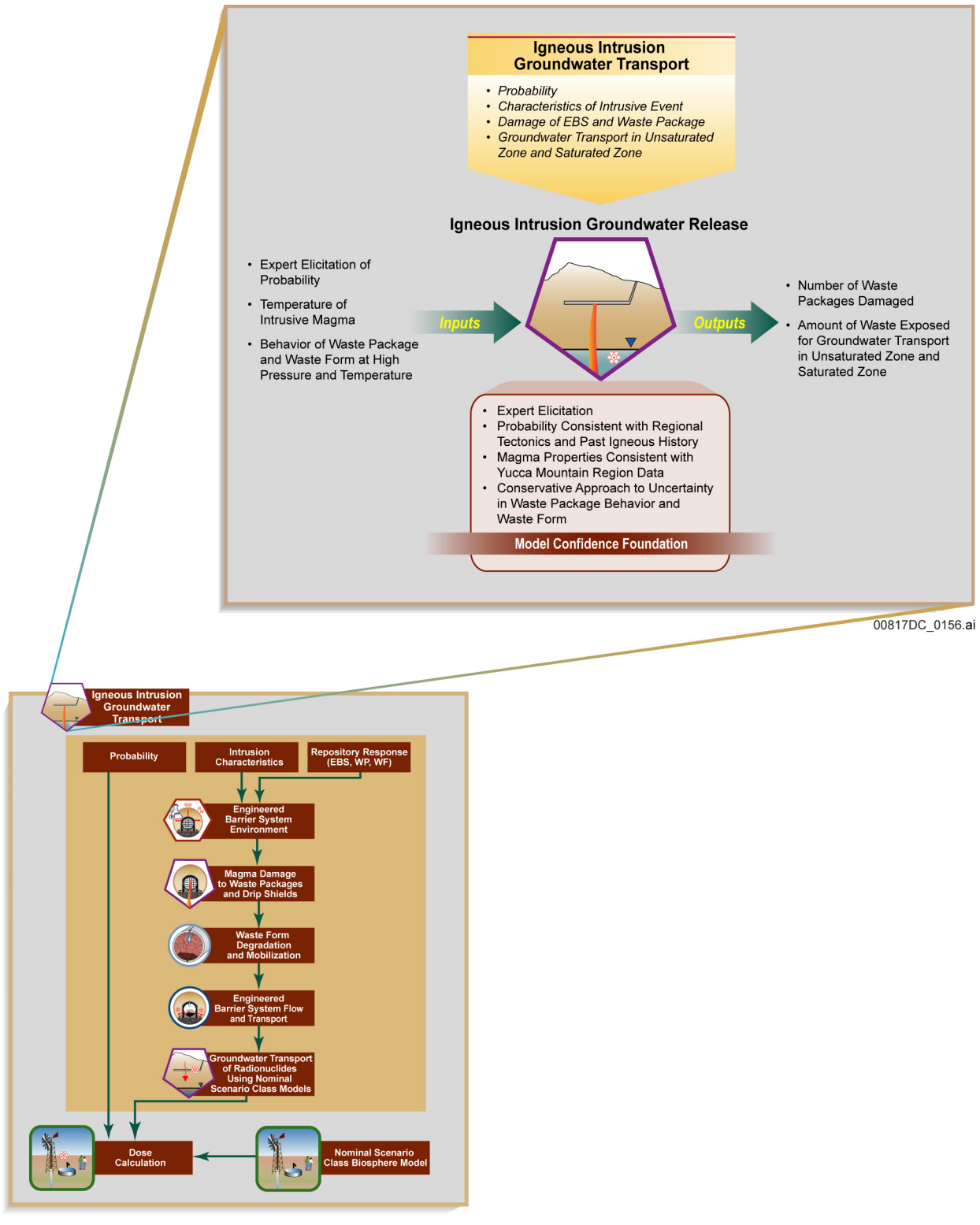

Figure 6.5-5. Inputs, Outputs, and Basis for Model Confidence for the TSPA-LA Igneous Intrusion Modeling Case

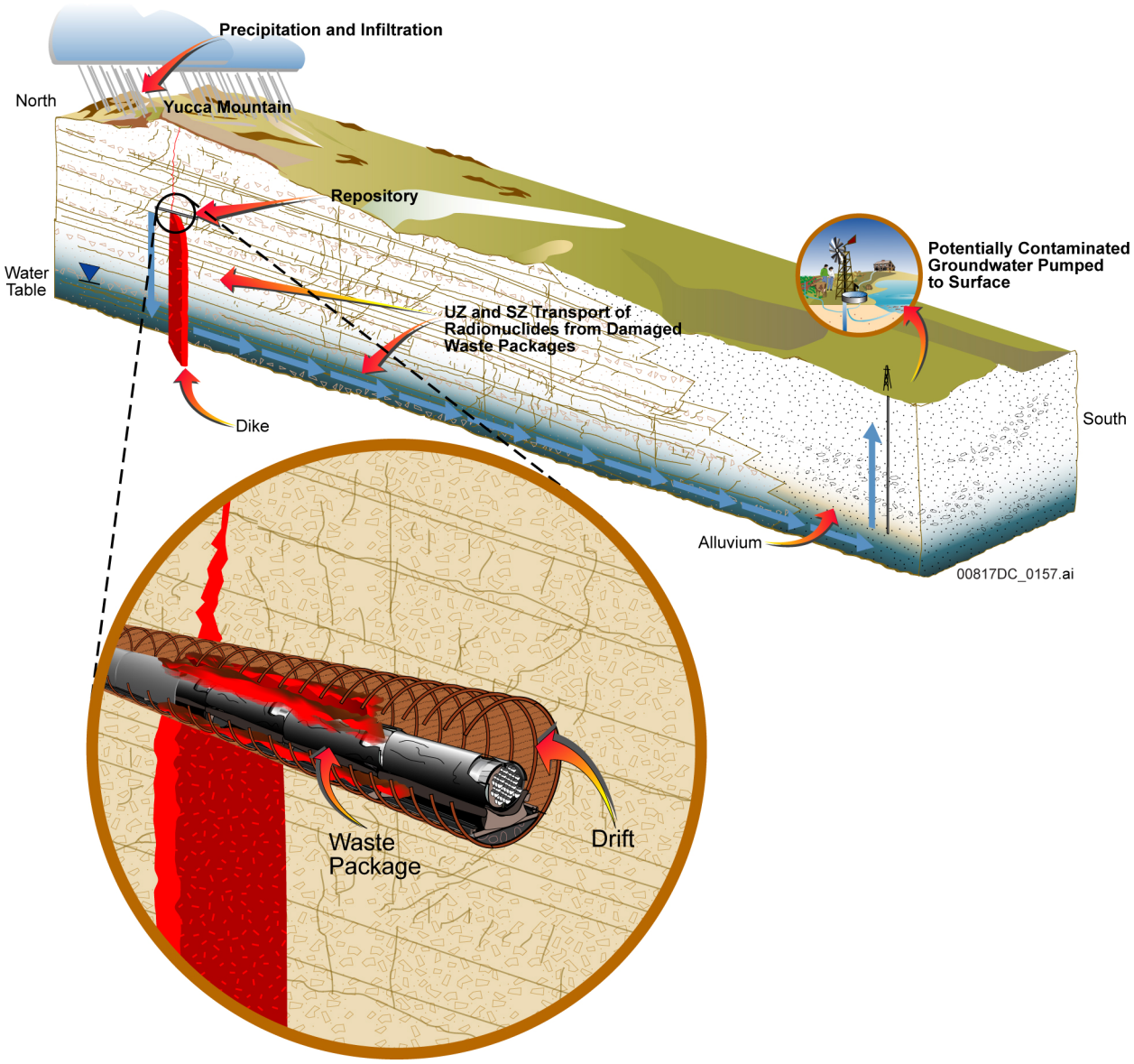

Figure 6.5-6. Schematic Diagram of the Intersection of an Igneous Dike with the Repository and Waste Packages

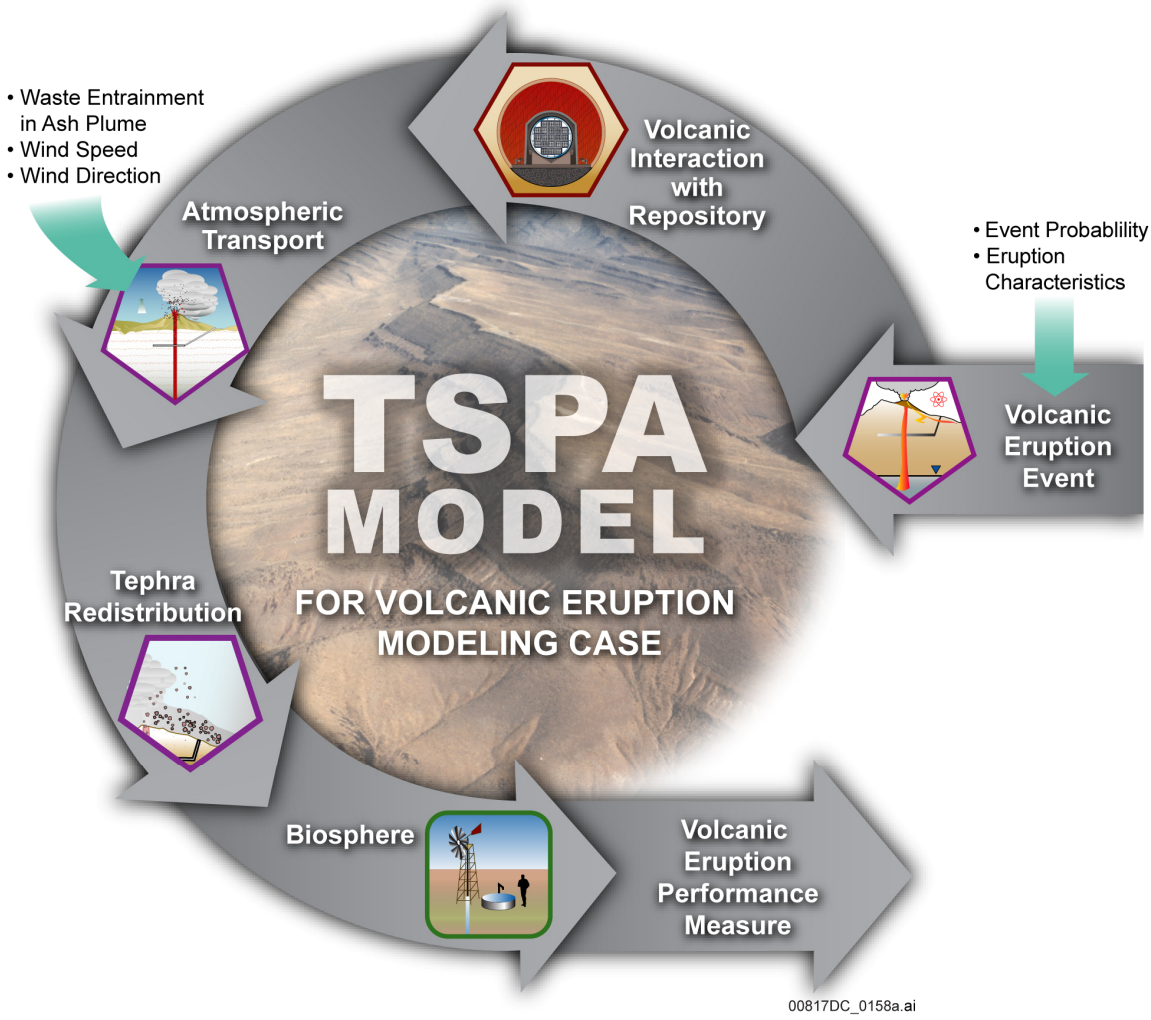

Figure 6.5-7. TSPA-LA Model Components for the Volcanic Eruption Modeling Case

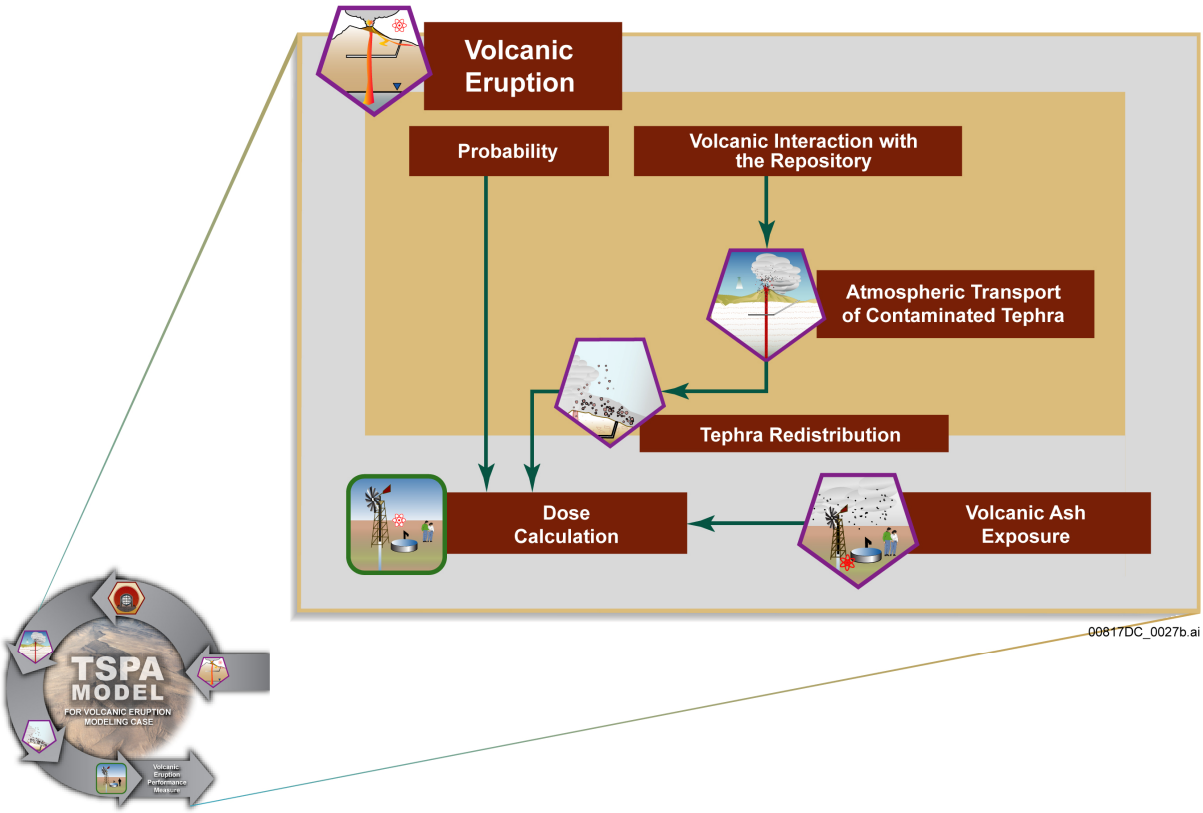

Figure 6.5-8. Information Flow Diagram for the TSPA-LA Volcanic Eruption Modeling Case

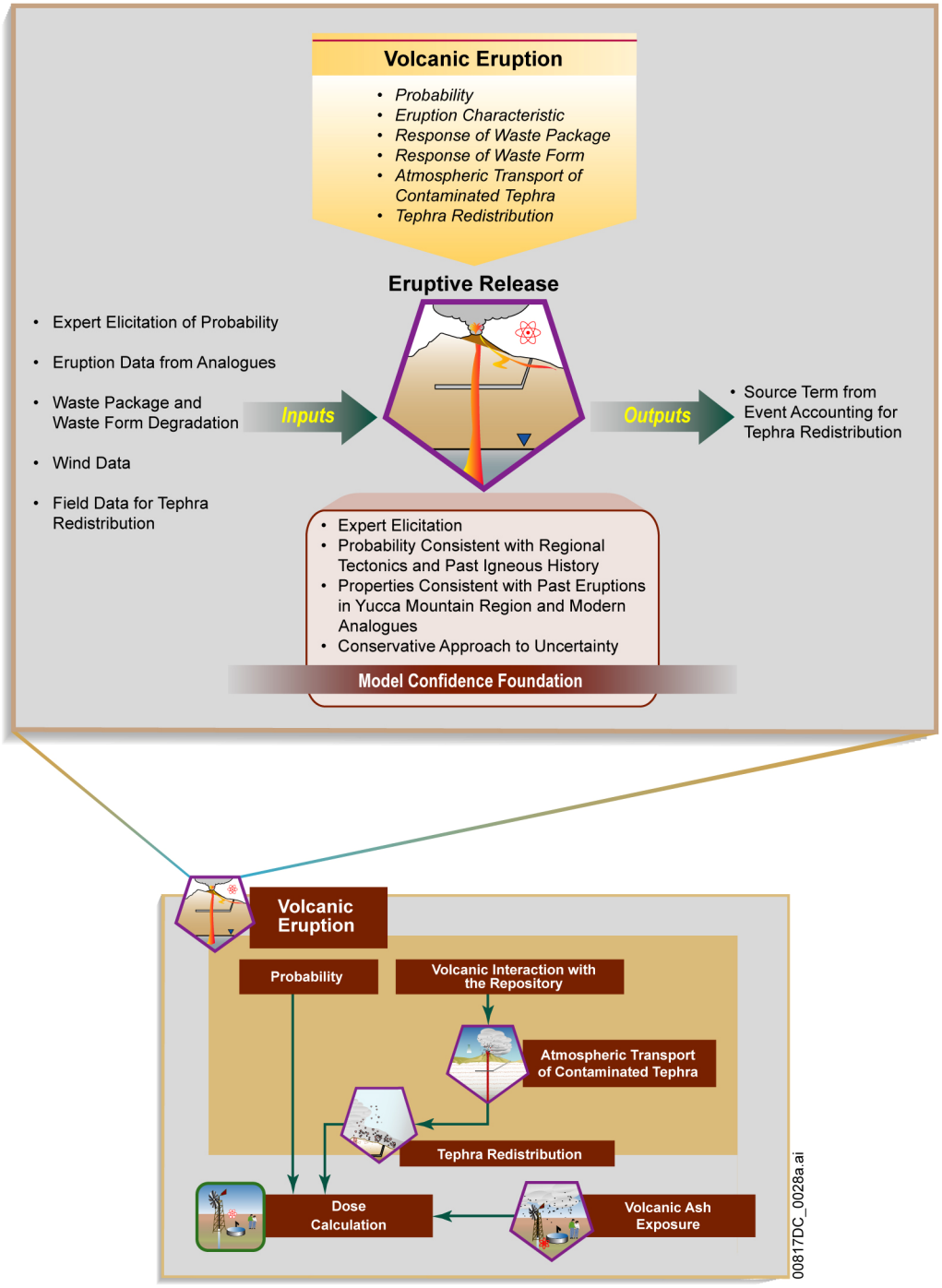

Figure 6.5-9. Inputs, Outputs, and Basis for Model Confidence for the TSPA-LA Volcanic Eruption Modeling Case

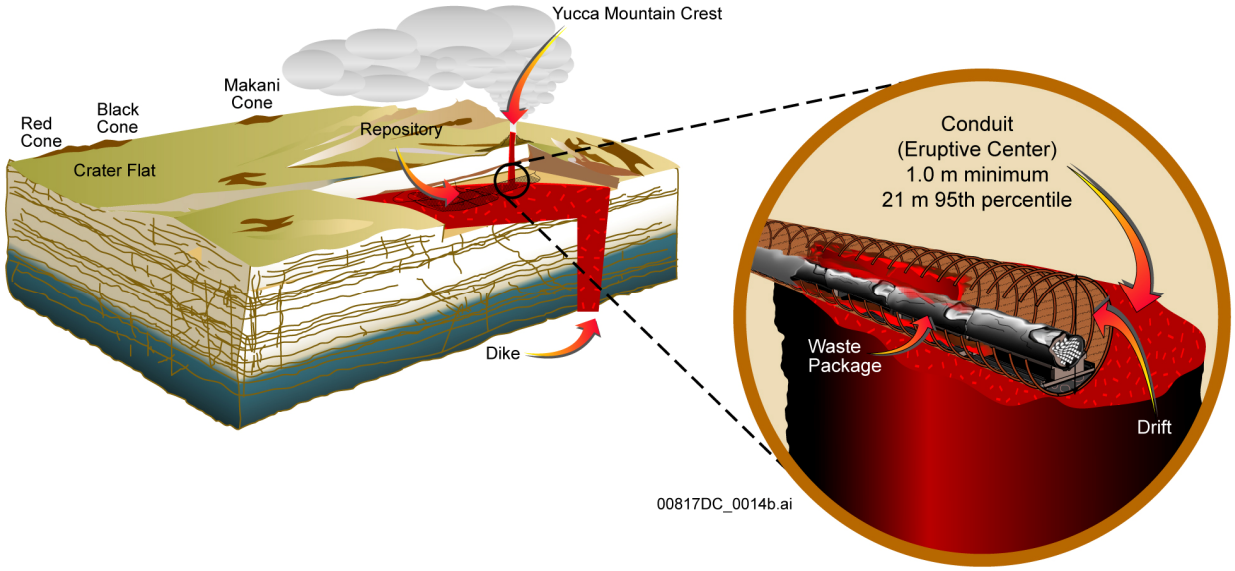

Figure 6.5-10. Schematic Diagram of the Intersection of an Igneous Dike and Eruptive Conduit with the Repository

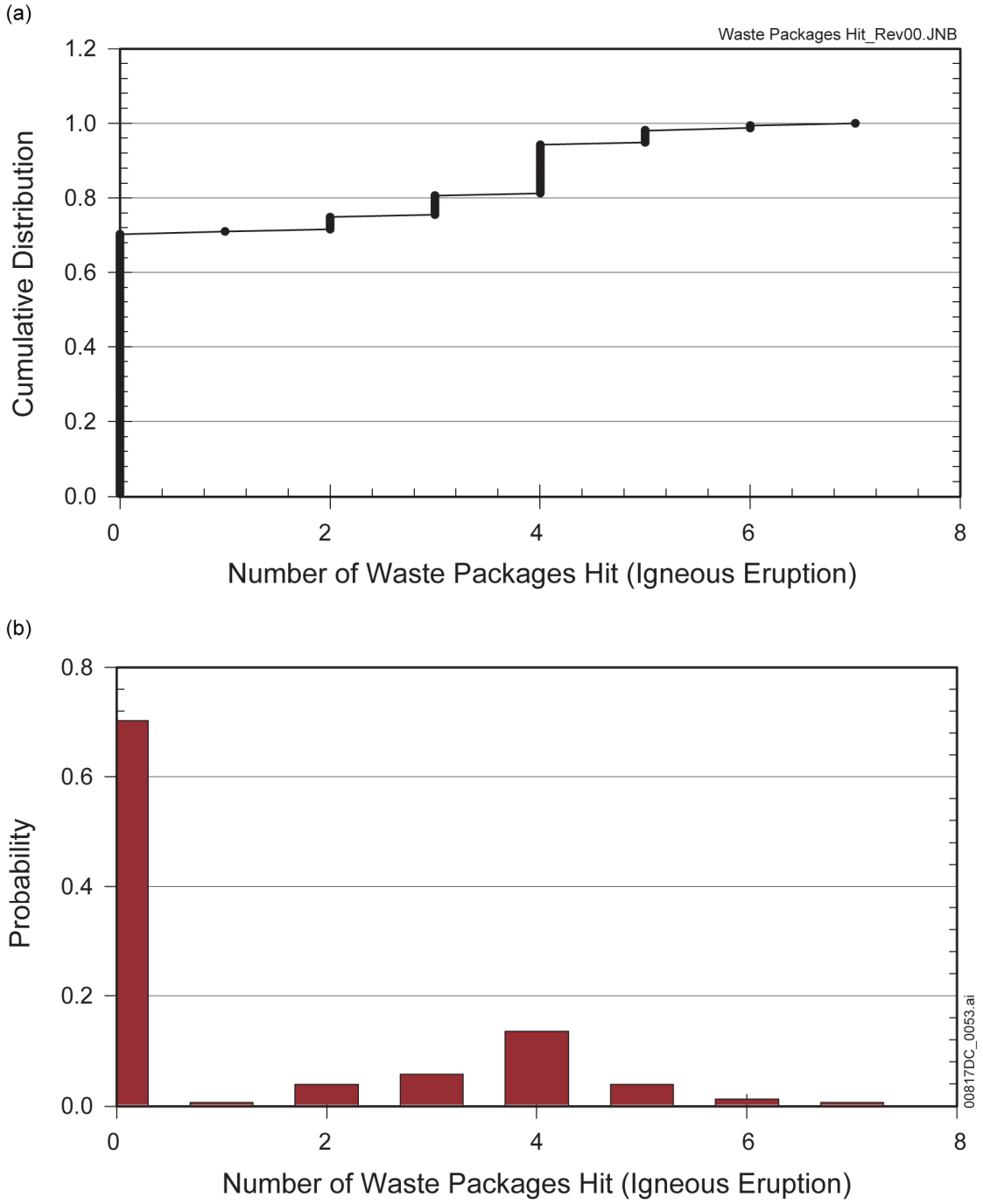

Source: DTN: SN0701PAWPHIT1.001_R2 [DIRS 182961].

Figure 6.5-11. Number of Waste Packages Hit by Conduits from a Volcanic Eruption

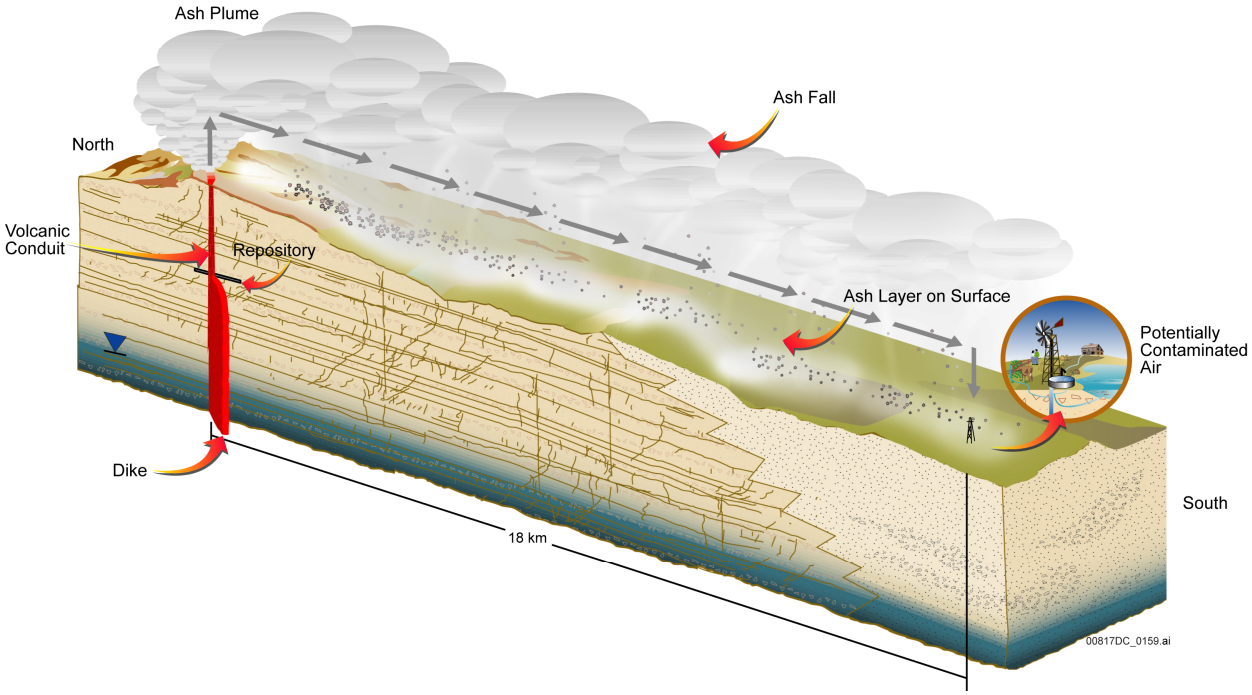

Figure 6.5-12. Schematic Representation of a Volcanic Eruption at Yucca Mountain, Showing Transport of Radioactive Waste in a Tephra Plume

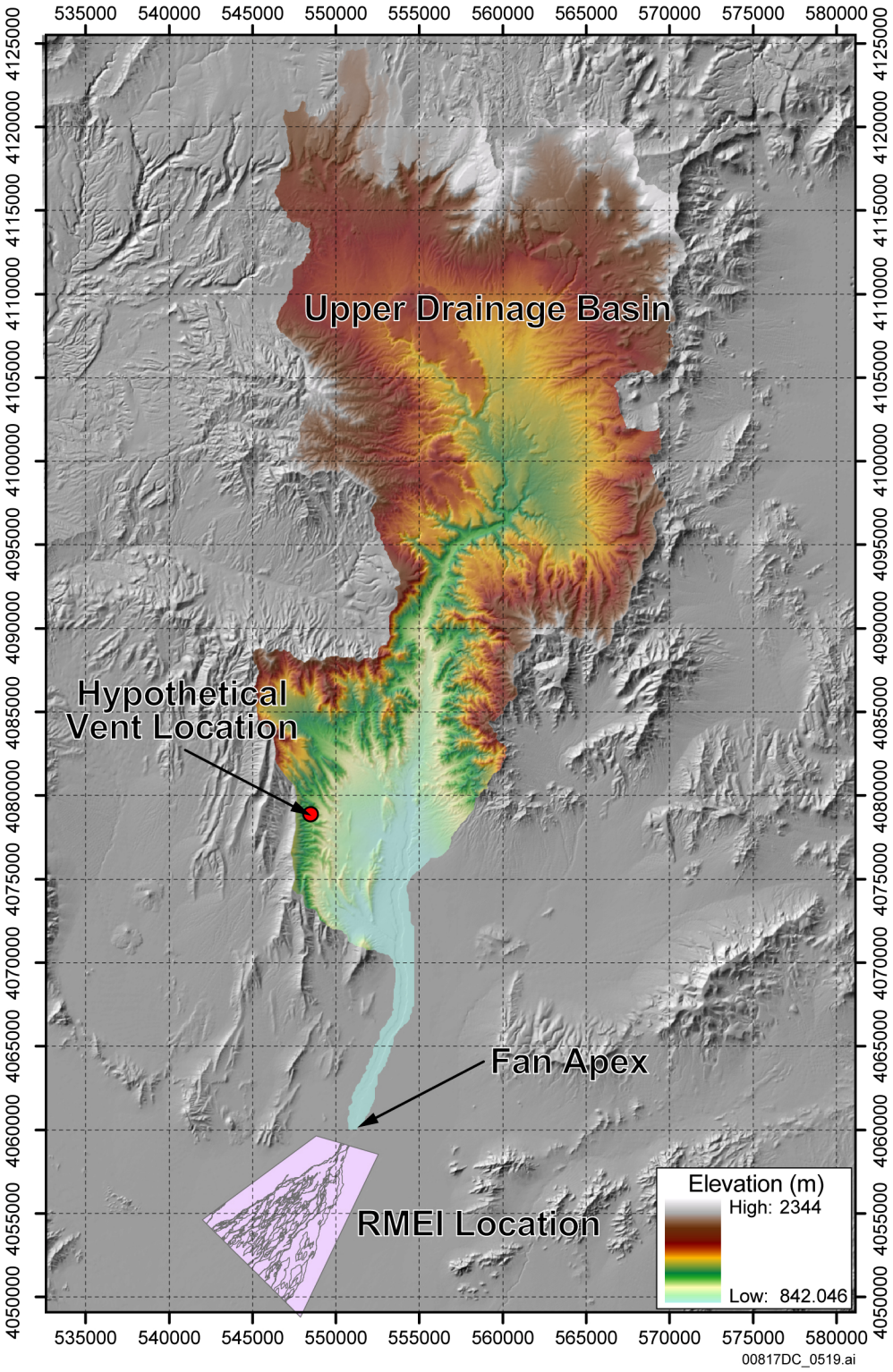

Source: SNL 2007 [DIRS 179347], Figure 1-2,

Figure 6.5-13. Schematic Diagram of Tephra Redistribution Model

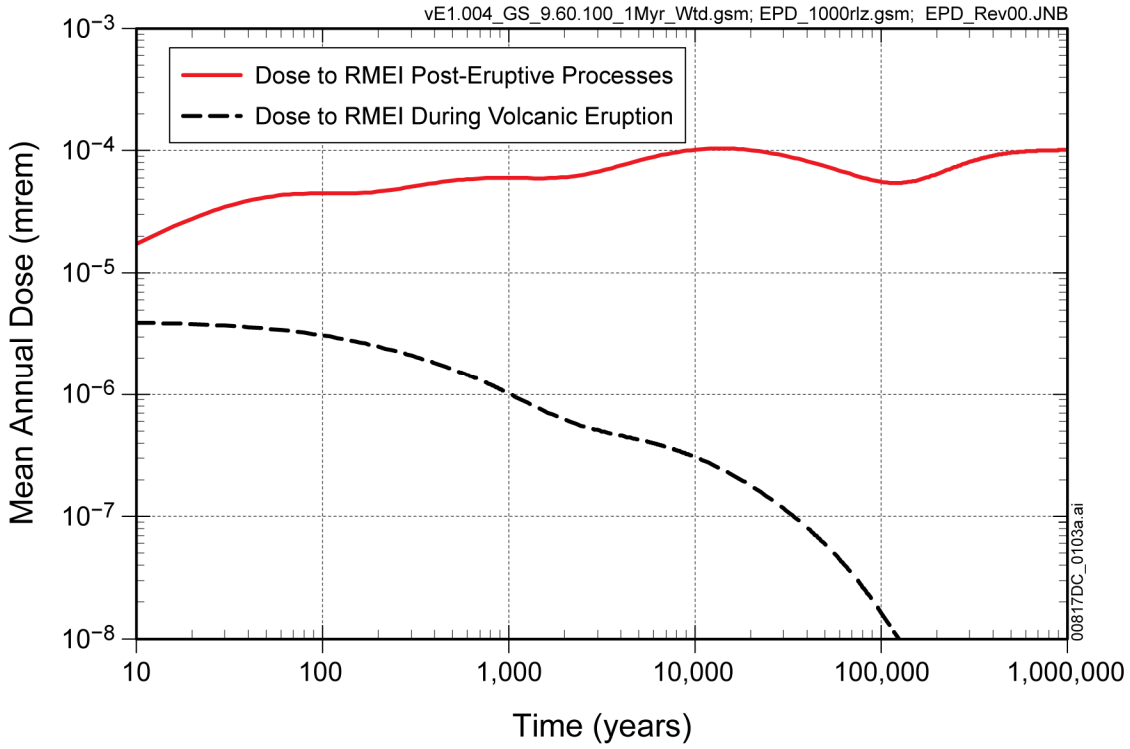

Source: Output DTN: MO0709TSPAREGS.000 [DIRS 182976].

Figure 6.5-14. Comparison of Dose to the RMEI for Post-Eruptive Processes and Dose to the RMEI During a Volcanic Eruption

6.6 TSPA-LA MODEL FOR THE SEISMIC SCENARIO CLASS

The Seismic Scenario Class describes future performance of the repository system in the event of seismic activity that could disrupt the repository system. The Seismic Scenario Class represents the direct effects of vibratory ground motion and fault displacement associated with seismic activity. Indirect effects of drift collapse and rockfall induced by vibratory ground motion are also considered in this scenario class. The Seismic Scenario Class considers the effects of the seismic hazards on DSs and WPs because damage to or failure of these components has the potential to initiate or increase releases of radionuclides by forming new diffusive or advective transport pathways. The Seismic Scenario Class also takes into account changes in seepage and drift wall condensation, WP and DS degradation, and in-drift thermal environment that might be associated with a seismic event. The conceptual models and abstractions for the mechanical response of EBS components to seismic hazards at a geologic repository are documented in *Seismic Consequence Abstraction* (SNL 2007 [DIRS 176828]). The structural response calculations and rockfall calculations that provide the basis for the seismic damage abstractions are documented in *Mechanical Assessment of Degraded Waste Packages and Drip Shields Subject to Vibratory Ground Motion* (SNL 2007 [DIRS 178851]).

The Seismic Scenario Class estimates the annual dose due to seismic activity by accounting for the probability of occurrence of activity, expressed in terms of its mean annual exceedance frequency (SNL 2007 [DIRS 176828], Section 6.1.7), and the associated consequences to EBS components. The estimate of annual dose takes into account the relevant processes that affect system performance. The Seismic Scenario Class is represented by two modeling cases. The first modeling case includes those WPs that fail solely due to the ground motion damage associated with the seismic event and it is denoted as the Seismic GM Modeling Case. Because nominal corrosion processes have the potential to alter the repository's susceptibility to damage during a seismic ground motion event, the Seismic GM Modeling Case includes these nominal processes when calculating consequences. The second modeling case includes only those WPs that fail due to fault displacement damage and it is denoted as the Seismic FD Modeling Case. Nominal corrosion processes are not included in the Seismic FD Modeling Case because the damage abstraction for fault displacement is based on a comparison of clearances between EBS components with fault displacements, independent of the thickness of EBS components. The mean annual dose calculated by the two modeling cases (Section 6.6.1.3.1) will be compared to the regulatory standard within 10,000 years after disposal, as required by the NRC Proposed Rule 10 CFR 63.303(a) [DIRS 178394], and the median annual dose will be compared to the regulatory standard for the period after 10,000 years of disposal and through the period of geologic stability, as required by the NRC Proposed Rule 10 CFR 63.303(b) [DIRS 178394]. The Individual Protection Standards for two periods are provided in 10 CFR 63.311 [DIRS 178394].

The two modeling cases in the Seismic Scenario Class have the same framework as the Nominal Scenario Class Modeling Case. This framework includes the TSPA-LA Model components that evaluate the mobilization and transport of radionuclides from the repository to the location of the RMEI. In other words, the mobilization of radionuclides in seeping water, the release of these radionuclides from the EBS, and the transport of these radionuclides through the UZ and SZ to the RMEI are based on the same model components for the Nominal Scenario Class as described in Section 6.3. The effects of the seismic event are taken into account in the changing

state of the EBS components, as required by the NRC proposed rule, 10 CFR 63.342(c)(1)(i) [DIRS 178394] and 10 CFR 63.102(j) [DIRS 180319], but not in the natural system components, which have been screened out by the FEPs screening process.

The calculational approach for the two Seismic Scenario Class modeling cases is discussed in Section 6.1.2.4.4.

Section 6.6 is organized as follows. Section 6.6.1 summarizes the model components and submodels of the Seismic Scenario Class. Sections 6.6.1.1 through 6.6.1.3 describe the ground motion damage and fault displacement damage conceptual models, the corresponding abstraction models, and their implementation in the TSPA-LA Model. Section 6.6.2 discusses the changes to other TSPA-LA Submodels that occur as a result of a seismic event. These include changes to the Drift Seepage Submodel and Drift Wall Condensation Submodel (Section 6.6.2.1), changes to the EBS TH Environment Submodel (Section 6.6.2.2), changes to the WP and DS Degradation Submodel (Section 6.6.2.3), and the potential effect of crown-seepage induced localized corrosion (Section 6.6.2.4). Model component consistency and conservatisms in assumptions and parameters are discussed in Section 6.6.3. In Section 6.6.4, alternative conceptual models (ACMs) are considered.

6.6.1 TSPA-LA Model Components and Submodels for the Seismic Scenario Class

The Seismic Scenario Class considers seismic events in the mean annual exceedance frequency range of 4.287×10^{-4} to 10^{-8} per year. The upper bound on the mean annual exceedance frequency is based on the minimum peak ground velocity (PGV) threshold for the onset of kinematic damage (SNL 2007 [DIRS 176828]), Section 6.4.3) and the lower bound is dictated by regulation (NRC proposed rule 10 CFR 63.342(b) [DIRS 178394]). If a seismic event breaches the WPs, radionuclides are mobilized and transported from the EBS into the repository host rock. The mobilized radionuclides can then be transported by water percolating through the UZ to the water table, and then to the accessible environment by flow and transport processes in the SZ.

The model components and submodels of the TSPA-LA Model for the Seismic Scenario Class are shown on Figure 6.6-1. Figure 6.6-2 shows the information flow within the TSPA-LA Model associated with the Seismic Scenario Class. Figure 6.6-3 indicates the major inputs and outputs of the model components and submodels of the Seismic Scenario Class, the processes included in the Seismic Scenario Class, and the foundation for confidence in the TSPA-LA Model. These figures indicate that the TSPA-LA Model framework for the Seismic Scenario Class is similar to that of the Nominal Scenario Class. However, some of the model components and submodels differ from those described in Section 6.3. These include the following:

- WP and DS Degradation Model Component
- Drift Seepage Submodel and Drift Wall Condensation Submodel of the UZ Flow Model Component
- EBS TH Environment Submodel of the EBS Environment Model Component.

Figure 6.6-4 provides a schematic illustration of the various elements of the Seismic Scenario Class. The figure shows the likely seismic effects within an emplacement drift of the repository, the subsequent radionuclide releases to the SZ, and their transport to the accessible environment.

In order to provide a complete description of the model components and submodels needed for the Seismic Scenario Class modeling cases, the model components and submodels that differ from those described in Section 6.3 are described in the following sections, according to their effects on repository performance.

6.6.1.1 Conceptual Model for Seismic Response of the Engineered Barrier System

The conceptual model for mechanical damage to the EBS associated with seismic activity is documented in *Seismic Consequence Abstraction* (SNL 2007 [DIRS 176828], Sections 6.1.1 to 6.1.3). The conceptual model for the mechanical response of the EBS components is summarized in the following sections.

6.6.1.1.1 Conceptual Model for Rockfall from Ground Motion

Rockfall induced by vibratory ground motion has the potential to fill the emplacement drifts during the period of geologic stability for dose assessment as defined in NRC proposed rule 10 CFR 63.302 [DIRS 178394]. Rockfall refers to the large rock blocks that may be ejected from the nonlithophysal units of the repository during vibratory ground motion. Rockfall also refers to the fractured and rubblized material that may surround the DS and fill the drifts during partial or complete collapse of drifts in lithophysal units of the repository. Detailed rockfall analyses have been performed for both lithophysal and nonlithophysal rock, under vibratory ground motion.

In the lithophysal zones, the rock mass has very low compressive strength and is permeated with void spaces of varying size (SNL 2007 [DIRS 176828], Section 6.7.1). The drifts in the lithophysal zone are predicted to collapse into small fragments with particle sizes of centimeters to decimeters under the loads imposed by vibratory ground motion. In the nonlithophysal zones, large rock blocks may be shaken loose from the drift walls and fall onto DSs in response to vibratory ground motion.

Drift collapse impacts the temperature and relative humidity of the outer surface of a WP in lithophysal regions of the repository because rubble fills the collapsed drift, essentially forming a thermal blanket covering the DSs and possibly the WPs if the DSs have failed as a barrier to rockfall. Drift collapse also impacts seepage flux and drift-wall condensation in the emplacement drifts in the lithophysal zones. The abstraction and implementation of the effect of drift collapse on seepage and temperature are discussed in more detail in Sections 6.6.2.1 and 6.6.2.2.

6.6.1.1.2 Conceptual Model for Drip Shield and Waste Package Failure from Ground Motion

The components of the EBS are illustrated on Figure 1-11. Mechanical processes that occur during a significant seismic event (i.e., an event with the capacity to degrade or rupture WPs and/or DSs) have the potential to compromise the functionality of the DSs as barriers to seepage

and rockfall and of the WPs as barriers to radionuclide release. For significant vibratory ground motions, impacts can occur between adjacent WPs and between a WP and its emplacement pallet, the surrounding DS, and the invert. Impacts can also occur between DSs and emplacement pallets, the invert, and the drift wall. Rockfall induced by vibratory ground motions can result in impacts on DSs in the postclosure period. Lithophysal rockfall induced by vibratory ground motion can result in static loads on DSs from the surrounding mass of fractured rock. Finally, mechanical loads may be generated by fault displacement within the repository block. In this case, EBS components may become sheared if fault displacement is greater than the available clearances between or around components.

DS Failure Mechanisms—The mechanical response of DSs to vibratory ground motion, which could adversely affect the ability of a DS to prevent flow from reaching a WP, was examined in *Seismic Consequence Abstraction* (SNL 2007 [DIRS 176828], Sections 6.8 and 6.10) and is described as follows:

- The static load from rockfall combined with the dynamic load during a seismic event may rupture DS plates or buckle the DS framework. Rupture or buckling compromises the capacity of a DS to deflect seepage and rockfall away from a WP (SNL 2007 [DIRS 176828], Sections 6.8.2 and 6.8.3).

- The static load from rockfall combined with the dynamic load during a seismic event may deform the plates on the crown of a DS. High levels of residual tensile stress may lead to accelerated degradation processes like SCC. The damaged or deformed area that exceeds a residual stress threshold (RST) is conceptualized to result in a tightly spaced network of stress corrosion cracks, providing a potential pathway for radionuclide transport and release (SNL 2007 [DIRS 176828], Sections 6.3 and 6.10).

- Impacts by large rock blocks in unfilled or partly filled drifts in nonlithophysal units may deform DSs or fail plates and axial stiffeners on the crown of a DS. Failed DS plates provide a potential pathway for seepage to contact the WPs (SNL 2007 [DIRS 176828] Section 6.10.2).

WP Failure Mechanisms—The potential failure mechanisms for the response of WPs to vibratory ground motion were examined in *Seismic Consequence Abstraction* (SNL 2007 [DIRS 176828], Sections 6.5, 6.6, and 6.9) and were described as follows.

- Dynamic loads may dent WPs, resulting in permanent structural deformation with residual tensile stress. The damaged or deformed area that exceeds a residual tensile stress threshold is conceptualized to result in a tightly spaced network of stress corrosion cracks. WP structural response was evaluated for three values of the residual tensile stress threshold for Alloy 22: 90 percent, 100 percent, and 105 percent of the yield strength of Alloy 22.The network of stress corrosion cracks is considered to immediately form once the residual tensile stress threshold is exceeded, providing potential pathways for radionuclide transport and release (SNL 2007 [DIRS 181953], Section 6.7). For WPs subject to SCC damage, the effective transport area for a damaged WP is much smaller than the total damaged area because transport occurs through a network of stress corrosion cracks, rather than through the total damaged area that exceeds the RST. The

effective area for flow and transport is based on the crack density model and associated scaling factor for Alloy 22 developed in *Stress Corrosion Cracking of Waste Package Outer Barrier and Drip Shield Materials* (SNL 2007 [DIRS 181953], Section 6.7). The distribution representing the scaling factor has a mean value of 0.00819 (Section 6.6.1.3.7).

- Dynamic loads on WPs free to move during a seismic event have the potential to result in a rupture (tear) of a WP if the local strain exceeds the ultimate tensile strain. Dynamic loading from a single impact may not produce tensile strains in the Alloy 22 outer corrosion barrier (OCB) that exceed the ultimate tensile strain. However, the extreme deformation from a major seismic event could weaken the OCB, potentially resulting in a ruptured OCB from a subsequent extreme seismic event (SNL 2007 [DIRS 176828], Section 6.1.2). WPs that have been ruptured provide potential pathways for seepage and for radionuclide transport and release. An abstraction for WP rupture from kinematic impacts has been included in the Seismic Scenario Class (Section 6.6.1.2.2.2). WP rupture occurs only for WPs free to move under intact DSs.

- The probability of rupture for WPs with degraded internals surrounded by rubble is zero because the strain on the OCB is always below the ultimate tensile strain for Alloy 22 (SNL 2007 [DIRS 178851], Section 6.5.1.4.1). However, a severely deformed OCB may be punctured by the sharp edges of fractured or partly degraded internal components. The WP internals are assumed to degrade as structural elements after the OCB is first breached. Extreme deformation of the cylindrical OCB can eliminate the free volume within the OCB, allowing the sharp corners or sharp edges from degraded internal elements to puncture the OCB when it is surrounded by lithophysal rubble (SNL 2007 [DIRS 176828], Section 6.1.2). The punctured area is conceptualized to be a small patch on the surface of the OCB (SNL 2007 [DIRS 176828], Section 6.9.1). WPs that have been punctured provide potential pathways for seepage and for radionuclide transport and release. An abstraction for puncture of WPs surrounded by rubble has been included in the Seismic Scenario Class (Section 6.6.1.2.2.2). WP puncture occurs only for WPs with degraded internals, surrounded by lithophysal rubble.

6.6.1.1.3 Fault Displacement Conceptual Model

The conceptual model for fault displacement was developed using data from known and hypothetical faults in the repository. The expected number of WP failures that could occur due to fault displacement is a small fraction of the total number of WPs in the repository. The number of failed WPs is estimated based on an understanding of the displacements that could occur on these faults and geometrical considerations, as described in *Seismic Consequence Abstraction* (SNL 2007 [DIRS 176828], Section 6.11). A fault displacement that occurs in an emplacement drift may cause a sudden discontinuity in the profile of the drift. This could result in one portion of the drift being displaced vertically relative to the adjacent section. Such a discontinuity in the drift could cause shearing of the WP and DS located over the fault if the fault displacement exceeds the available clearance in the EBS. The comparison of fault displacements with available clearances defines the potential for damage to EBS components from fault displacement.

Two distinct cases were considered in analyzing the clearances between EBS components: (1) an intact DS, and (2) a failed DS. The first case represents the as-emplaced configuration of the EBS, shortly after repository closure, and is expected to be applicable to the first 10,000 years after repository closure. The second case represents the late time response of the EBS after DS framework and DS plates have failed and rockfall has partly filled the emplacement drifts and surrounded WPs with rubble. The results of the analyses representing failed DSs with WPs surrounded by rubble were deemed appropriate for use in the TSPA-LA Model, since they are conservative relative to unfailed DS results (SNL 2007 [DIRS 176828], Section 6.11.1.3).

Given the complexity of the response of EBS components and the invert to a fault displacement, a simplified failure criterion was applied to determine shear failure in a collapsed drift. If the fault displacement exceeds one-quarter of the outer diameter of the OCB (about 0.4 meters to 0.5 meters), the WP fails from shear (SNL 2007 [DIRS 176828], Section 6.11.1.2). This simple failure criterion is appropriate because shear failure from fault displacement only occurs from extremely low-frequency, high-amplitude fault displacements, corresponding to a mean annual exceedance frequency of less than or equal to 2.5×10^{-7} per year (SNL 2007 [DIRS 176828], Table 6-67). Fault displacement in excess of these values is conservatively considered to fail WPs and the overlying DSs through direct shearing, allowing advective flow through the sheared components. The cladding within the affected WPs would also be failed, but cladding failure is not analyzed because the compliance case for TSPA-LA Model not taking credit for the cladding. The damage abstraction for cladding is included in the Performance Margin Analysis found in Appendix C.

6.6.1.2 Abstraction Model for Seismic Response of the Engineered Barrier System

The mechanical response of EBS components to a seismic event will be highly dependent on the in-drift configuration of EBS components and on the structural integrity of the EBS components at the time of the seismic event. The future configuration of the EBS components has been represented by three idealized configurations, as shown on Figure 6.6-5. Figure 6.6-5 (a) represents the as-emplaced EBS configuration, with an intact DS and minimal rockfall in the drifts. In this configuration, WPs can move freely beneath DSs. Figure 6.6-5 (b) represents an intermediate state of the system where the legs of a DS have buckled under combined rockfall/seismic load (i.e., DS framework failed), but DS plates remain intact. In this configuration, a DS may collapse onto a WP, inhibiting free movement of the WP and emplacement pallet during the seismic event. Figure 6.6-5 (c) represents the end state of the system, in which rubble surrounds WPs after failure of DS plates. The transition between these configurations is determined by fragility curves for DS framework and plates, based on the intensity of the seismic event and on the thickness of DS components and accumulated rockfall load at the time of the seismic event. The structural integrity of the DS is determined by structural response calculations (SNL 2007 [DIRS 178851], Sections 6.4.3 and 6.4.4).

This potential for DS failure leads to three distinct damage mechanisms for WPs. The first mechanism, referred to as kinematic damage, exists when WPs are free to move beneath DSs (Figure 6.6-5(a)). The second and third damage mechanisms occur when the motion of WPs is restricted and are shown on Figure 6.6-5(b) and Figure 6.6-5(c). These mechanisms are referred

to as damage for a WP beneath (loaded by) a buckled DS and damage for a WP surrounded by rubble, respectively.

The future state of the internal structures within WPs is also important for the damage mechanisms. This internal structure includes a 2-inch thick inner vessel of stainless steel, a TAD canister (for CSNF), and the basket structure that supports the fuel rod assemblies within the WPs. The internal structures add structural strength to the WPs. These internal structures may degrade much faster than Alloy 22, depending on the in-package chemical environment, the residual stress near welds in the inner vessel, and the potential for galvanic contact between the Alloy 22 OCB and the stainless steel inner vessel. Given the uncertainties related to these long-term degradation processes, the future state of the internals is represented as either intact or degraded. The internals remain intact structurally until the first breach of the OCB, after which time they are treated as a degraded material with minimal strength and minimal cohesion. Breach refers to any penetration of the OCB. First breach will usually occur from SCC in the lid welds or in response to seismic events (SNL 2007 [DIRS 176828], Section 6.1.3).

The timing of the first seismic event that breaches a WP is a function of the type of WP. The CSNF WP has two independent stainless steel vessels, the inner vessel and its lids, and the TAD canister. The CDSP WP has only the inner vessel and its lids. The CSNF WP is demonstrably more robust based on a comparison of the probabilities of damage to WPs with intact internals (Section 6.6.1.2.2.2).

The assumption (SNL 2007 [DIRS 176828], Assumption 5.4) that the internal structures degrade by the time of the next seismic event after the OCB is first breached adds conservatism to the seismic WP damage abstraction. Since the Poisson frequency of seismic events is 4.287×10^{-4} per year (Section 6.6.1.3.2), the typical time interval between seismic events is about 2,300 years. However, stainless steel internal structures may remain structurally intact for much more than 2,300 years if in-package chemical conditions remain similar to a fresh water environment, which is the expected condition until after DS failure (SNL 2007 [DIRS 176828], Section 6.1.3). Because seismic damage to a WP is much greater when the internals are degraded, due to the much lower structural strength, this nearly instantaneous degradation of the internals maximizes seismic-related damage to the WP.

A probabilistic seismic hazard analysis (PSHA) was performed to assess the seismic hazards of vibratory ground motion and fault displacement at Yucca Mountain. The PSHA (CRWMS M&O 1998 [DIRS 103731]) provides quantitative hazard results to support an assessment of the repository's long-term performance and to form the basis for developing seismic design criteria. The PSHA methodology for vibratory ground motions is standard practice for deriving vibratory ground motion hazards for design purposes. In addition, probabilistic fault displacement analyses were conducted to provide quantitative assessments of the location and amount of differential ground displacement that might occur. Both analyses provide hazard curves, which express the annual frequency of exceeding various amounts of ground motion (or fault displacement) (SNL 2007 [DIRS 176828], Section 6.4.1). The Seismic Scenario Class for the TSPA-LA Model uses the mean hazard curves for PGV and fault displacement. Each mean hazard curve is defined as the mean estimate or average of a distribution of hazard curves. For annual frequencies of exceedance less than about 10^{-5} to 10^{-6}, the mean curve typically lies above the 80th percentile of the distribution because the average is

dominated by the larger values of the distribution. The use of mean hazard curves is conservative relative to median hazard curves, and provides an accurate representation for the mean dose. The mean hazard curve for ground motion defines the relationship between the estimate of mean annual exceedance frequency, and the amplitude of the vibratory ground motion, measured by the PGV of the first horizontal component of the ground motion(SNL 2007 [DIRS 176828], Section 1.1, footnote 1, p. 1-2). Analysis of the limits for maximum shear strain in the lithophysal rock typical of geologic conditions at Yucca Mountain led to a determination of a mean bounded hazard curve for horizontal PGV at the repository emplacement level. Figure 6.6-6 (DTN: MO0501BPVELEMP.001_R0 [DIRS 172682], file: *Bounded Horizontal Peak Ground Velocity Hazard at the Repository Waste Emplacement Level.xls*) shows the mean bounded hazard curve. The effect of fault displacement on the EBS is evaluated in terms of mean fault displacement hazard curves developed for faulting conditions mapped within the immediate vicinity of Yucca Mountain (SNL 2007 [DIRS 176828], Section 6.11.3).

6.6.1.2.1 Abstraction for Rockfall Volume from Ground Motion

The probability of lithophysal rockfall from a seismic event was abstracted, based on computational results for 15 ground motions at the 0.4 m/s, 1.05 m/s, and 2.44 m/s PGV levels and five rock mass categories (SNL 2007 [DIRS 176828], Section 6.7.1.1, Table 6-28). The probability of rockfall was calculated based on a weighted average of the results for each rock mass category, since the rock mass categories are not equally probable. The resulting piecewise linear definition for the probability of rockfall is given in *Seismic Consequence Abstraction* (SNL 2007 [DIRS 176828], Equation 6.7-1):

$$P_{rockfall} = Min(1.0, Max(0.0, (1.288)PGV - 0.353)) \quad \text{(Eq. 6.6-1)}$$

When rockfall occurs, the volume of lithophysal rock that collapses per meter of drift length is represented by a gamma distribution with mean and standard deviations (SDs) that are quadratic functions of PGV (Figure 6.6-7).

The lithophysal rock volume from multiple seismic events is defined as the sum of the volumes from the individual seismic events. Examination of the mean volume on Figure 6.6-7 shows that rock volume in the lithophysal units will accumulate fairly rapidly. The total rock volume from multiple seismic events is an important parameter because it defines the static load of rubble based on the fraction of the drift filled by rubble. This fraction is defined as the total rubble volume (from multiple seismic events) divided by the rubble volume needed to fill a drift (the effective drift volume after collapse). The effective drift volume after collapse is estimated to be 30 m^3/m to 120 m^3/m for both lithophysal and nonlithophysal zones (SNL 2007 [DIRS 176828], Section 6.7.1.5).

Calculations for the nonlithophysal zones evaluated the response of a 21.74-meter-long section of drift in nonlithophysal rock for the 1.05 m/s, 2.44 m/s, and 5.35 m/s PGV levels. The volume of nonlithophysal rock that collapses per meter of drift length was represented by a gamma distribution with mean and SD that are quadratic functions of PGV. The mean and SD are shown on Figure 6.6-7. Examination of the mean curves shows that the mean rockfall volume in the lithophysal rock is a factor of 32 to 188 greater than the mean rockfall volume in the

nonlithophysal rock for the 1.05 m/s and 2.44 m/s PGV levels, respectively (SNL 2007 [DIRS 176828], Section 6.7.2.1).

The results for nonlithophysal rockfall show probabilities of rockfall that are similar to those for rockfall in the lithophysal zones, except at the 0.4 m/s level, where the calculations could not be compared (SNL 2007 [DIRS 176828], Section 6.7.2.2). Therefore, the probability of rockfall in the nonlithophysal zones is set to be the same as the probability of rockfall in the lithophysal zones, based on the comparison at higher PGV levels than 0.4 m/s.

6.6.1.2.2 Abstraction for Drip Shield and Waste Package Degradation from Ground Motion

Three types of calculations form the basis of the seismic damage abstractions for the WP and DS. The three types of calculations are: (1) three-dimensional kinematic calculations for EBS damage due to vibratory ground motion, appropriate for the early postclosure period, when the DSs are intact and the WPs can move freely beneath the DSs; (2) calculations for deformation and damage of a DS under static and dynamic conditions with intact and degraded EBS components; and (3) calculations for a WP surrounded by rubble that estimate damage after the DS plates have failed (SNL 2007 [DIRS 178851], Section 7.2.1).

Three-dimensional kinematic calculations are used to examine the motion and impact of multiple WPs, pallets, and DSs in an emplacement drift. The objective of these analyses is to define the history of impact parameters for collisions of the WPs, pallets, and DSs as a function of the applied ground motion time histories, and to determine the associated probability of rupture and damaged areas on a WP. Seventeen separate ground motion time histories are used at each of four different PGV levels. A separate kinematic calculation is performed for each ground motion time history at each PGV level, and separate kinematic models are used for CSNF WPs and CDSP WPs.

The kinematic calculations are appropriate when the DS is intact and the WP can move freely beneath the DS. At late times, when the degraded DS plates may fail from rockfall and seismic loads, the WP will be surrounded by rubble. The direct loads from this rubble may cause damage to the WP in response to vibratory ground motion. Rubble in the lithophysal zone is most relevant here because the small particle size of the lithophysal rubble means it can more easily slip or fall through gaps or tears in the plates of the DS and because the lithophysal zones encompass approximately 80 to 85 percent of the emplacement drifts in the repository. The damage induced by the rubble surrounding the WP is based on the two-dimensional coupled rockfall/structural response of the Alloy 22 outer barrier during vibratory ground motion. Damage is determined directly from the finite-difference output for the stress and strain state of the outer barrier. The input data for the calculations of a single WP surrounded by rubble include 17 ground motion time histories at four PGV levels, elastic and plastic properties of the outer barrier, and the bulk properties of degraded WP internals (SNL 2007 [DIRS 178851], Section 6.5.1.1).

6.6.1.2.2.1 Drip Shield Fragility Abstraction

The fragility analysis for DSs defines the probability of failure as a function of the thickness and plastic load capacity of DS components, the static rockfall load on DSs, and the vertical component of peak ground acceleration (PGA) for the seismic event (SNL 2007 [DIRS 176828], Section 6.8). Fragility curves were developed for two modes of failure: (1) rupture or tearing of DS plates, and (2) buckling or collapse of the sidewalls and/or crown of a DS. A third failure mode, from lateral WP impacts to the DS or from longitudinal impacts of the WP on the bulkhead support beams, was considered but not incorporated into the TSPA-LA Model. This third failure mode is not represented in the TSPA-LA Model for two reasons. First, lateral impact of the WP on the DS does not cause catastrophic failure of the DS. Second, high velocity longitudinal impacts of the WP on the bulkhead support beams exposed on the underside of the crown of the DS occur infrequently, even at the 4.07 m/s PGV level (SNL 2007 [DIRS 176828], Section 6.8.5).

The fragility analysis is based on the vertical component of PGA because the average loads on the crown are significantly greater than the average loads on the sidewalls of a DS, indicating that vertical loads are likely to be the critical loads for failure. The vertical component of PGA is defined by a probability distribution that is conditional on the PGV level for a seismic event. The static load from rockfall was based on lithophysal rubble. Rockfall in lithophysal rock has significantly greater volume (SNL 2007 [DIRS 176828], Section 6.7.2.1) than rockfall in nonlithophysal rock, resulting in greater static loads from lithophysal rubble than from nonlithophysal rubble. The load from lithophysal rubble was treated as uniform on the crown on a DS because the typical particulate sizes in the lithophysal rubble are less than the typical dimensions of DS plates.

Plate Failure

Finite-element calculations were performed to define the plastic (nonlinear) load-bearing capacity of the curved plates on the crown of a DS (SNL 2007 [DIRS 176828], Section 6.8.2.1). These calculations defined the magnitude of the uniform load that causes an element of the plate to exceed the failure criteria for Titanium Grade 7, which are based on both accumulated plastic strain and maximum stress (SNL 2007 [DIRS 178851], Section 6.4.3.1.3). For these calculations, the ultimate plastic load capacity of a DS was determined as a function of plate thickness, the static load from rubble in the drifts, and the vertical PGA. Calculations to represent degraded states of the system were performed for 15-mm-, 10-mm-, and 5-mm-thick plates. The plate thicknesses correspond to 0-mm, 5-mm, 10-mm and 13-mm thickness reductions from the initial plate thickness of 15-mm. The probability of DS plate failure as a function of PGV is illustrated on Figure 6.6-8, for 10 percent, 50 percent, and 100 percent rockfall load (i.e., for drifts that are 10 percent, 50 percent, and 100 percent filled with rubble).

If DS plates fail from a seismic event, then all DSs fail as a barrier to seepage (no spatial variability) and this failure is a permanent change for the rest of the realization. See Section 6.6.3.2 for a discussion of spatial variability.

After DS plate failure, the mechanical response of WPs to seismic events is determined by the abstraction, discussed below, for a WP surrounded by rubble.

Framework Failure

A series of dynamic calculations was performed, using selected ground motions for the 2.44 m/s and 4.07 m/s PGV levels, to determine the failure modes of DS framework. Based on these results, the failure mode for the fragility analysis for DS framework was determined to be buckling or collapse of the sidewalls of a DS. Finite-element calculations were carried out to define the plastic (nonlinear) load-bearing capacity of DS framework with intact plates. These calculations defined the magnitude of the load on the crown that caused the side or leg of a DS to buckle. The thickness of all DS components, including the plates and the individual structural members in the framework, was reduced by a constant value of 0-mm, 5-mm, or 10-mm for these calculations. The thickness reduction was taken in the smaller dimension for each structural member in the framework (SNL 2007 [DIRS 176828], Section 6.8.3.2).

The probability of DS framework failure as a function of PGV is illustrated on Figure 6.6-9, for 10 percent, 50 percent and 100 percent rockfall load. Comparison with Figure 6.6-8 shows that the probability of framework failure is always higher than the probability of plate failure, for a given rockfall load and PGV. The framework is expected to collapse before the plates rupture (SNL 2007 [DIRS 176828], Section 6.12.2, Step 13(c)).

If DS framework fails for a seismic event, then DSs do not fail as a barrier to seepage. Plate failure must subsequently occur for seepage to pass through the DS. There is no spatial variability (Section 6.6.3.2) for DS collapse (all DSs collapse), and the framework remains collapsed for the rest of the realization. After DS failure, the mechanical response of WPs to seismic events is a function of the state of the internals. If the internals are intact, the abstraction for a WP surrounded by rubble applies as given below. If the internals are degraded, the kinematic damage abstraction for a WP, under an intact DS but with degraded internals, applies.

Abstraction for Drip Shield Damage from Rockfall Loading

Before DS plates fail, DSs accumulate damage from vibratory ground motion and from rockfall induced by vibratory ground motion. In the lithophysal units, the accumulation of rubble from multiple seismic events and the dynamic motion during a seismic event can generate SCC damaged areas on DSs. These damaged areas are regions that exceed the residual (tensile) stress threshold for DS plates, potentially leading to a network of stress corrosion cracks. The damaged area occurs on the crown of a DS; damage to the sides was not abstracted because any seepage through the sides is considered unlikely to drip onto a WP. The damaged areas in the lithophysal zones were analyzed as a function of the thickness of DS plates, the rockfall load on DSs, and the vertical component of PGA for the seismic event. The abstraction for damaged area on DSs in the lithophysal zones is discussed in Section 6.10.1 of *Seismic Consequence Abstraction* (SNL 2007 [DIRS 176828]). Because DS damage in lithophysal zones is in the form of a network of stress corrosion cracks and because advective flow through stress corrosion cracks in DSs has been screened out (DTN: MO0706SPAFEPLA.001_R0 [DIRS 181613], FEP 2.1.03.10.0B), the abstraction for DS damage due to rockfall loading in the lithophysal units has not been included in the TSPA-LA Model file.

Abstraction for Drip Shield Damage from Rock Block Impacts

Before DSs fail in the nonlithophysal units, rock blocks can impact DSs in an unfilled or partially filled drift. Rock block impacts may result in damaged areas on DS plates and, in more extreme cases, may result in tearing or rupture of the plates and failure of the axial stiffeners beneath the crown of a DS. Section 6.10.2 of *Seismic Consequence Abstraction* (SNL 2007 [DIRS 176828]) develops abstractions for damaged area and plate failures for DSs in unfilled or partly filled drifts in the nonlithophysal units of the repository. The abstractions developed there support the screening arguments for excluding DS damage due to rock block impacts in the nonlithophysal units. The screening analysis is documented in DTN: MO0706SPAFEPLA.001_R0 [DIRS 181613], FEP 1.2.03.02.0B. As a result, DS damage due to rock block impacts in nonlithophysal units is excluded from the TSPA-LA Model.

6.6.1.2.2.2 Waste Package Damage Abstraction

Throughout this section reference is made to damage estimates for WPs based on calculations for an OCB at two thicknesses, 23 mm and 17 mm. The 23-mm thick OCB provides representation of an intact or almost intact WP. The 17-mm thick OCB provides a representation for a degraded WP at late times after repository closure. If the OCB thickness is between 17 mm and 23 mm, linear interpolation is used to define the damaged area (i.e., the area that exceeds the RST) within the damage abstractions. If the OCB thickness is greater than 23 mm, damage estimates at 23 mm are used. If the OCB thickness is less than 17 mm, damage estimates at 17 mm are used.

A 17-mm-thick OCB is appropriate for late times after repository closure. The median corrosion rate of Alloy 22 at 60ºC is less than 7 nm/yr, based on a medium uncertainty level in the distributions for general corrosion rate (SNL 2007 [DIRS 178519] Figure 6-23). The value of 60ºC is appropriate because it is an upper bound on OCB temperature beyond 10,000 years after repository closure (SNL 2007 [DIRS 178851], Figure 1-3), and because it is consistent with the structural response calculations for the seismic scenario (SNL 2007 [DIRS 178851], Assumption 5.7, Section 5). The 17-mm-thick OCB, which corresponds to an 8.4-mm ≈ 8-mm thickness reduction, will occur at a time of $(8 \times 10^{-3}\ \text{m})/(7 \times 10^{-9}\ \text{m/yr}) \approx 1{,}100{,}000$ years. More detailed corrosion calculations require a probabilistic analysis, but this estimate indicates that the 17-mm-thick OCB provides a reasonable representation for seismic response at the end of the period for assessment of repository performance.

The adequacy of the 17-mm thick OCB to represent the degraded states that may occur up to one million years after repository closure has been confirmed by a stand-alone probabilistic analysis of WP degradation. The stand-alone analysis model is a modified version of the TSPA-LA Model. The model components not pertaining to WP and DS degradation have been removed, to allow increased computational speed and to allow more detailed results to be saved. All epistemically uncertain parameters have been retained and all aleatory parameters related to WP and DS degradation have been retained. The sampling sequence is identical to the TSPA-LA Model 300-realization unified sampling Seismic GM Modeling Case (Section 6.6.1.3.1). The stand-alone model is documented in output DTN: MO0709TSPAWPDS [DIRS 183170].

Stress Corrosion Cracking Damage to CSNF and CDSP Waste Packages under Intact Drip Shields

Kinematic and structural response calculations were performed to develop damage estimates for the failed WP surface area for CSNF and CDSP WPs under intact DSs (SNL 2007 [DIRS 176828], Sections 6.5.1 through 6.5.4 and 6.6.1 through 6.6.4). As described in *Seismic Consequence Abstraction* (SNL 2007 [DIRS 176828], Sections 6.5 and 6.6), kinematic damage abstractions were developed for three future states of CSNF and CDSP WPs:

- 23-mm-thick OCB with intact internals
- 23-mm-thick OCB with degraded internals
- 17-mm-thick OCB with degraded internals.

The probability of damage to CSNF or CDSP WPs for the j^{th} seismic event is defined as a function of (1) the state of the internals (intact or degraded), (2) the PGV for the j^{th} seismic event, (3) the value of RST for the i^{th} realization, and (4) the OCB thickness (SNL 2007 [DIRS 176828] Sections 6.5.1.2, 6.5.2.2, 6.6.1.2, and 6.6.2.2). Figures 6.6-10 and 6.6-11 illustrate these probabilities, for the three states of the WP (23-mm, intact; 23-mm, degraded; and 17-mm, degraded). When the WP internals are intact the probability of damage is much lower for CSNF WPs, than for CDSP WPs.

If CSNF or CDSP WPs are damaged by the j^{th} seismic event, then their conditional damaged area is represented by a gamma distribution. Separate gamma distributions were defined for three states of WPs: (1) 23-mm-thick OCB with intact internals, (2) 23-mm-thick OCB with degraded internals, and (3) 17-mm-thick OCB with degraded internals. The values for the mean and SD of these gamma distributions are derived in Sections 6.5.1.3, 6.5.2.3, 6.6.1.3, and 6.6.2.3 of Seismic Consequence Abstraction (SNL 2007 [DIRS 176828]). Figures 6.6-12 and 6.6-13 illustrate the quadratic fits for mean damaged area for the CSNF and CDSP WPs, respectively. The means are a function of PGV and there is a separate gamma distribution for the three values of RST (90 percent, 100 percent, and 105 percent of yield strength). For CSNF and CDSP WPs with degraded internals, the damage abstractions show consistently higher SCC damage for the CSNF WPs, compared to the CDSP WPs.

Note that for the CSNF WP with intact internals damage occurs only at the 4.07 m/s PGV level (the probability is zero for all other PGVs – Figure 6.6-10). In this particular case, the single point results are conservative for all values of PGV less than 4.07 m/s and all values of the RST greater than 90 percent. In addition, the magnitude of the conditional damaged area is less than 0.006 which is a very small fraction of the cylindrical surface area of the CSNF WP of 33.64 m^2 (SNL 2007 [DIRS 176828], Sections 6.5.1.3). Therefore, the conditional damage at 4.07 m/s and 90 percent RST is considered to represent the damage at all values of PGV and RST in the TSPA-LA Model (SNL 2007 [DIRS 176828], Section 6.5.1.3).

For either intact or degraded internals, there is no WP-to-WP spatial variability for the conditional damaged area (Section 6.6.3.2). For a single package, the damaged area is randomly located on the cylindrical surface of the OCB. The total damaged area increases with each seismic event that causes damage to the WP OCB. Damaged area cannot exceed the total surface area of a CSNF or CDSP WP.

Rupture of CSNF and CDSP Waste Packages under Intact Drip Shields

CSNF or CDSP WPs that can move freely beneath a DS can rupture from the accumulation of severe deformation due to multiple impacts, which can accumulate in either one seismic event or multiple seismic events. The probability of rupture for the 23-mm-thick OCB with intact internals was determined to be zero (SNL 2007 [DIRS 176828], Sections 6.5.1.1 and 6.6.1.1). However, for CSNF or CDSP WPs with degraded internals, the effect of multiple WP-to-pallet impacts was assessed by evaluating the severity of accumulated deformation. The degree of deformation was used to define the probability of rupture. A minor degree of deformation indicated that no rupture occurred, consistent with the observation that the strain in the OCB is below the ultimate tensile strain for Alloy 22 for individual impacts. A significant degree of deformation was interpreted as causing an incipient rupture, in the sense that a second severe impact, during a subsequent seismic event, would have the potential to cause rupture. Finally, if two severe impacts occurred during the same seismic event, then the accumulation of severe deformation was interpreted as causing immediate rupture in the OCB. The probability of incipient rupture and the probability of immediate rupture for CSNF or CDSP WPs with degraded internals are abstracted as power laws in Sections 6.5.2.1 and 6.6.2.1 of *Seismic Consequence Abstraction* (SNL 2007 [DIRS 176828]). Figure 6.6-14 compares the probability for incipient and immediate rupture of the CSNF and CDSP WPs. For a given PGV, CSNF WPs have a higher rupture probability.

When a WP is ruptured, the failed area is determined by sampling a uniform distribution for failed area, with a lower bound of 0 m^2 and an upper bound equal to the cross-sectional area of the WP OCB. This failed area allows advective flow through and advective and diffusive transport out of ruptured CSNF or CDSP WPs. Once the WP is ruptured, there is no further damage from rupture in successive events, and the WPs remain ruptured for the remainder of the realization.

Stress Corrosion Cracking Damage to CSNF and CDSP Waste Packages Surrounded by Rubble

Structural response calculations were performed to develop damage estimates for the failed WP surface area of a CSNF WP surrounded by rubble (SNL 2007 [DIRS 176828], Sections 6.9.1 through 6.9.9). Two damage abstractions were developed for a WP with degraded internals that is surrounded by lithophysal rubble:

- 23-mm-thick OCB with degraded internals
- 17-mm-thick OCB with degraded internals.

Damage for WPs with intact internals was not calculated for WPs surrounded by rubble. A WP becomes surrounded by rubble after DS framework and DS plates have failed during a seismic event. This is expected to occur at late times after repository closure. For CDSP WPs the OCB is likely to be breached by SCC at these times, resulting in degraded internals. In contrast, the probability of SCC damage to CSNF WPs with intact internals under intact DSs is zero except at 4.07 m/s PGV levels. Therefore, CSNF WPs are not likely to have degraded internals at the time of DS failure. Regardless of the time scale, the damage abstractions for degraded internals will result in greater damaged area relative to the response with intact internals, so this approach is

conservative. Separate abstractions were not developed for CSNF and CDSP WPs surrounded by rubble because it was considered that the results for the CSNF WPs provide a reasonable estimate of damage to the CDSP WP (SNL 2007 [DIRS 176828], Sections 6.9.10).

Lithophysal rubble was selected for the dynamic load on WPs. The analysis acknowledges that large rock blocks would tend to have point loading contacts in localized areas on a WP, but the cumulative loading from the lithophysal rubble is expected to be significantly greater because the volume of lithophysal rubble is much greater than the volume of nonlithophysal rockfall (SNL 2007 [DIRS 176828], Table 6-32 and Figure 6-58).

The probability of damage for the j^{th} seismic event was abstracted as a function of the value of PGV for the j^{th} seismic event, the value of RST for the i^{th} realization, and of the OCB thickness (SNL 2007 [DIRS 176828], Section 6.9.2). Figure 6.6-15 illustrates these probabilities, for the two states of the WP (23-mm degraded and 17-mm degraded).

If WPs are damaged by the j^{th} seismic event, then the conditional damaged area is represented by a gamma distribution. Separate gamma distributions were defined for two states of WPs: (1) 23-mm-thick OCB with degraded internals, and (2) 17-mm-thick OCB with degraded internals. The mean and SD of the gamma functions are quadratic equations in RST (SNL 2007 [DIRS 176828], Section 6.9.3). For the 23-mm thick and the 17-mm thick OCB, relatively few data points showed SCC damage (SNL 2007 [DIRS 176828], Sections 6.9.3 and 6.9.5). Therefore, the abstraction for damage was done at a single PGV level (4.07 m/s). It was considered to be conservative to use the conditional damage at the 4.07 m/s PGV level for all values of PGV (SNL 2007 [DIRS 176828], Section 6.9.3). Figure 6.6-16 shows the quadratic fit for the mean damage area as a percent of the total surface area, for the 23-mm and 17-mm thick OCB.

There is no WP-to-WP spatial variability for the conditional damaged area (SNL 2007 [DIRS 176828], Section 6.9.9). Spatial variability is also discussed in Section 6.6.3.2. For a single package, the damaged area is randomly located on the cylindrical surface of the OCB. The total damaged area increases with each seismic event that causes damage to the OCB. The damaged area cannot exceed the total surface area of a CSNF or CDSP WP.

Puncture of CSNF and CDSP Waste Packages Surrounded by Rubble

For a WP surrounded by rubble, loss of WP integrity is conceptualized to occur from puncture by sharp internal fragments, rather than rupture of the OCB due to impact with other EBS components. The probability of puncture for the 23-mm-thick and 17-mm-thick OCBs is abstracted as a power law in PGV (SNL 2007 [DIRS 176828], Section 6.9.1). Figure 6.6-17 shows the probability of puncture for 23-mm and 17-mm OCBs. Comparison with Figure 6.6-14 shows that puncture can be more likely than rupture, particularly for 17-mm OCBs and at lower PGVs.

When WPs are punctured, the failed area is determined by sampling a uniform distribution, with a lower bound of 0 m^2 and an upper bound of 0.10 m^2. The upper bound of the uniform distribution is based on two estimates for the area of a hypothetical puncture. If the puncture occurs from a sharp fragment of a fuel rod, the corresponding hole is likely to be quite small. In

the second estimate, one of the fuel basket plates is conceptualized to form a lengthwise slice through the OCB (SNL 2007 [DIRS 176828], Section 6.9.1). The upper bound of 0.10 m^2 represents the maximum estimated area from either mechanism.

This failed area allows advective flow through punctured WPs and advective and diffusive transport out of the punctured WPs. Once a WP is penetrated, there is no further damage from penetrations in successive events and the WPs remain punctured for the remainder of the realization.

6.6.1.2.3 Fault Displacement Abstraction

In addition to the damage from vibratory ground motion, it is possible that WP and DS failures may occur due to fault displacement. Damage to WPs by fault displacement occurs when the fault displacement exceeds the available clearances between or around EBS components. Two distinct cases were considered in analyzing the clearances between EBS components (Section 6.6.1.1.3). The maximum allowable displacement, for six different WP types (SNL 2007 [DIRS 176828], Tables 6-58 and 6-59), was determined for the two cases, one with an intact DS and a second with a failed DS. The values corresponding to the second case (failed DSs) are used for the TSPA-LA Model because these values result in more failures than for the first case, with an intact DS.

Fault displacement hazard curves for 15 faulting conditions mapped within the immediate vicinity of Yucca Mountain were used to provide displacement values as a function of the mean annual exceedance frequency (SNL 2007 [DIRS 176828], Section 6.11.3). The inventory of WP types was split into two groups (CSNF and CDSP WP). WPs of similar design and similar waste type were grouped together. The WP designs with the smallest diameter in the group are chosen to represent the clearance for all packages in that group. The clearance is given by one-quarter of the outer diameter of the OCB, so the smallest diameter results in the least clearance for all WPs in the group. The probability of finding a WP in each group on a fault was calculated based on the total length of the WP types in the group versus the total length of all emplaced WPs (rather than the number of each type of WP divided by the total number of WPs). The hazard curve data is combined with the clearance data and the probability of finding a WP from each group on a fault to give the expected number of WP failures as a function of mean annual exceedance frequency. The expected number of WPs that could fail from fault displacement was found to be a small fraction of the total number of WPs in the repository. If a WP fails from fault displacement, then the surrounding DS also fails from fault displacement (if it hasn't already failed in a previous seismic event). The results are summarized in Table 6.6-1. The table indicates that damage to WPs and DSs from fault displacement is not expected if the mean annual frequency of occurrence is greater than 2.5×10^{-7} per year (DTN: MO0703PASEISDA.002_R4 [DIRS 183156], Table 1-14).

Shearing of the WP and DS over the fault can occur if the fault exceeds the available clearance in the EBS (SNL 2007 [DIRS 176828], Section 6.11). When a WP fails by fault displacement, the failed area is determined by sampling a uniform distribution with a lower bound of zero and an upper bound equal to the area of a WP lid. The lower bound is appropriate for mean annual exceedance frequencies near 10^{-7} per year because a WP that is minimally pinned from fault displacement is expected to have only minor crimping and is unlikely to rupture. The upper

bound is appropriate for a large fault displacement that shears a WP near its lid. In this case, the lid welds have the potential to fracture, separating the lid from the package and potentially exposing the entire waste form to seepage and release (SNL 2007 [DIRS 176828], Section 6.11.5). The use of a uniform distribution is appropriate because reasonable upper and lower bounds can be defined and because the use of this type of distribution maintains the uncertainty in the damaged area for this abstraction.

In the TSPA model the failed area is conceptualized to be a shear that lies in a plane normal to the central axis of a WP. The failed area can be represented as a circumferential band around a WP for transport calculations in the TSPA. Once WPs fail in shear, there is no further damage on successive events and WPs remain failed for the remainder of the realization. The resulting damage is assumed to allow flow into WPs (if seepage is present) and allow advective and diffusive transport out of WPs. When a WP fails from fault displacement, the associated DS is also presumed to fail, causing damage to the total surface area of the DS. A sheared DS will allow all seepage to pass through no flux splitting (SNL 2007 [DIRS 176828], Section 6.11.5). A damage abstraction for the cladding in a fault-failed WP was not developed because the TSPA-LA Model does not take credit for cladding as a barrier to radionuclide releases (SNL 2007 [DIRS 180616], Section 6.2.1.2[a]).

6.6.1.2.4 Treatment of Uncertainty

The TSPA-LA Model includes parameter uncertainty in the Seismic Scenario Class at two levels: in the implementation of the abstraction in the TSPA-LA Model, and in the underlying process models used in the development of the Seismic Consequences Abstraction. The term parameter uncertainty encompasses uncertainty in input parameters for process level models (like ground motions) and uncertainty in random variables for seismic damage, such as the damaged areas.

Uncertainty can be characterized as epistemic (representing limited data and knowledge) or aleatory (representing variability or natural randomness in a process). Uncertainty in the Seismic Scenario Class is directly represented in the TSPA-LA Model by defining uncertain parameters that are sampled either once per realization (epistemic parameters) or multiple times per realization (i.e., at the occurrence of each seismic event (aleatory parameters)). Table 6.6-2 lists the parameters that represent uncertainty in the Seismic Scenario Class. In this table the parameters are categorized according to whether they represent epistemic or aleatory uncertainty.

The uncertainty in the input parameters to the underlying process models, and its propagation in the TSPA-LA Model, is discussed in Section 8.2 of Seismic Consequence Abstraction (SNL 2007 [DIRS 176828]), and summarized as follows:

- The structural response calculations for the responses of WPs that are affected by vibratory ground motion include three principal sources of uncertainty: (1) the ground motion time histories (aleatory uncertainty); (2) the metal-to-metal friction coefficient (epistemic uncertainty); and (3) the metal-to-rock friction coefficient (epistemic uncertainty) (SNL 2007 [DIRS 176828], Section 8.2, Acceptance Criterion 3). The variations of these uncertain input parameters are simultaneously included in the 17 structural response calculations at each seismic hazard level. This is accomplished by a

Latin Hypercube Sampling (LHS) procedure that ensures robust sampling of the uncertain parameters over their full ranges (SNL 2007 [DIRS 178851], Sections 6.3.1, 6.4.4.5, and 6.5.1.1).

- All rockfall analyses include the ground motion time histories as a major source of aleatory uncertainty. Fifteen ground motions represent the uncertainty in the seismic forcing functions. Note that the rockfall calculations predate the WP calculations and for these earlier calculations only 15 of the 17 ground motion histories were used (SNL 2007 [DIRS 176828], Section 6.1.3). In the lithophysal units, the rock compressive strength is an uncertain input parameter that is represented as five discrete levels of rock strength. The computational results for probability of lithophysal rockfall are based on 15 realizations with LHS for the ground motion histories and the rock strengths. In the nonlithophysal units, the synthetic fracture pattern that defines the fracture geometry is an uncertain input parameter that is used in the rockfall analyses for the nonlithophysal units. The nonlithophysal analysis evaluated the response of a 25-meter long section of drift in nonlithophysal rock with randomly selected fracture patterns paired with randomly selected ground motion time histories (BSC 2004 [DIRS 166107], Section 6.3.1).

- The calculations of damaged areas on WPs that are due to vibratory ground motion exhibit substantial variability (primarily aleatory uncertainty) induced by the uncertainties in seismic ground motions and other input parameters. This variability in damaged area is represented as conditional probability distributions that are provided to and sampled in the TSPA-LA Model.

6.6.1.3 Implementation in the TSPA-LA Model

The potential for deformation and rupture/puncture of EBS components from multiple seismic events within a given realization of the TSPA-LA Model, is described in the following sections. These sections are aligned with the separate elements of the seismic damage abstractions. A realization of the TSPA-LA Model represents one of many future potential histories of the repository. Each realization generally has a unique value for each random variable that represents epistemic (knowledge) uncertainty, such the RST for initiation of potential stress corrosion cracking. Each realization also has a unique sequence of seismic events whose timing and intensity capture the aleatory uncertainty (i.e., the randomness) in the seismic process.

6.6.1.3.1 TSPA-LA Modeling Cases

The implementation of the Seismic Damage Abstraction involves two modeling cases, the Seismic GM Modeling Case and the Seismic FD Modeling Case.

Seismic GM Modeling Case

The Seismic GM Modeling Case calculates mean annual dose due to damage to WPs resulting from vibratory ground motion. This modeling case also accounts for fragility of the DSs under the combined loads from vibratory ground motion and accumulated rockfall around the DS. In addition, corrosion processes are included in the Seismic GM Modeling Case calculation for

1,000,000 years, and the dose due to corrosion processes is calculated as part of the Seismic GM Modeling Case for 1,000,000 years. The Seismic GM Modeling Case does not include damaged areas (due to SCC) on the DS because advective flow through the DS has been screened out by FEP 2.1.03.10.0B, *Advection of Liquids and Solids Through Cracks in the Drip Shield* (DTN: MO0706SPAFEPLA.001_R0 [DIRS 181613]). This modeling case also does not include failure of the DSs from large rock block impacts in nonlithophysal units because these processes have been screened out by FEP 1.2.03.02.0B, *Seismic-Induced Rockfall Damages EBS Components* (DTN: MO0706SPAFEPLA.001_R0 [DIRS 181613]).

The Seismic GM Modeling Case for 10,000 years and the Seismic GM Modeling Case for 1,000,000 years use different numerical techniques to calculate mean annual dose. These are described in the following paragraphs.

The TSPA-LA Model calculates the mean annual dose for the Seismic GM Modeling Case for 10,000 years using a three-step process. First, a LHS of uncertain TSPA-LA Model parameters is generated. Each element of the LHS is a vector, specifying a value for each epistemically uncertain parameter. For each element in the LHS, a number of annual dose histories are computed using GoldSim. Each annual dose history represents a single seismic ground motion event, which occurs at a specified time, and results in a specified damage area to each WP simulated. The mobilization and transport of radionuclides is evaluated using the Nominal Scenario Class submodels for radionuclide transport in the EBS, UZ, and SZ.

Second, for each element in the LHS, the expected annual dose history is calculated by Equation 6.1.2-22, using the annual dose histories computed for each element of the LHS. The integral in Equation 6.1.2-22 accounts for the uncertainty in the number of seismic events, the time of each event, and the damaged area. The integral is evaluated numerically by EXDOC software (Section 6.1.5). The mean annual dose history is calculated as the average of the expected annual dose histories from the set of realizations.

Because relatively few seismic events (approximately 5) occur within 10,000 years, and the probability of damage to CDSP WPs is much greater than that of damage to the CSNF WPs, the expected dose for the Seismic GM Modeling Case for 10,000 years relies on a number of simplifying approximations:

- Corrosion of WP and DS materials is bounded by a 2 mm thickness reduction to the WP and a 2 mm thickness reduction to the DS
- Only CDSP WPs are considered because the probability of damaging the CSNF WP is very low during the first 10,000 years
- Rupture and puncture events are not considered
- The DS remains intact and functional
- Seepage and temperature are not altered due to rockfall.

Section 7.3.2 provides justification for these approximations. Calculation of the mean annual dose for the Seismic GM Modeling Case for 1,000,000 years also begins by generating an LHS of uncertain TSPA-LA Model parameters. For each element in the LHS, a number of annual dose histories are computed using GoldSim. Each annual dose history is associated with a sequence of seismic events generated by GoldSim. The effects of corrosion on EBS components are included, and rockfall and damage to EBS components are accumulated as seismic events occur. The mobilization and transport of radionuclides is evaluated using the Nominal Scenario Class submodels for radionuclide transport in the EBS, UZ, and SZ.

The expected annual dose history is calculated by Equation 6.1.2-24, using the annual dose histories computed for each element of the LHS. The mean annual dose history is calculated as the average of the expected annual dose histories from the set of realizations.

Seismic FD Modeling Case

The Seismic FD Modeling Case calculates mean annual dose due to damage caused by fault displacements. This modeling case accounts for damage to WPs and DSs through direct shearing which allows advective flow through the sheared components. Corrosion processes are not included in the Seismic FD Modeling Case. The modeling case considers a single seismic event. This modeling case does not consider rockfall accumulation in the drifts, however, after the seismic event occurs drifts are considered to be filled with rockfall.

Calculation of the mean annual dose for the Seismic FD Modeling Case for either 10,000 years or 1,000,000 years also begins by generating an LHS of uncertain TSPA-LA Model parameters, and, for each element of the LHS, computing a number of annual dose histories using GoldSim. Each annual dose history is associated with a single seismic fault displacement event occurring at a specified time, and resulting in a specified damage area to each WP represented. The effects of the fault displacement are applied to the DS and to the drift, and the mobilization and transport of radionuclides is evaluated using the Nominal Scenario Class submodels for radionuclide transport in the EBS, UZ, and SZ.

The expected annual dose history is calculated by Equation 6.1.2-25, using the annual dose histories computed for each element of the LHS. The integral in Equation 6.1.2-25 accounts for the uncertainty in the time of the seismic fault displacement event, the uncertainty in the damaged area caused by the seismic event, and the number of WPs affected; this equation is evaluated numerically by EXDOC (Section 6.1.5). The mean annual dose history is calculated as the average of the expected annual dose histories from the set of realizations. Table 6.6-3 summarizes the calculations for the two modeling cases.

The computational approach used in GoldSim in the implementation of the Seismic Scenario Class is described in DTN: MO0703PASEISDA.002_R4 ([DIRS 183156], Section 1.1). The input parameters required by the Seismic Scenario Class model components are taken from the TSPA Input Database.

6.6.1.3.2 Seismic Event Time and Magnitude Calculations for the 1,000,000-Year Ground Motion Case

For the Seismic GM Modeling Case 1,000,000-year simulation, each realization includes multiple seismic events. In the discussions that follow, a particular seismic event, the j^{th} event, will be considered representative of all seismic events in a particular Monte Carlo realization. The time of the j^{th} event is determined by GoldSim's random time internal (Poisson) event generator (GoldSim Technology Group 2007 [DIRS 181727], Appendix B) using a Poisson frequency of ($\lambda_{max} - \lambda_{min}$). The values of λ_{min} and λ_{max} are set to 1×10^{-8} per year and 4.287×10^{-4} per year, respectively (DTN: MO0703PASEISDA.002_R4 [DIRS 183156], Table 1-15). The Poisson frequency is then given by (4.287×10^{-4} per year – 1×10^{-8} per year) = 4.287×10^{-4} per year.

The mean annual exceedance frequency for the j^{th} event is sampled from a uniform distribution between λ_{min} and λ_{max}. The bounds are chosen to encompass all mean annual exceedance frequencies with the potential to result in significant damage to DSs or WPs. The range of mean annual exceedance frequencies, spans the response of the system from no damage to the regulatory probability limit at 10^{-8} per year (DTN: MO0703PASEISDA.002_R4 [DIRS 183156], Table 1-15).

After the value of the mean annual exceedance frequency has been determined for the j^{th} event, the corresponding value of the PGV is calculated. The relationship between the PGV and the mean annual exceedance frequency (bounded hazard curve) is represented in the model by a one-dimensional table (DTN: MO0703PASEISDA.002_R4 [DIRS 183156], Table 1-15). Interpolation between points on the hazard curve is based on a piecewise linear interpolation with the values of log(λ) and log (PGV) at the individual points.

6.6.1.3.3 Methodology for Damage Abstraction Implementation

The seismic damage abstractions are generally based on a three-part approach:

1. The probabilities of incipient rupture (which may lead to rupture during a subsequent timestep), immediate rupture, or puncture are defined as a function of horizontal PGV and the thickness of the OCB. If rupture or puncture occurs, the resulting rupture area or puncture area is defined using a bounding, uniform distribution. The probabilities of incipient rupture, immediate rupture, or puncture are represented as a power-law function of PGV. The rationale for two types of rupture, incipient and immediate, is explained in Section 6.6.1.2.2.2.

2. The probability of damage is defined as a function of PGV, RST, and the thickness of the WP. Damaged area is defined as the area that exceeds the RST and is thereby susceptible to potential SCC. Damaged area represents the physical area of a dented region with high residual stress. Damaged area is significantly greater than the effective area for transport through a network of stress corrosion cracks, as explained in Section 6.6.1.1.2.

   The probability of nonzero damaged area, or more simply the probability of damage, is usually represented as a lookup table that uses PGV and RST as the independent variables.

The typical lookup table for probability of damage at a given OCB thickness has 12 entries defined by four values of PGV (0.4 m/s, 1.05 m/s, 2.44 m/s, and 4.07 m/s) and by three values of RST (90 percent, 100 percent, and 105 percent of the yield strength of Alloy 22). A piecewise linear interpolation scheme is used between the points in the lookup table, avoiding the need for a functional fit to a probability surface.

3. When nonzero damaged area occurs, a conditional probability distribution for the magnitude of the conditional damaged area is defined as a function of PGV, RST, and the thickness of the OCB. The conditional damaged areas are always nonzero areas, by definition.

This approach is useful because it eliminates zero values from the conditional probability distributions in Step 3. A similar approach is applied for rockfall induced by a seismic event, based on Steps 2 and 3, as described in the next section.

6.6.1.3.4 Implementation of Rockfall for the 1,000,000-Year Ground Motion Case

Lithophysal Rockfall Calculation

The probability of rockfall was abstracted as a linear function of PGV (Equation 6.6-1). The occurrence of rockfall is determined by comparing the calculated probability of rockfall for the j^{th} seismic event, $P_{rockfall}$, to a random number between 0 and 1, R_j , corresponding to the j^{th} seismic event

$$If \quad R_j \le P_{rockfall} \quad \text{then} \quad RV_{LITH,j} > 0 \qquad \text{(Eq. 6.6-2)}$$

$$else \quad RV_{LITH,j} = 0$$

where $RV_{LITH,\,j}$ is the volume of lithophysal rockfall. The random number is resampled for each seismic event because the uncertainty in the probability of rockfall is related to the aleatory uncertainty in 17 ground motion time histories.

For each seismic event where rockfall occurs, the volume of lithophysal rock that collapses per meter of drift length is represented by a gamma distribution with mean (μ) and SD (σ) that are quadratic functions of PGV (DTN: MO0703PASEISDA.002_R4 [DIRS 183156], Section 1.1, Step 5c and Table 1-16). If the PGV determined from the bounded hazard curve is less than 0.4 m/s, then the values at 0.4 m/s are used in the volume calculations (DTN: MO0703PASEISDA.002_R4 [DIRS 183156], Table 1-16), since Equations 6.6-4 and 6.6-5 may produce negative values of the mean and/or SD for PGVs less than 0.4 m/s.

$$PGV_{rf} = MAX(PGV, 0.4 m/s), \qquad \text{(Eq. 6.6-3)}$$

$$\mu = (20.307)\left(PGV_{rf}\right)^2 - (18.023)PGV_{rf} + 4.0102, \qquad \text{(Eq. 6.6-4)}$$

$$\sigma = -(3.5613)\left(PGV_{rf}\right)^2 + (18.018)PGV_{rf} - 6.6202. \qquad \text{(Eq. 6.6-5)}$$

The total volume of lithophysal rock that collapses per meter of drift length after the j^{th} seismic event, $TV_{LITH,j}$, is the sum of the volumes for the first j seismic events.

$$TV_{LITH,j} = \sum_{k=1}^{j} RV_{LITH,k} \quad \text{(Eq. 6.6-6)}$$

The volume of lithophysal rock that must collapse to fill the drift ($V_{L,i}$) is defined as a uniform distribution between 30 m^3 per meter to 120 m^3 per meter of drift length. This parameter is sampled once per realization (DTN: MO0703PASEISDA.002_R4 [DIRS 183156], Section 1.1, Step 5e).

The fraction of the drift that is filled after the j^{th} seismic event, FD_j, is defined as the ratio of the total volume of collapsed lithophysal rock after the j^{th} seismic event to the volume that is required to fill the drift ($V_{L,i}$), for the i^{th} realization (DTN: MO0703PASEISDA.002_R4 [DIRS 183156], Equation 1-11).

$$FD_{LITH,j} = MIN\left(\frac{TV_{LITH,j}}{V_{L,i}}, 1.0\right) \quad \text{(Eq. 6.6-7)}$$

The fraction of drift filled by lithophysal rubble ($FD_{LITH,j}$) is a parameter used in DS fragility calculations.

Nonlithophysal Rockfall Calculation

The probability of nonlithophysal rockfall has been abstracted to be the same as the probability of lithophysal rockfall (Section 6.6.1.2.1). Thus the probability of occurrence of nonlithophysal rockfall is given in Equation 6.6-2.

For each seismic event where rockfall occurs, the volume of nonlithophysal rock that collapses per meter of drift length is represented by a gamma distribution with mean (μ) and SD (σ) that are quadratic functions of PGV (DTN: MO0703PASEISDA.002_R4 [DIRS 183156], Table 1-16):

$$\mu = (-0.0142)(PGV)^2 + (0.2064)PGV + 0.0387 \quad \text{(Eq. 6.6-8)}$$

$$\sigma = (-0.037)(PGV)^2 + (0.3057)PGV + 0.0696. \quad \text{(Eq. 6.6-9)}$$

The total volume of nonlithophysal rock that collapses per meter of drift length after the j^{th} seismic event, the volume of nonlithophysal rock that must collapse to fill a drift, and the fraction of the drift that is filled after the j^{th} seismic event are all defined in an analogous fashion to the definitions for lithophysal rockfall.

The fraction of a drift filled by nonlithophysal rubble is a parameter used by the drift seepage abstraction (Section 6.6.2.1) for the Seismic GM Modeling Case for 1,000,000 years.

6.6.1.3.5 Implementation of Drip Shield Plate and Framework Damage from Ground Motion

Plate Fragility

DS plate fragility is defined as the probability of rupturing a plate during a seismic event. Plate fragility is a function of *PGV* for the j^{th} seismic event, of the thickness of DS plates, and of the static load on plates from rockfall. The thickness of DS plates is a feed from WP and DS Degradation Model Component (Section 6.3.5) of the TSPA-LA Model, based on the time of the event, the top-side (upper surface of the DS) and bottom-side (lower surface of the DS) corrosion rates for Titanium Grade 7, and the initial plate thickness. The static load is defined by the fraction of the drift that is filled with lithophysal rubble ($FD_{LITH,j}$), as discussed in Section 6.6.1.3.4 and the resulting failure probability is applied to all zones of the repository.

Four two-dimensional look-up tables represent the probability of failure of DS plates at 0 percent, 10 percent, 50 percent, and 100 percent rockfall load (Figure 6.6-8 and DTN: MO0703PASEISDA.002_R4 [DIRS 183156], Table 1-2). Each of these tables is a function of PGV and DS plate thickness. A two-stage linear interpolation process is used to determine the probability. The first step in this interpolation is to linearly interpolate within each of the four sections of Table 1-2 (DTN: MO0703PASEISDA.002_R4 [DIRS 183156]) using the values of PGV for the j^{th} event and of the plate thickness at the time of the j^{th} event. This first interpolation produces four failure probabilities for drifts that are 0 percent, 10 percent, 50 percent, and 100 percent filled with rubble. A second linear interpolation using the value of $FD_{LITH,j}$ (Equation 6.6-7) for the j^{th} event versus the failure probabilities at these four points determines the probability of DS plate failure. Plate failure is determined by comparing the calculated probability of failure for the j^{th} seismic event to a random number, R_j, between 0 and 1, corresponding to the j^{th} seismic event (DTN: MO0703PASEISDA.002_R4 [DIRS 183156], Section 1.1, Step 7c)

$$If \quad R_j \le P_{plate\ failure} \quad then \quad Plate\ Failure = true$$

$$else \quad Plate\ Failure = false\ .$$

For the j^{th} seismic event, the random number, R_j , used above is the same random number as was used in Section 6.6.1.3.4 for the determination of the occurrence of rockfall. This random number is also used for the determination of DS framework failure and WP damage. The reason for this is that a more intense ground motion is likely to simultaneously cause rockfall, WP damage, and DS failure because the intensity of the ground motion for a given PGV level is the major driver of system response. The probabilities of rockfall, WP damage, and DS failure are therefore expected to be highly correlated, rather than independent random variables (DTN: MO0703PASEISDA.002_R4 [DIRS 183156], Section 1.1, Step 5b). This random number is resampled for each event because the uncertainty in these probabilities is primarily caused by the aleatory uncertainty in the ground motions (DTN: MO0703PASEISDA.002_R4 [DIRS 183156], Section 1.1, Step 9c).

The consequence of plate failure is that all DSs fail as a barrier to seepage for the remainder of the simulation (DTN: MO0703PASEISDA.002_R4 [DIRS 183156], Section 1.1, Step 9d). In

addition, the damage abstraction for WPs under failed DSs (Section 6.6.1.2.2.2) will be applied to all WPs for the remainder of the simulation.

Framework Fragility

DS framework fragility is defined as the probability of collapsing the sides of a DS during a seismic event. Framework fragility is a function of PGV for the j^{th} seismic event, of the reduction in thickness of DS framework, and of the static load on the crown of a DS from rockfall. The reduction in thickness of DS plates is a feed from the WP and DS Degradation Model Component (Section 6.3.5) of the TSPA-LA Model, based on the time of the event, the external (upper surface of the DS) corrosion rate for Titanium Grade 7, and the corrosion rate multiplier that converts the Titanium Grade 7 corrosion rate to a corrosion rate appropriate for Titanium Grade 29 (DTN: SN0704PADSGCMT.002_R1 [DIRS 182188]). The external (upper surface) corrosion rate is appropriate because the predicted failure mode for the DS framework is collapse of the legs, and the supporting bulkheads on the sides of the DS are located on the exterior side of the DS plates. The external (upper surface) corrosion rate is applied to both sides of the framework components (double-sided corrosion). Double-sided corrosion is considered appropriate since the width of the bulkheads and stiffeners in the axial direction of the DS is usually less than the depth of the bulkheads and stiffeners normal to the plates. In this geometry, the thickness reduction of the width is the important parameter for buckling of the legs. Both sides of the bulkhead or stiffener that are perpendicular to the width will be exposed to the in-drift environment and experience general corrosion (DTN: MO0703PASEISDA.002_R4 [DIRS 183156], Section 1.1, Step 8; and SNL 2007 [DIRS 176828], Section 6.8.3.3). The static load is defined by the fraction of the drift that is filled with lithophysal rubble.

The calculation of probability of framework failure (i.e., buckling of the sidewalls) is analogous to that for plate failure. The probability is represented by four look-up tables, each a function of PGV and framework thickness reduction (Figure 6.6-9) and DTN: MO0703PASEISDA.002_R4 ([DIRS 183156], Table 1-3). A two-stage linear interpolation process is used to determine the probability of framework failure. The first step in this interpolation is to linearly interpolate within each of the four sections of Table 1-3 (DTN: MO0703PASEISDA.002_R4 [DIRS 183156]) using the values of PGV for the j^{th} event and of the reduction in framework thickness at the time of the j^{th} event. This first interpolation produces four conditional failure probabilities, for drifts that are 0 percent, 10 percent, 50 percent, and 100 percent filled with rubble. A second linear interpolation using the value of $FD_{LITH,j}$ for the j^{th} event versus the failure probabilities at these four points determines the probability of collapse. Framework failure is determined by comparing the calculated probability for the j^{th} seismic event to the same random number used to determine DS plate failure for the j^{th} seismic event (DTN: MO0703PASEISDA.002_R4 [DIRS 183156], Section 1.1, Step 8c).

If DS framework fails, DSs are considered collapsed but are not considered failed as a barrier to seepage. Two calculations were done to represent the response of CSNF (TAD-bearing) WPs, one with intact internals and one with degraded internals (SNL 2007 [DIRS 176828], Section 6.8.4). The expected damage for a CSNF WP surrounded by rubble was found to provide an upper bound for the damage to a CSNF WP with intact internals loaded by a collapsed DS. The results for degraded internals showed a higher level of damage which was consistent with the kinematic damage abstractions for CSNF WPs with degraded internals.

Separate calculations were not performed for CDSP WPs loaded by collapsed DSs. Since the calculations for the CSNF WPs were performed quasi-statically, it was anticipated that the response of the CDSP WPs would be very similar (SNL 2007 [DIRS 176828], Section 6.8.4). Therefore, after DS framework failure, but before DS plate failure, the damage abstractions for WPs surrounded by rubble are applied, if the WP internals are still intact. When the WP internals become degraded (after the first damage-causing event), the damage abstractions for WPs under intact DSs, but with degraded internals, apply until the DS plates also fail (DTN: MO0703PASEISDA.002_R4 [DIRS 183156], Section 1.1, Step 8e).

6.6.1.3.6 Implementation of WP Rupture and Puncture from Ground Motion

The rupture of a CSNF or CDSP WP that can move freely beneath a DS can occur only up until the time of DS plate failure. After DS plate failure, WPs are surrounded by rubble and the failure mechanism is abstracted to be WP puncture.

Ruptured Waste Packages

The probability of rupture for CSNF or CDSP WPs with intact internals is zero. For WPs with degraded internals, two rupture probabilities are calculated; one for incipient rupture, one for immediate rupture. For both CSNF and CDSP WPs, they are given by power laws in PGV (DTN: MO0703PASEISDA.002_R4 [DIRS 183156], Eq. 1-12, Eq. 1-13, Eq. 1-17, Eq. 1-18, and Table 1-17). There are three possible rupture states: immediate rupture, PR_{immed}; incipient rupture, PR_{incip}; and no rupture, PR_{none} (given by one minus the sum of the two rupture probabilities). The appropriate state is determined using a random number R_{ruptue}, and a counter, C, with the following logic:

$$\begin{array}{llll} \textit{If} & R_{rupture} < PR_{none} & \textit{then} & C = 0 \\ \textit{else if} & R_{rupture} < PR_{none} + PR_{incip} & \textit{then} & C = 1 \\ \textit{else} & & & C = 2\,. \end{array}$$

A counter value of 1 indicates an incipient condition for rupture after a single severe impact. A counter value of 2 indicates immediate rupture. The value of the counter is retained, so if an event is deemed to be incipient (C=1) and a subsequent seismic event is also deemed to be incipient, then a rupture will occur during the subsequent seismic event. Independent random numbers (not correlated) are used for the determination of rupture for CSNF and CDSP WPs.

When a WP is ruptured, the failed area is determined by sampling a uniform distribution with a lower bound of 0 m^2 and an upper bound equal to the cross-sectional area, 2.78 m^2 and 3.28 m^2 for CSNF and CDSP WPs, respectively (DTN: MO0703PASEISDA.002_R4 [DIRS 183156], Table 1-20). This failed area allows advective flow into and advective and diffusive transport out of ruptured CSNF or CDSP WPs.

Punctured Waste Packages

The probability of rupture for a WP surrounded by rubble is represented by two power laws in PGV (DTN: MO0703PASEISDA.002_R4 [DIRS 183156], Equations 1-22 and 1-23 and Table 1-17), one that applies to WPs with 23-mm-thick OCBs and one that applies to WPs with

17-mm-thick OCBs. For thicknesses greater than 23 mm or less than 17 mm, the 23-mm power law and 17-mm power law are used, respectively, for the probabilities of puncture. For intermediate thicknesses, linear interpolation is used.

The determination of the occurrence of puncture is done by comparing the calculated probability of puncture to a random number between 0 and 1. This random number is not correlated with any of the other random numbers used either for assessing the probability of rockfall, WP crack damage, or rupture (Section 6.6.1.3.4). If the random number is less than or equal to the calculated probability of puncture, then all CSNF or CDSP WPs are punctured by this seismic event. Note that the evaluation of puncture is done separately for CSNF and CDSP WPs because the probability depends on WP OCB thickness, which in turn depends on general corrosion rate.

When WPs are punctured, the failed area is determined by sampling a uniform distribution with a lower bound of 0 m^2 and an upper bound of 0.1 m^2 (DTN: MO0703PASEISDA.002_R4 [DIRS 183156], Section 1.1, Step 15c and Table 1-17). This failed area allows advective flow through the punctured WP and advective and diffusive transport out of the punctured WP.

6.6.1.3.7 Implementation of Waste Package Stress Corrosion Cracking Damage from Ground Motion

The damage to WP OCB surface has been abstracted to occur as a dense network of stress corrosion cracks (Sections 6.6.1.2.3 and 6.6.1.2.4). Both the probability of WP damage and the conditional probability distributions for the amount of damage have been abstracted to be functions of the PGV level for the seismic event and of the RST threshold for Alloy 22. Residual stress threshold (RST) for Alloy 22 is a random variable that is sampled once per realization from a uniform distribution between 90 and 105 percent of the yield strength of Alloy 22 (DTN: MO0703PASEISDA.002_R4 [DIRS 183156], Table 1-15). The random variable is sampled once per realization because it represents the epistemic uncertainty in the RST.

The abstractions for probability of WP damage and for the conditional damaged area are functions of whether or not the WP internals are degraded. The internals are considered intact until the first event that causes damage, or breach by nominal general corrosion processes, if this occurs first. After this time, WPs are considered to have degraded internals and the probability and damage abstractions for degraded internals are used.

Probability of WP Damage

The probability of WP damage is represented as a look-up table that uses PGV and RST as the independent variables. The typical look-up table for probability of damage at a given WP OCB thickness has up to six values of PGV (forming the rows of the table) and three values of RST (90 percent, 100 percent, and 105 percent of the yield strength of Alloy 22). A piecewise linear interpolation scheme is used between the points in each look-up table, avoiding the need for a functional fit to a probability surface. Figures 6.6-10, 6.6-11, and 6.6-15 illustrate these probabilities.

The determination of damage is done by comparing the calculated probability of damage to a random number between 0 and 1. The random number (R_j) is the same random number used for the determination of rockfall and DS fragility for the j^{th} seismic event (Sections 6-6.1.3.4

and 6.6.1.3.5). If the random number is less than or equal to the calculated probability of damage, then all CSNF or CDSP WPs are damaged by the j^{th} seismic event and the internals of CSNF or CDSP WPs are considered degraded for all subsequent seismic events.

Probability of Damage to CSNF and CDSP Waste Packages under Intact Drip Shields

For WPs under an intact DS, with intact internals, two look-up tables represent the probability of damage to a WP with OCB thickness 23 mm. One table represents the CSNF WPs and one represents the CDSP WPs. A single table look-up is done in each table to obtain the probability of damage.

For WPs under an intact DS, with degraded internals, there are four look-up tables that represent the probability of damage to WPs, two representing CSNF and CDSP WPs at OCB thickness 23 mm and two representing CSNF and CDSP WPs at OCB thickness 17 mm. The current WP thickness is used to interpolate between the values from the look-up tables at 23 mm and 17 mm. The probability of damage is set equal to the value at 23 mm if the average OCB thickness is greater than 23 mm. The probability is set equal to the value at 17 mm if the average OCB thickness is less than 17 mm.

Probability of Damage to CSNF and CDSP Waste Packages Surrounded by Rubble

For WPs surrounded by rubble, four look-up tables represent the probability of damage to CSNF and CDSP WPs of thickness 23 mm and 17 mm with degraded internals. Two tables represent the probability of CSNF WP failure at 23 mm and 17 mm OCB thicknesses and two tables represent the probabilities of CDSP WP failure at 23 mm and 17 mm OCB thicknesses. The current WP thickness is used to interpolate between the values from the look-up tables at 23 mm and 17 mm. If the current WP thickness lies outside this range, the 23 mm or 17 mm table values are used.

Calculation of WP Damage Area

The conditional (nonzero) damaged areas are represented by gamma distributions. The parameters for the gamma distributions are their mean and SDs. All gamma distributions are resampled for each event.

The damage abstractions for WPs with degraded internals are derived for two different thicknesses of the WP OCB, 23 mm and 17 mm. These are both represented by gamma distributions that must be sampled at the same level of probability (i.e., in a correlated manner) to allow interpolation between the two thicknesses. Three independent random numbers are used to maintain this correlation, one for damage to CSNF WPs under intact DSs, one for CDSP WPs under intact DSs, and one for damage to WPs surrounded by rubble. These random numbers are resampled for each event to represent the aleatory uncertainty in the ground motions.

If the OCB thickness is greater than 23 mm, the damaged area is conservatively set equal to the value at 23 mm. The damaged area is set equal to the value at 17 mm if the average OCB thickness is less than 17 mm.

The total damaged area increases with each seismic event that causes damage to the OCB. Total damaged area for CSNF or the CDSP WPs is the sum of the damaged areas for the first through j^{th} seismic events. Total damaged area cannot exceed the total surface area of a CSNF or CDSP WP, respectively.

Seismically damaged areas are represented as a dense network of stress corrosion cracks. The effective area for transport through the crack network is determined by the product of the total damaged area and the crack density per unit surface area. The crack density model developed for Alloy 22 was abstracted as a uniform distribution between 0.00327 and 0.0131 (DTN: MO0702PASTRESS.002_R2 [DIRS 180514], file: Model Output.doc, Table 8-15). This parameter represents epistemic uncertainty and is sampled once per realization.

Damage Area for CSNF and CDSP Waste Packages under Intact Drip Shields

The mean and SDs of the gamma distribution for damaged area for CDSP WPs with intact internals under intact DSs are quadratic functions in PGV and have coefficients that are linear in RST (DTN: MO0703PASEISDA.002_R4 [DIRS 183156], Tables 1-5 and 1-17). The parameters for CSNF WPs with intact internals under intact DSs are based on computational results at PGV = 4.07 m/s and RST = 90 percent, which will have the maximum damaged area and apply to all values of PGV and RST (DTN: MO0703PASEISDA.002_R4 [DIRS 183156], Section 1.1, Table 1-7, Step 14a, and Table 1-17). In spite of this conservatism, damage will still be zero at most values of PGV and RST because the damage is conditional on the probability of damage, and this probability is 0 except for a single point in the first five lines of Table 1-6 in Step 13(a) (DTN: MO0703PASEISDA.002_R4 [DIRS 183156]). There are two pairs of gamma distributions representing the damaged area for CSNF and CDSP WPs with degraded internals under intact DSs. One pair represents CSNF WPs and one pair represents CDSP WPs. Their means and SDs are quadratic functions in PGV and have coefficients that are linear in RST (Figure 6.6-13 and DTN: MO0703PASEISDA.002_R4 [DIRS 183156], Tables 1-7, 1-5, and 1-17).

Damage Area for CSNF and CDSP Waste Packages Surrounded by Rubble

There are two gamma distributions representing the conditional damaged area for CSNF WPs with 23-mm and 17-mm thick OCBs surrounded by rubble (degraded DSs). Their means and SDs are quadratic functions of RST, with no PGV dependence (Section 6.6.1.2.3) (Figure 6.6-16 and DTN: MO0703PASEISDA.002_R4 [DIRS 183156], Tables 1-9 and 1-17). The damage to CDSP WPs is represented by the same gamma distributions as those used for CSNF WPs, although the thicknesses of the OCBs for the CDSP and CSNF WPs may be different at the time of the j^{th} seismic event.

6.6.1.3.8 Waste Package Thickness Calculations

WPs and overlying DSs are partitioned among the five percolation subregions according to the partitioning described in Section 6.3.2.2.1. In the Seismic GM Modeling Case, the calculations for the probability and damaged area are a function of WP OCB thickness, which depends on the general corrosion rate of Alloy 22. The general corrosion calculation depends on temperature, and other parameters that vary at the percolation subregion level and with fuel type

(Section 6.3.5.1.2). Therefore, the time-dependent WP OCB thickness will be different for each of the five percolation subregions and for each of the two fuel types.

The general corrosion rate of the Titanium Grade 7 DSs is given by a distribution that is independent of percolation subregion parameters and will be the same for all DSs (Section 6.3.5.1.2).

The abstractions for WP degradation used in the Seismic GM Modeling Case require the spatially-averaged thickness of the WP OCB as a function of time. This calculation is done as part of the WP and DS Degradation Submodel calculations. The WAPDEG V4.07 software is run 10 times, once for each percolation subregion and fuel type, to produce a time history of WP thickness. This calculation is done separately from the calculation of WP breach used to feed the EBS Flow and Transport Model Component (Sections 6.3.6 and 6.3.8) for nominal corrosion processes. The general corrosion rate used for the feed to the Seismic GM Modeling Cases is done with an average rate rather than an extreme patch approximation to the general corrosion rate discussed in Section 6.3.5.1.2. The method discussed in Section 6.3.5.1.2 used the highest of four sampled corrosion rates (from the two-parameter Weibull distribution) to analyze general corrosion of the WP patch. For the purposes of the seismic abstractions, the average of the four sampled corrosion rates was used to generate the general corrosion rate fed to the WAPDEG v4.07 software (output DTN: MO0707WPDRIPSD.000 [DIRS 183005]). The GetThk_LA v1.0 (STN: 11229-1.0-00 [DIRS 181040]) software was used to post-process the thickness file output by the WAPDEG v4.07 software and generate a one-dimensional table of mean WP OCB thickness versus time. This mean thickness is a spatially-averaged WP OCB thickness over all the WPs in a particular percolation subregion for each fuel type.

Since the nominal corrosion processes calculated by the WAPDEG V4.07 software calculations are included in the Seismic GM Modeling Case, the inside-out corrosion that occurs after a seismic event has damaged a WP must be accounted for. The mean time of the first seismic event that causes WP damage must be passed as an input to the WAPDEG V4.07 calculations. However, the WAPDEG 4.07 calculations are done at the beginning of the simulation, before any seismic calculations are done. Therefore, a separate *a priori* calculation of the time that WPs are first damaged by a seismic event is carried out.

CSNF and CDSP WPs are considered to have intact internals before the first seismic damage event and the probability of damage for WPs with intact internals under intact DSs is not a function of WP thickness (Figures 6.6-10 and 6.6-11; and DTN: MO0703PASEISDA.002_R4 [DIRS 183156], Tables 1-4 and 1-6). However, for CSNF WPs, damage is not likely to occur before DS failure. In this case, the abstraction for the probability of damage for WPs surrounded by rubble with a 17 mm thickness is used as a conservative estimate of the probability of first failure time (Figure 6.6-15; and DTN: MO0703PASEISDA.002_R4 [DIRS 183156], Table 1-8). This estimate is conservative because it gives the highest possible probability of failure for a WP surrounded by rubble. The same approximation is used for CDSP WPs if the WP damage does not occur before DS failure. However, in the case of CDSP WPs, the probability of WP damage under intact DSs is higher (Figures 6.6-11).

6.6.1.3.9 Implementation of Fault Displacement Damage

The two simulations for Seismic FD Modeling Case are both run using pre-specified parameters (Table 6.6-3). The fraction of damage is set at 0.028, 0.056, or 0.084, for CSNF WPs, and at 0.0335, 0.067, or 0.101, for CDSP WPs. These values represent 1/3, 2/3, 3/3 of the ratio of lid area to WP surface area, for CSNF and CDSP WPs respectively.

The time of the seismic event is set to be 1,000 years, 20,000 years, 80,000 years, 200,000 years, 400,000 years, or 800,000 years, for the 1,000,000-year Seismic FD Modeling Case. For the 10,000-year Seismic FD Modeling Case, the time of the seismic event is set to be either 200 years, 800 years, 2,000 years, 4,000 years, 8,000 years, or 18,000 years.

The time at which the drifts fill with rubble is set to be the time of the seismic event. The DS damage fraction is set to 1.0.

The number of failed WPs is set to 100. This number is chosen so that there will be failed WPs in each percolation subregion. The dose calculation is then scaled by the ratio of the expected number of WP failures divided by 100 (Section 6.1.2.4.3, Equation 6.1.2-24).

For model development purposed, a unified sampling Seismic FD Modeling Case is also run. In the unified sampling case a single seismic event is modeled. The time of the seismic event is determined by sampling a log uniform distribution that spans the simulation duration. The mean annual exceedance frequency is sampled from a log uniform distribution with an upper bound of 2.5×10^{-7} per year, the largest frequency for for which fault displacement damage will occur (Section 6.6.1.2.3) and the same lower bound as for the Seimsic GM Modeling Case (10^{-8} per year). The expected number of WP failures due to fault displacement is extracted from a table over a series of mean annual exceedance frequency intervals for each of two WP groups (DTN: MO0703PASEISDA.002_R4 [DIRS 183156], Tables 1-14 and 1-20) and is rounded to the nearest integer. Note that inspection of the failure numbers shows that the maximum number of failures for the CSNF and CDSP WP groups is approximately 159 and 53, respectively. The failed area is determined by sampling a uniform distribution with a lower bound zero and upper bound equal to the area of the CSNF or CDSP WP lid (Section 6.6.1.2.3).

The amount of rubble in a drift following a seismic fault displacement event is 112 m^3/m in the lithophysal zones and 2.9 m^3/3 in the nonlithophysal zones output (SNL 2007 [DIRS 176828], Figure 6-63).

The DSs and cladding corresponding to fault-failed WPs are also considered to be completely failed (DTN: MO0703PASEISDA.002_R4 [DIRS 183156], Section 1.1, Step 21)

6.6.2 Interaction of Seismic Scenario Class Submodels with other TSPA-LA Submodels

The rockfall accumulation calculations described in Section 6.6.1.3.4 have consequences with respect to other TSPA-LA submodels.

6.6.2.1 Drift Seepage Submodel and Drift Wall Condensation Submodel Modifications for Seismic Disruption

The Drift Seepage Submodel's (Section 6.3.3.1) drift seepage simulations produce response surfaces in the form of look-up tables for the seepage flux into the degraded drifts. The values of the independent variables in the look-up tables are local percolation flux, permeability, and capillary strength. For the Seismic Scenario Class, drift collapse occurs in both lithophysal and nonlithophysal zones. Partial collapse, followed by full collapse, can occur in the lithophysal units. The switch from noncollapsed to collapsed conditions depends on rockfall volume in the drifts. For lithophysal rock, if rockfall volumes in the drifts are less than or equal to 5 m^3/m of drift length, the intact drift seepage response surface table is utilized in the analysis. If rockfall volumes in the drifts are greater than 60 m^3/m of drift length, the collapsed drift seepage response surface is utilized in the analysis. If rockfall volumes (per unit drift length) in the drifts are between 5 m^3/m and 60 m^3/m, seepage values are linearly interpolated between the two response surfaces (Section 6.3.3.1.3). In the nonlithophysal units, once a specified degree of drift collapse has occurred, the intact-drift seepage model is no longer appropriate. Therefore, in the nonlithophysal zone, if rockfall volumes in the drifts are less than or equal to 0.5 m^3/m, the intact drift seepage response surface is utilized; if not, the percolation rates are utilized instead of seepage rates (Section 6.3.3.1.3).

The rockfall volume in the drifts is a feed from the seismic rockfall calculations to the drift seepage calculations. The rockfall volumes in the lithophysal and nonlithophysal zones are calculated as described in Section 6.6.1.3.4, for the Seismic GM Modeling Case 1,000,000–year simulation, which uses GoldSim-sampled event sequences. For the 1,000,000-year Seismic FD Modeling Case and the 10,000-year Seismic FD Modeling Case simulations, rockfall volumes are pre-specified (Table 6.6-3). The Drift Wall Condensation Abstraction (Section 6.3.3.2.2) calculates a probability of condensation occurrence on the drift walls at a WP location and, if condensation occurs, a rate of condensation. For the Seismic Scenario Class, drift collapse is expected in the lithophysal regions but is not expected in the nonlithophysal units. Condensation occurs on drift walls above DSs in the nonlithophysal units at all times. In contrast, there is no condensation in the lithophysal units after drift collapse. The Seismic Scenario Class modeling cases calculate the time of drift collapse in terms of the time at which rubble fills the lithophysal drifts. For the Seismic GM Modeling Case 1,000,000-year simulation, this calculation is described in Section 6.6.1.3.4. For the 1,000,000-year Seismic FD Modeling Case and the 10,000-year Seismic FD Modeling Case simulations, drift collapse times are pre-specified (Section 6.6-4) and are set to either the time of the first seismic event or are set to be non-collapsed.

6.6.2.2 Engineered Barrier System Thermal-Hydrologic Environment Submodel Modifications for Seismic Disruption

Seismically induced ground motion can cause drift collapse in the lithophysal zones, requiring an adjustment to the temperature and relative humidity histories to account for the presence of rubble on WPs. The adjusted temperature and relative humidity histories for the Seismic Scenario Class modeling cases are provided by a supplemental analysis performed on the EBS TH Environment Submodel thermal-hydrology data (DTN: LL0702PA027MST.082_R0 [DIRS 179590]). The data tracking number provides eight files containing time-dependent

temperature adjustments and eight files containing time-dependent relative humidity adjustments: one file for each of the six representative CSNF and two representative CDSP WP/DS pairs (Section 6.3.2.2). Each file contains two types of temperature/relative humidity adjustments, one associated with a collapsed drift with low thermal-conductivity rubble and one associated with a collapsed drift with high thermal-conductivity rubble. The assignment of a low or high thermal-conductivity adjustment is based on sampling a discrete distribution with equal probability for high or low (SNL 2007 [DIRS 181383], Section 6.2.10.3).

The Seismic GM and FD Modeling Cases calculate the time required to fill the drift with rockfall, after which the adjustments apply. For the Seismic GM Modeling Case 1,000,000-year simulation, this time is based on the calculations described in Section 6.6.1.3.4. For the 1,000,000-year Seismic FD Modeling Case and the 10,000-year Seismic FD Modeling Case simulations, drift fill times are pre-specified (Section 6.6.1.3.9) and are set to either the time of the first seismic event or the end of the simulation. The adjusted temperature and relative humidity values are used for both lithophysal and nonlithophysal zones in the TSPA-LA Model because the TSPA-LA Model does not distinguish between the lithophysal and nonlithophysal components of a percolation subregion.

6.6.2.3 Waste Package and Drip Shield Degradation Submodel Modifications for Seismic Disruption

Nominal corrosion processes are included in the Seismic GM Modeling Case when calculating consequences after 10,000 years. When WPs are first damaged by a seismic event, the resulting cracks will impact the nominal corrosion processes. In particular, corrosion on the inner surface of a WP OCB (inside-out corrosion) will be initiated. An *a priori* calculation is done to determine the time of the first seismic event that causes WP damage and this time is fed to the input vector for the WAPDEG V4.07 software. This time will be different for CSNF and CDSP WPs. The WAPDEG V4.07 software will initiate an inside-out corrosion event at that time, thus accelerating the corrosion processes that ultimately lead to WP breach. This effect is also included in the separate WAPDEG V4.07 calculations that determine mean WP thickness for each percolation subregion. These calculations are used by the Seismic GM Modeling Case as input to the WP damage calculations (Section 6.6.1.3.8).

6.6.2.4 Waste Package Localized Corrosion Initiation Submodel for Seismic Disruption

The Seismic Scenario Class does not include the potential effect of crown-seepage initiated localized corrosion on the WP outer surface. Although crown-seepage induced localized corrosion is possible for both the Seismic GM and FD Modeling Cases, a stand-alone localized corrosion initiation analysis has been carried out to determine that the environmental conditions required for localized corrosion initiation are present only for the first 4,000 years after repository closure. Beyond this time, the chemistry of the seepage water is benign, and localized corrosion no longer occurs. This stand-alone analysis is documented in Section 6.3.5.2. The temperature, pH, chloride-ion concentration, and nitrate-ion concentrations in aqueous solutions on the WP outer surface are the primary factors that determine the potential for initiating localized corrosion. In addition, localized corrosion can only occur if crown seepage water contacts the WP outer surface, i.e., if the DS is failed.

In the Seismic GM Modeling Case simulations, there is a low probability (Figure 7.3.2-16) of DS plate failure occurring before 4,000 years. Section 7.3.2.6.1.3.2 discusses the justification for not considering localized corrosion due to these early DS failures. In the Seismic FD Modeling Case simulations, DS can be failed at early times, where environmental conditions are suitable for localized corrosion initiation. However, it is assumed that the advective damage due to the fault displacement is sufficient to account for the effects of localized corrosion. This assumption has been verified by simulation runs which show that the dose is insensitive to increasing the fraction of damaged area beyond 1/3 of the WP cross-sectional area (Section 7.3.2.7 and Figure 7.3.2-25).

A description of localized corrosion of the WP outer surface is provided in Section 6.3.5.2. Section 6.3.5.2 describes the Localized Corrosion Initiation Analysis and Localized Corrosion Penetration Rate Abstraction that form the components of the Localized Corrosion Initiation Submodel. Section 6.3.5.2.1 provides the conceptual models for these localized corrosion processes, and Section 6.3.5.2.2 describes the model abstractions.

For the localized corrosion initiation analysis, a temperature constraint is applied to the seepage flux after drift collapse in the lithophysal zones. Specifically, seepage onto WPs is set to zero for the period of above-boiling temperatures by using a 100°C threshold temperature at a WP surface. This constraint implies that seepage can enter the drift and be diverted through the rubble to the invert beneath a WP, but it cannot contact a WP surface until the surface temperature drops to less than 100°C. This threshold temperature is based on a sensitivity study of seepage arrival times at a DS crown for a collapsed drift that is filled with rubble (SNL 2007 [DIRS 181383], Section 6.3.7.3 and Table 6.3-44). This study considers rubble with high and low values of thermal conductivity and seepage magnitudes that vary between 10 liter/yr/WP and 1,000 liter/yr/WP. The temperature threshold of 100°C is a reasonable upper bound to the ranges of WP temperatures that significantly delay the arrival of seepage at a DS crown. A 100°C temperature is, therefore, an appropriate threshold to limit the presence of liquid seepage in a rubble-filled drift. This temperature constraint on seepage flux after drift collapse is applied only in the Localized Corrosion Initiation and Propagation Analysis. The constraint is not applied to the calculation of seepage flux in the Drift Seepage Submodel (Section 6.3.3.1).

The Localized Corrosion Initiation Analysis also accounts for changes in temperature and relative humidity due to the presence of rubble after a seismic event. The Localized Corrosion Initiation Analysis uses the same eight WP emplacement configurations to calculate temperature and relative humidity adjustments discussed in Section 6.6.2.2, for the purposes of localized corrosion initiation. The rubble fill time is based on the calculations described in Section 6.6.1.3.4 for the lithophysal zones. In addition, the Localized Corrosion Initiation Analysis does distinguish between lithophysal and nonlithophysal regions and, therefore, the temperature and relative humidity adjustments are applied only when a WP location lies in the lithophysal zone. For the nonlithophysal zones, examination of Tables 6-30 and 6-31 in *Seismic Consequence Abstraction* (SNL 2007 [DIRS 176828]) shows that all of the calculated rockfall volumes are significantly less than those in the lithophysal zones at the same PGV level. Therefore, the temperature and relative humidity adjustments are not applied in the nonlithophysal zones.

6.6.3 Model Component Consistency and Conservatisms in Assumptions and Parameters

To enhance understanding of the complex interactions within the TSPA-LA Model, a discussion of consistency among model components and submodels and identification of conservative assumptions in abstractions, process models, and parameter sets supporting the Seismic Scenario Class are discussed below.

6.6.3.1 Consistency of Assumptions

Degradation of the Internal Structures After Breach of Outer Corrosion Barrier—In the Seismic GM Modeling Case calculations once the OCB is breached due to seismic damage it is assumed that the internal structure of the WP would degrade as a structural element, quickly leading to an overall loss of WP structural strength by the time of next seismic event. As a result the damage abstractions for the fully degraded internals are applied after the WP is breached for the first time. This is a conservative assumption and inconsistent with the slow degradation of steel internals modeled in the EBS Transport model, where the stainless steel is expected to last for tens of thousands of years on average thus maintaining the integrity of the WP for much longer duration than the time to the next seismic event.

Effect on the TSPA-LA Model—Using the WP damage abstraction for the fully degraded internals subsequent to the seismic event that leads to the first breach is conservative as it would lead to larger damage area on the WP due to lower structural strength of the WP. This would likely result in a greater diffusive release rate out of the WP.

6.6.3.2 Identification of Conservatisms in Submodels and Abstractions

Conservatism in Ground Motion Calculations—The use of a bounded hazard curve for PGV does not mean that all three components of a ground motion are bounded. Only one horizontal component of the ground motion is scaled to a given PGV value on the bounded hazard curve (SNL 2007 [DIRS 176828], Section 6.4.3). In developing the time histories used in the kinematic and structural response calculations, the second horizontal component and the vertical component are not directly scaled, but rather are allowed to vary to maintain the inter-component variability of the original accelerogram. This means that these components can vary substantially even when the PGV for the first horizontal component is at a fixed value. This inter-component variability reflects the aleatory uncertainty inherent in vibratory ground motions. In some cases, this results in PGV values for these components that exceed the maximum scaled value for the first horizontal component. Thus, the damage abstractions, although parameterized using one horizontal component, in some cases represent damage associated with larger PGVs on the other components. Thus, although the hazard curve for horizontal PGV is bounded, the damage abstractions include larger, unbounded PGVs on the other components as given in Acceptance Criterion 3, Propagation of Uncertainty into TSPA (SNL 2007 [DIRS 176828], Section 8.2). Alternate ground motions with bounded components are not available to quantify this conservatism.

Seismic Failure Criteria—The seismic abstractions for WPs and DSs make use of two failure criteria: a RST and the ultimate tensile strain. If the residual stress from mechanical damage exceeds the stress threshold for the barrier, then the affected area(s) are represented as a network

of stress corrosion cracks. The RST for WPs is based on a uniform distribution between 90 percent and 105 percent of the yield strength for Alloy 22. The RST for Titanium Grade 7 is conservatively set to a constant value of 80 percent of its yield strength (and for Titanium Grade 29 at 50 percent of its yield strength). These thresholds are conservative estimates for the initiation of SCC (SNL 2007 [DIRS 181953], Sections 6.2.2 (Alloy 22), 6.8.3.1.3 (Titanium Grade 7), and 6.8.3.2.3 (Titanium Grades 25 and 29)). The potential for tearing or rupture of EBS components is based on the ultimate tensile strain for Alloy 22 and Titanium Grade 7, with a conservative knockdown factor of 2 (the maximum value), which adjusts the uniaxial data for ultimate tensile strain in a multidimensional stress field .

Spatial Variability—Spatial variability in the mechanical response of EBS components to vibratory ground motion has not been represented in the TSPA-LA Model. Damage to the WP and DS from vibratory ground motion is constant throughout the repository for each seismic event. Although spatial variability is not included within the TSPA-LA Model, it has been included in the kinematic calculations through the variability of friction factors on a package-by-package basis and in the abstraction of damaged areas for the two or three central WPs in the kinematic calculations. Lack of spatial variability is not important for estimating the mean annual dose from the Seismic Scenario Class. The mean dose is accurately estimated because the sum of the mean doses from groups of WPs with different damage levels is equal to the mean of the sum of the doses from the individual groups. Using a constant mean value for the damage is an accurate approach for calculating the mean annual dose from the repository (SNL 2007 [DIRS 176828], Section 1.2).

Conservatism in Hazard Curve—The development of hazard curves for vibratory ground motion and fault displacement included an expert elicitation—(*Probabilistic Seismic Hazard Analyses for Fault Displacement and Vibratory Ground Motion at Yucca Mountain, Nevada,* Milestone SP32IM3, September 23, 1998 (CRWMS M&O 1998 [DIRS 103731]). Evaluations by multiple experts were made within a structured process designed to minimize uncertainty due to uneven or incomplete knowledge and understanding (Budnitz et al. 1997 [DIRS 103635]). The weighted alternative interpretations were expressed by the use of logic trees. Each pathway through the logic tree represented a weighted interpretation of the seismotectonic environment of the site for which a seismic hazard curve was computed. The result of computing the hazard for all relevant pathways was a distribution of hazard curves representing the full variability and uncertainty in the hazard at Yucca Mountain. The Seismic Scenario Class for the TSPA-LA Model uses the mean hazard curves for PGV and for fault displacement. Each mean hazard curve is defined as an average of the distribution of hazard curves and each typically lies above the 80th percentile of the distribution for high intensity ground motions (i.e., at low annual exceedance frequencies) because the average is dominated by the larger values of the distribution (SNL 2007 [DIRS 176828], Section 6.4.1). The use of the mean hazard curves ensures a conservative representation of the seismic hazard in the TSPA-LA Model. An analysis that includes a suite of hazard curves to represent epistemic uncertainty was done as part of the PMA (Appendix C).

Conservatism in Initiation of Inside-Out Corrosion Processes—Corrosion on the inner surface of a WP OCB (inside-out corrosion) is initiated at the time of the first seismic event that causes WP damage. An *a priori* calculation is done to determine the time of the first seismic event that causes WP damage. The probability that a CSNF WP with intact internals under intact

DSs will be damaged by a seismic event is small (Figure 6.6-10). Therefore, DS failure is likely to occur before a damaging seismic event occurs. If such a WP has not been damaged, its internals will still be intact even though it is under a failed DS and surrounded by rubble. However, there is no abstraction for probability of damage for a CSNF WP with intact internals under a failed DS. Such a WP is also likely to have a reduced shell thickness. Therefore the probability of damage to a CSNF WP with degraded internals and an OCB thickness of 17 mm is used as a surrogate to the damage on a CSNF WP with intact internals under a failed DS. This is a conservative assumption, as can be seen from an examination of Figure 6.6-15.

6.6.4 Alternative Conceptual Model(s) for Seismic Scenario Modeling Cases

A brief description of the Seismic Scenario Class ACMs is presented below. The Seismic Scenario Class ACMs are also summarized in Table 6.6-4.

Lithophysal and Nonlithophysal Rock—Alternative modeling approaches were evaluated for the conceptual and computational models of lithophysal and nonlithophysal rockfall (BSC 2004 [DIRS 166107], Section 7.4). A standard approach for solving excavation stability problems is the use of numerical models based on continuum mechanics. Continuum models use constitutive relations to describe the mechanical behavior of a material. The use of a continuum model requires that the mechanical effects of fractures be lumped into the constitutive relationships. Continuum models are unable to predict instabilities such as fracture and rockfall (BSC 2004 [DIRS 166107], Section 7.4.1).

The ACM based on continuum mechanics (BSC 2004 [DIRS 166107], Section 7.4.1) was not used to represent rockfall. The estimation of rockfall requires that the modeling technique and mechanical material model be capable of representing fracture of the rock mass and separation of the intact rock mass into blocks. The discontinuum approach is more suitable for these purposes and was therefore adopted for modeling the drift degradation processes that occur after a seismic event (BSC 2004 [DIRS 166107], Section 7.4.2).

Fault Displacement WP Damage Abstraction—The damage abstraction for fault displacement was compared to an ACM proposed by Waiting et al. (SNL 2003 [DIRS 164449], described in *Seismic Consequence Abstraction* (SNL 2007 [DIRS 176828], Section 6.11.6). The ACM considered the probability-weighted number of WP failures from fault displacement and the number of fault intersections with emplacement drifts. The ACM, based on the use of historical data for fault displacement in the western United States, provided results that are consistent with the base case model for both the probability weighted number of WP failures and the number of fault intersections with the emplacement drifts (SNL 2007 [DIRS 176828], Section 6.11.6).

The ACM based on historical western United States data was not used in the TSPA-LA Model. The damage abstraction used in the TSPA-LA Model is based on hazard curves specific to Yucca Mountain. Nevertheless, the agreement between the two models is very good and this adds confidence to the TSPA-LA Model damage abstraction.

Effective Cross-sectional Area for Transport—The effective cross-sectional area for transport out of Alloy 22 WPs through a network of stress corrosion cracks is given by a crack area density based on two conceptual models (SNL 2007 [DIRS 181953], Section 6.7.3). The first

conceptual model is based on a hexagonal array of randomly oriented cracks, while the second conceptual model is based on a hexagonal array of cracks in parallel rows. The distribution for crack area density used in the TSPA-LA Model is based on both conceptual models. An alternative conceptual model for crack area density is presented in *Stress Corrosion Cracking of Waste Package outer barrier and Drip Shield Materials* (SNL 2007 [DIRS 181953] Section 6.7.4). The alternative model considers a circular geometry circumscribed by a single through-wall crack.

The ACM was not used for the TSPA-LA Model implementation of seismic crack density. The hexagonal geometry represents a high effective density of individual cracks and the two hexagonal geometry conceptual models are considered conservative representations. The ACM analysis which uses circular geometry is considered a limiting realistic case (SNL 2007 [DIRS 181953], Section 6.7.2).

Conditional Probability Distributions for Damaged Areas—The seismic consequence abstractions have considered ACMs for the conditional probability distributions representing damaged areas on the WP, damaged areas on the DS, and the volume of rockfall from a seismic event. These alternate distributions include the gamma, normal, log-normal, Weibull and triangular distributions, as presented in Sections 6.5.1.4, 6.5.2.4, 6.6.1.4, 6.6.2.4, 6.7.1.3, 6.7.2.4, 6.9.4, and 6.10.2.8 of *Seismic Consequence Abstraction* (SNL 2007 [DIRS 176828]). Gamma distributions generally provided simpler and more accurate representations of the statistical observations than normal, log-normal, log-triangular, and Weibull distributions. The exception to the use of gamma distributions is that the fragility analyses (for DS plates and framework) have used log-normal representations to simplify manipulation of products and quotients of random variables.

The alternative conditional probability distributions for WP damaged areas were investigated, in the sections noted above, but not used since gamma distributions provided the simplest and most accurate representation of the data.

Table 6.6-1. Expected Waste Package Failure Due to Fault Displacement

Annual Exceedance Frequency (1/yr)	Expected Number of Failures – CSNF (TAD) Group	Annual Exceedance Frequency (1/yr)	Expected Number of Failures – CDSP Group
$> 2.2 \times 10^{-7}$	0	$> 2.5 \times 10^{-7}$	0
1.4×10^{-7} to 2.2×10^{-7}	19.5	1.6×10^{-7} to 2.5×10^{-7}	6.5
7.8×10^{-8} to 1.4×10^{-7}	27.7	8.6×10^{-8} to 1.6×10^{-7}	9.3
2.6×10^{-8} to 7.8×10^{-8}	30.7	2.9×10^{-8} to 8.6×10^{-8}	10.3
1×10^{-8} to 2.6×10^{-8}	158.8	1×10^{-8} to 2.9×10^{-8}	53.2

Source: DTN: MO0703PASEISDA.002_R4 [DIRS 183156], Table 1-14. See NOTES: for an explanation of the values in rows 4 and 5 of columns 2 and 4.

NOTE: TAD = transportation, aging, and disposal (canister); CSNF = commercial spent nuclear fuel; CDSP = co-disposed (waste package).

Table 6.6-2. Uncertain Inputs Used in the Seismic Scenario Class

TSPA-LA Parameter Name	Description	Units	Distribution	Remarks
Epistemic Parameters				
Stress_Thresh_A22_a (RST)	Residual stress threshold of Alloy 22.	None	Uniform(90,105)	DTN: MO0703PASEISDA.002_R4 [DIRS 183156], Table 1-15
Vol_Rubble_Max_Lith_a (MAX_RUBBLE_VOLUME)	Volume of lithophysal rock that must fall to fill the drift.	m^3/m	Uniform(30,120)	DTN: MO0703PASEISDA.002_R4 [DIRS 183156], Table 1-16
Vol_Rubble_Max_NonLith_a (MAX_BLOCK_VOLUME)	Volume of nonlithophysal rock that must fall to fill the drift.	m^3/m	Uniform(30,120)	DTN: MO0703PASEISDA.002_R4 [DIRS 183156], Table 1-16
DS_Crack_Area_Density_a	Crack area per unit of seismic DS damage.	None	Uniform(0.00467, 0.01875)	MO0702PASTRESS.002_R2 [DIRS 180514], file: Model Output DTN.doc, Table 8-15
WP_Crack_Area_Density_a	Crack area per unit area of seismic WP damage.	None	Uniform(0.00327, 0.0131)	MO0702PASTRESS.002_R2 [DIRS 180514], file: Model Output DTN.doc, Table 8-15
Aleatory Parameters				
Exceedance_Frequency_a (LAMBDA)	Annual exceedance frequency for the seismic hazard.	1/yr	Uniform(Seismic_Lambda_Min, Seismic_Lambda_Max) Seismic_Lambda_Min=$1x10^{-8}$ (LAMBDA_MIN) Seismic_Lambda_Max=$4.287x10^{-4}$ (LAMBDA_MAX)	DTN: MO0703PASEISDA.002_R4 [DIRS 183156], Table 1-15
Rubble_Vol_Lith_a (LITH_VOL)	Distribution used to calculate the rubble area deposited around the DS / WP in the last seismic event.	m^3/m	Gamma Distribution Mean: LITH_MU SD: LITH_SIGMA	DTN: MO0703PASEISDA.002_R4 [DIRS 183156], Table 1-16
Rubble_Vol_NonLith_a (NONLITH_VOL)	Distribution used to calculate the rubble volume deposited around the DS / WP in the last seismic event (nonlithophysal zones).	m^3/m	Gamma Distribution Mean: NONLITH_MU SD: NONLITH_SIGMA	DTN: MO0703PASEISDA.002_R4 [DIRS 183156], Table 1-16
Ln_Dyn_Load_DS (DS_LOAD_LN)	Dynamic load on the DS due to a seismic event.	None	Normal Distribution Mean: DSLOAD_LAMBDA SD: 0.536 (DSLOAD_BETA_	DTN: MO0703PASEISDA.002_R4 [DIRS 183156], Table 1-18

Table 6.6-2. Uncertain Inputs Used in the Seismic Scenario Class (Continued)

TSPA-LA Parameter Name	Description	Units	Distribution	Remarks
Aleatory Parameters (continued)				
Corr_TAD_Dam_DS_Intact_a	Random number for maintaining correlation while sampling the TAD-bearing WP damage gamma distributions for intact DSs.	None	Uniform(0,1)	DTN: MO0708TSPAGENT.000, file: AB-TSPA-DTN-5 (PEF 132)
Corr_CDSP_Dam_DS_Intact_a	Random number for maintaining correlation while sampling the CDSP WP damage gamma distributions for intact DSs.	None	Uniform(0,1)	DTN: MO0708TSPAGENT.000, file: AB-TSPA-DTN-5 (PEF 132)
Corr_WP_Dam_DS_Failed_a	Random number for maintaining correlation while sampling the WP (CDSP and TAD) damage gamma distributions for failed DSs.	None	Uniform(0,1)	DTN: MO0708TSPAGENT.000, file: AB-TSPA-DTN-5 (PEF 132)
Gamma_A_Intact_TAD (DA_TADi23_GAMMA)	Damage to a TAD-bearing WP of thickness 23 mm with intact internals under an intact DS.	m^2	Gamma Distribution Mean: 0.00408 (DA_TADi23_MU) SD: 0.0013 (DA_TADi23_SIGMA)	DTN: MO0703PASEISDA.002_R4 [DIRS 183156], Table 1-17
Gamma_A_Degrdd_TAD (DA_TADd23_GAMMA)	Damage to a TAD-bearing WP of thickness 23 mm with degraded internals under an intact DS.	m^2	Gamma Distribution Mean: DA_TADd23_MU SD: DA_TADd23_SIGMA	DTN: MO0703PASEISDA.002_R4 [DIRS 183156], Table 1-17
Gamma_B_Degrdd_TAD (DA_TADd17_GAMMA)	Damage to a TAD-bearing WP of thickness 17 mm with degraded internals under an intact DS.	m^2	Gamma Distribution Mean: DA_TADd17_MU SD: A_TADd17_SIGMA	DTN: MO0703PASEISDA.002_R4 [DIRS 183156], Table 1-17
Gamma_A_Intact_CDSP (DA_CDSPi23_GAMMA)	Damage to a CDSP WP of thickness 23 mm with degraded internals under an intact DS.	m^2	Gamma Distribution Mean: DA_CDSPi23_MU SD: DA_CDSPi23_SIGMA	DTN: MO0703PASEISDA.002_R4 [DIRS 183156], Table 1-17
Gamma_A_Degrdd_CDSP (DA_CDSPd23_GAMMA)	Damage to a CDSP WP of thickness 23 mm with degraded internals under an intact DS.	m^2	Gamma Distribution Mean: DA_CDSPd23_MU SD: DA_CDSPd23_SIGMA	DTN: MO0703PASEISDA.002_R4 [DIRS 183156], Table 1-17
Gamma_B_Degrdd_CDSP (DA_CDSPd17_GAMMA)	Damage to a CDSP WP of thickness 17 mm with degraded internals under an intact DS.	m^2	Gamma Distribution Mean: DA_CDSPd17_MU SD: DA_CDSPd17_SIGMA	DTN: MO0703PASEISDA.002_R4 [DIRS 183156], Table 1-17

Table 6.6-2. Uncertain Inputs Used in the Seismic Scenario Class (Continued)

TSPA-LA Parameter Name	Description	Units	Distribution	Remarks
Aleatory Parameters (continued)				
Gamma_A_Degrdd_WP_NoDS (DA_23_GAMMA)	Damage to a CDSP WP of thickness 23 mm with degraded internals under a degraded DS.	m^2	Gamma Distribution Mean: DA_23_MU SD: DA_23_SIGMA	DTN: MO0703PASEISDA.002_R4 [DIRS 183156], Table 1-17
Gamma_B_Degrdd_WP_NoDS (DA_17_GAMMA)	Damage to a CDSP WP of thickness 17 mm with degraded internals under a degraded DS.	m^2	Gamma Distribution Mean: DA_17_MU SD: DA_17_SIGMA	DTN: MO0703PASEISDA.002_R4 [DIRS 183156], Table 1-17
RN_DSF_a (RN_DSF)	Random number to determine rockfall damage, WP damage, and drip shield plate and/or framework failure.	None	Uniform(0,1)	DTN: MO0703PASEISDA.002_R4 [DIRS 183156], Table 1-15
RN _Rupture_TAD_a	Random number used to determine rupture TAD of WPs under intact DSs, due to multiple impacts.	None	Uniform(0,1)	DTN: MO0708TSPAGENT.000, file: AB-TSPA-DTN-5 (PEF 132)
RN_Rupture_CDSP_a	Random number used to determine rupture of CDSP WPs under intact DSs, due to multiple impacts.	None	Uniform(0,1)	DTN: MO0708TSPAGENT.000, file: AB-TSPA-DTN-5 (PEF 132)
RN_Puncture_a (RN_PUNC)	Random number used to determine puncture of WPs under failed DSs, due to multiple impacts.	None	Uniform(0,1)	DTN: MO0703PASEISDA.002_R4 [DIRS 183156], Table 1-17
TAD_Rupture_Area_a (FAILED_AREA_TAD)	Failed area of the TAD-bearing WP due to WP rupture damage.	m^2	Uniform(0, 2.78)	DTN: MO0703PASEISDA.002_R4 [DIRS 183156], Table 1-20
CDSP_Rupture_Area_a (FAILED_AREA_CDSP)	Failed area of the CDSP WP due to WP rupture damage.	m^2	Uniform(0, 3.28)	DTN: MO0703PASEISDA.002_R4 [DIRS 183156], Table 1-20
Puncture_Area_a (PP_AREA)	Failed area when WPs surrounded by rubble are punctured.	m^2	Uniform(0, 0.1)	DTN: MO0703PASEISDA.002_R4 [DIRS 183156], Table 1-17
TAD_Failed_Area_a (FAILED_AREA_TAD)	Failed area of the TAD WP due to fault displacement damage.	m^2	Uniform(0,2.78)	DTN: MO0703PASEISDA.002_R4 [DIRS 183156], Table 1-20
CDSP_Failed_Area_a (FAILED_AREA_CDSP)	Failed area of the CDSP WP due to fault displacement damage.	m^2	Uniform(0,3.28)	DTN: MO0703PASEISDA.002_R4 [DIRS 183156], Table 1-20

NOTE 1: CDSP (WP) = co-disposed; TAD (WP) = transportation, aging, and disposal (canister); PGV = peak ground velocity; SD = standard deviation.

NOTE 2: In some cases the TSPA parameter name is different than the parameter name in the DTN. In these cases the parameter name in the DTN is noted in brackets.

Table 6.6-3. Seismic Ground Motion and Fault Displacement Modeling Cases Using Pre-Specified Parameters

Modeling Case	Seismic Event Time (yr)	CSNF WP Damage Fraction (fraction of WP surface area)	CDSP WP Damage Fraction (fraction of WP surface area)	Number of Failed CSNF WPs	Number of Failed CDSP WPs	Rubble Volume Accumulated (m^3/m)	Rubble Fill Time (yr)	DS Damage Fraction (fraction of WP surface area)
Seismic 1M yr FD Case[a]	1,000 20,000 80,000 200,000 400,000 800,000	0.028 0.056 0.084	0.0335 0.067 0.101	0 100	100 0	120	Seismic Event Time	1.0
Seismic 10k yr FD Case[b]	200 800 2,000 4,000 8,000 18,000	0.028 0.056 0.084	0.0335 0.067 0.101	0 100	100 0	120	Seismic Event Time	1.0
Seismic 10k yr GM Case[c]	100 1,000 3,000 6,000 12,000 18,000	0	1.00×10^{-7} 1.00×10^{-6} 0.00001 0.001	0	3416	0	2,000,000	0.0
Seismic 1M yr GM Case	Section 6.6.1.3.1	Section 6.6.1.3.4	Section 6.6.1.3.4	Section 6.6.1.3.4	Section 6.6.1.3.4	Section 6.6.1.3.2	Section 6.6.1.3.2	Section 6.6.1.3.3

Sources: [a]Output DTN: MO0708TSPAGENT.000 [DIRS 183000], folders: PL-TSPA-DTN-9. (PEF 126)
Output DTN: MO0708TSPAGENT.000 [DIRS 183000], folder: PL-TSPA-DTN-8 (PEF 125)
Output DTN: MO0708TSPAGENT.000 [DIRS 183000], folder: PL-TSPA-DTN-7 (PEF 124)

NOTES: For each modeling case run defined above, the model cycles through all possible combinations of the aleatory parameters one realization at time, holding the epistemic sample number constant. For the Seismic one-million year FD Modeling Case and the Seismic 10,000 year FD Modeling Case, there are
[b] 108 possible combinations of aleatory parameters. For the Seismic 10,000 year GM Modeling Case there are 24 possible combinations of aleatory
[c] parameters.

Table 6.6-4. Alternative Conceptual Models Considered for the Seismic Scenario Class

Alternative Conceptual Models	Key Assumptions	Assessment and Basis
Alternative modeling approaches were evaluated for the conceptual and computational models of lithophysal and nonlithophysal rock (BSC 2004 [DIRS 166107], Section 7.4).	A standard approach for solving excavation stability problems is the use of numerical models based on continuum mechanics. Continuum models use constitutive relations to describe the mechanical behavior of a material. The use of a constitutive model requires that the mechanical effects of fractures be lumped into the constitutive relationships.	Continuum models are unable to predict instabilities, such as fracture and rockfall (BSC 2004 [DIRS 166107], Section 7.4.1). The discontinuum approach is more suitable for representing fracture of the rock mass and separation of the intact rock mass into blocks and was therefore adopted for modeling the drift degradation processes that occur after a seismic event (BSC 2004 [DIRS 166107], Section 7.4.2).
An alternative damage abstraction for fault displacement damage was proposed by Waiting et al., described in Seismic Consequence Abstraction (SNL 2007 [DIRS 176828], Section 6.11.6).	The ACM considered the probability-weighted number of waste package failures from fault displacement and the number of fault intersections with emplacement drifts. The ACM, based on the use of historical data for fault displacement in the western United States.	The results provided by the ACM are consistent with the base-case model for both the probability-weighted number of WP failures and the number of fault intersections with the emplacement drifts (SNL 2007 [DIRS 176828], Section 6.11.6).
An alternative conceptual model for crack area density was presented in Section 6.7.4 (SNL 2007 [DIRS 181953]).	The alternative model considered a circular geometry circumscribed by a single through-wall crack. The base case model combines two conceptual models based on hexagonal geometry (SNL 2007 [DIRS 181953], Section 6.7.3).	The hexagonal geometry represents a high effective density of individual cracks and the two hexagonal geometry conceptual models are considered conservative representations. The ACM analysis which uses circular geometry is considered a limiting realistic case (SNL 2007 [DIRS 181953], Section 6.7.2).
Alternative conceptual models for the conditional probability distributions representing damaged areas on the waste package, damaged areas on the drip shield, and the volume of rockfall from a seismic event were considered.	These alternate distributions included the gamma, normal, log-normal, Weibull and triangular distributions, as presented in Sections 6.5.1.4; 6.5.2.4; 6.6.1.4; 6.6.2.4; 6.7.1.3; 6.7.2.4; 6.9.4; and 6.10.2.8 of Seismic Consequence Abstraction (SNL 2007 [DIRS 176828]).	Gamma distributions generally provided simpler and more accurate representations of the statistical observations than normal, log-normal, log-triangular, and Weibull distributions. The exception to the use of gamma distributions is that the fragility analyses (for drip shield plates and framework) have used log-normal representations to simplify manipulation of products and quotients of random variables.

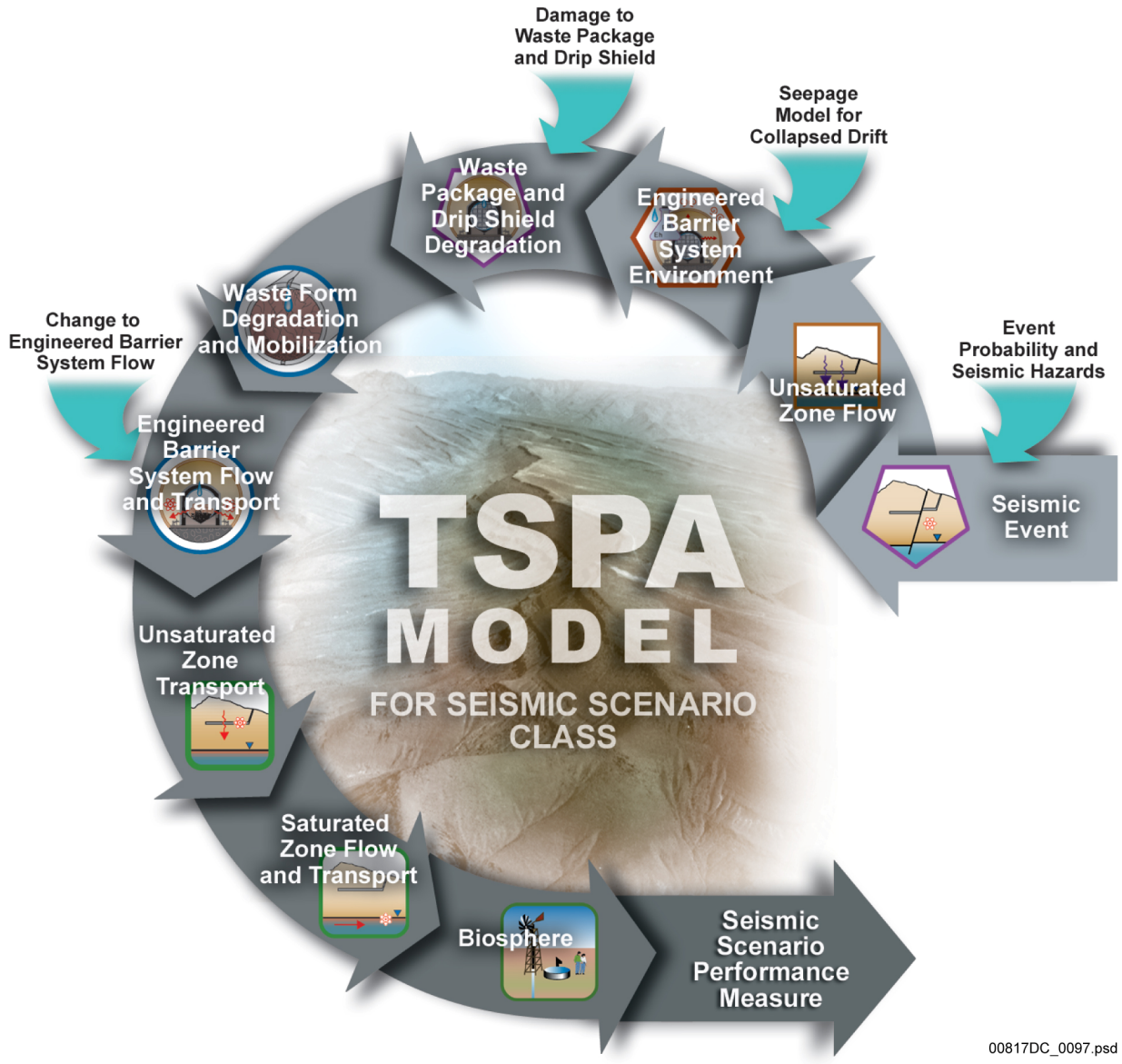

Figure 6.6-1. Schematic Representation of the TSPA-LA Model Components for the Seismic Scenario Class

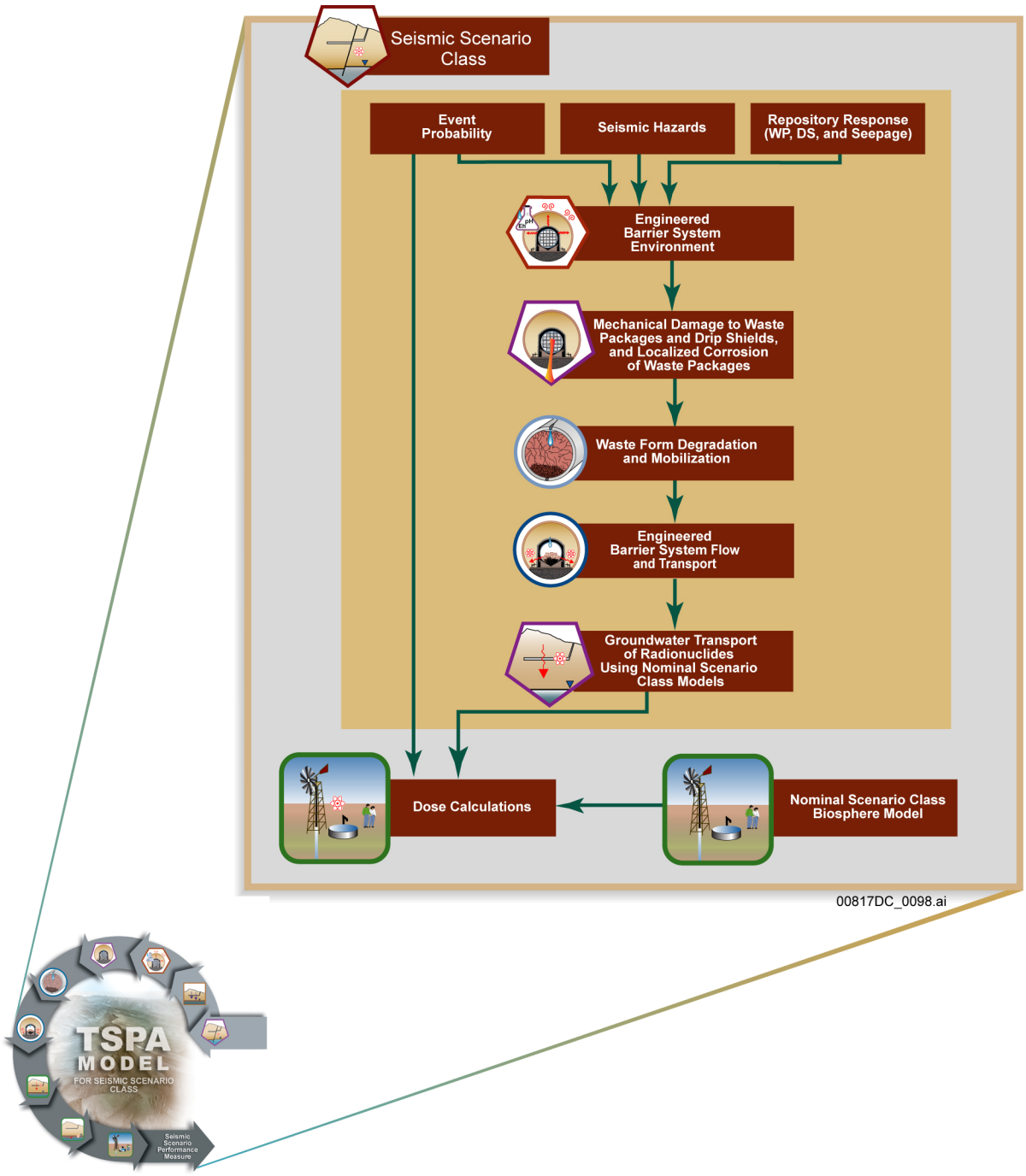

Figure 6.6-2. Information Flow Diagram for the Seismic Scenario Class in the TSPA-LA Model

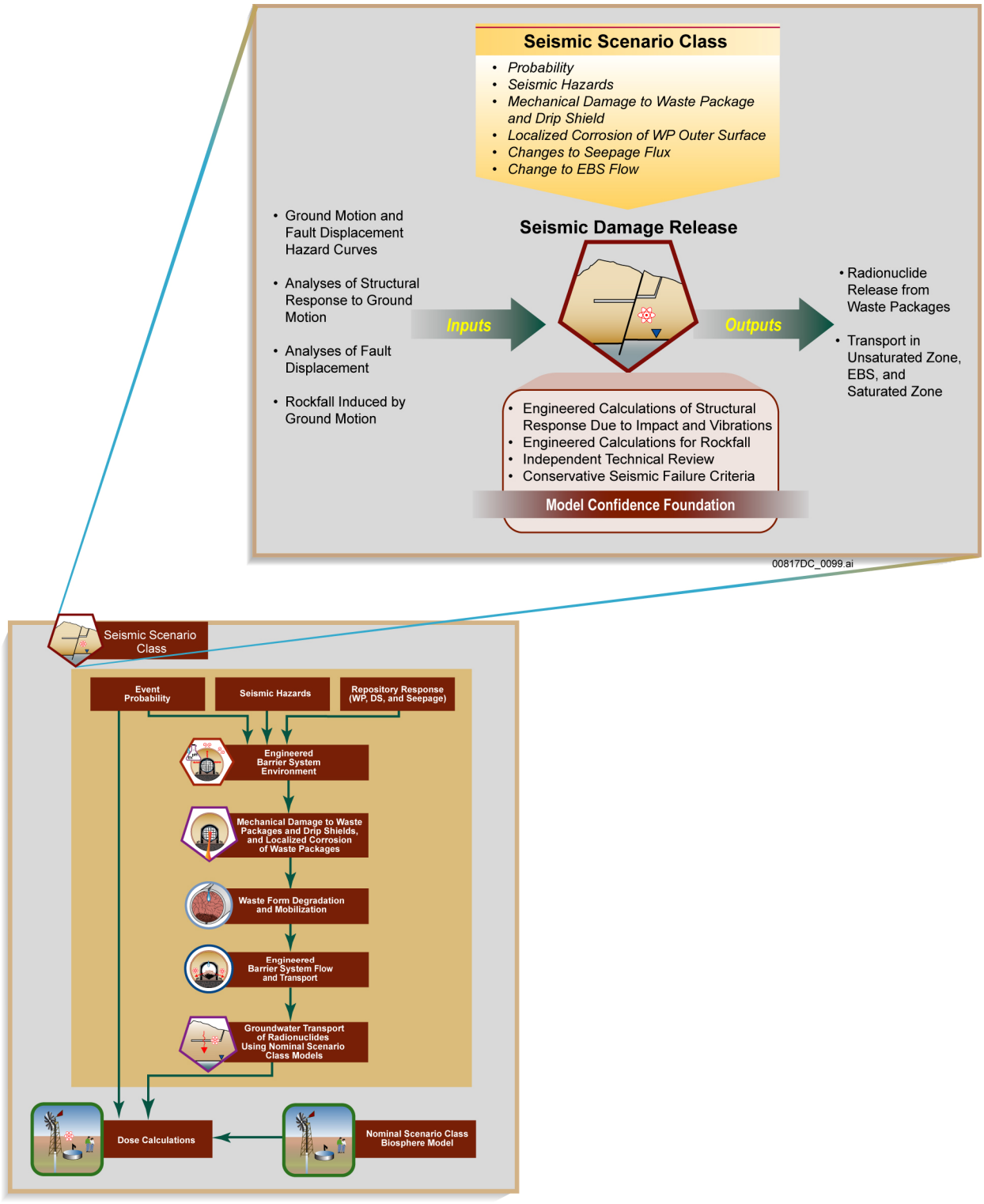

Figure 6.6-3. Inputs, Outputs, and Basis for Model Confidence for the Seismic Scenario Class

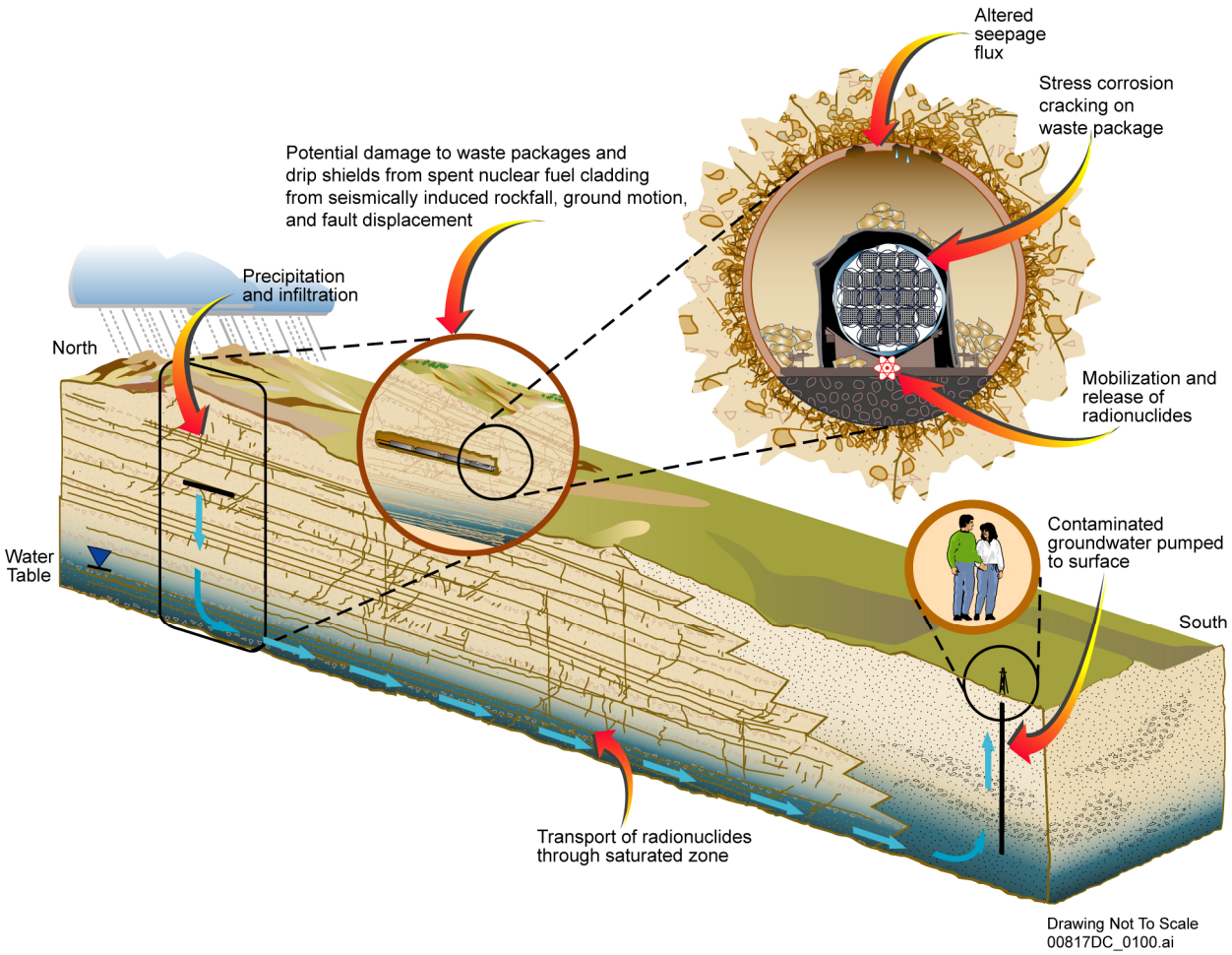

Figure 6.6-4. Schematic Illustration of the Seismic Scenario Class, the Seismic Effects within a Drift, and Subsequent Radionuclide Releases to the Accessible Environment

Figure 6.6-5. Schematic Representation of Future Configurations of EBS Components for Seismic Damage Abstraction

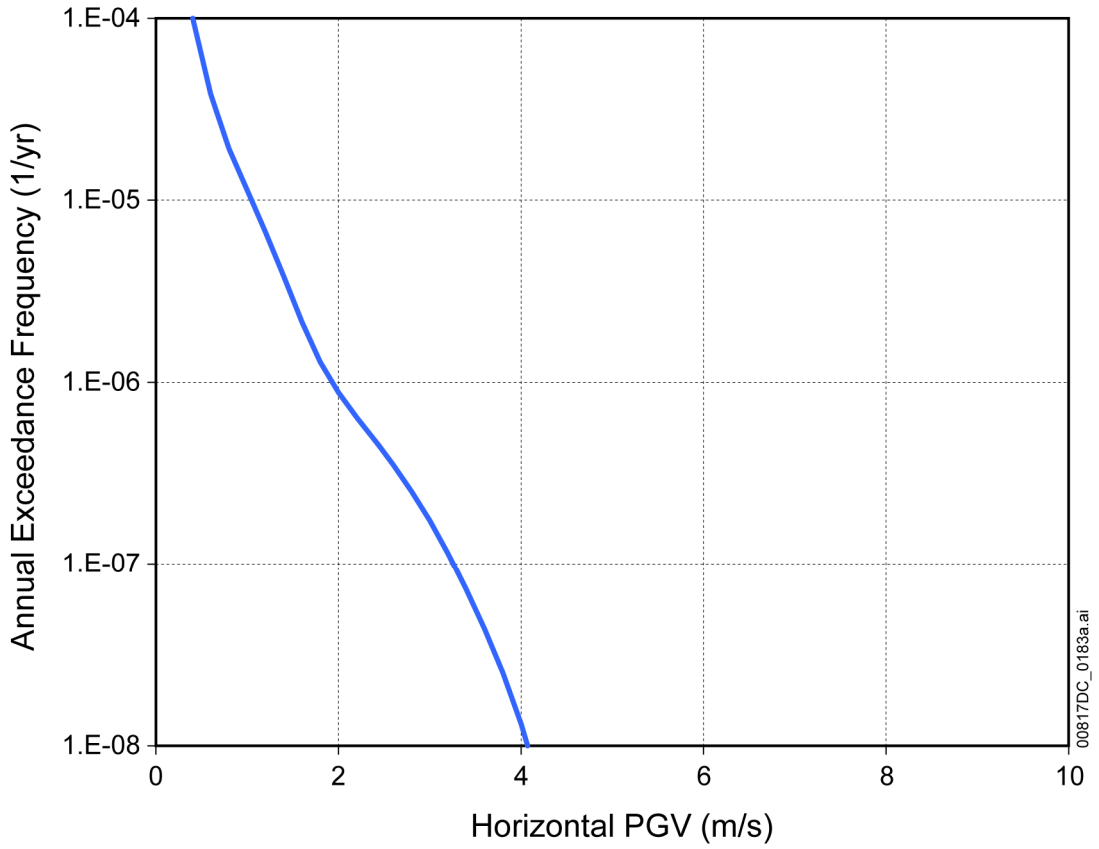

Source: DTN: MO0501BPVELEMP.001_R0 [DIRS 172682], *Bounded Horizontal Peak Ground Velocity Hazard at the Repository Waste Emplacement Level.xls*.

NOTE: Data is plotted on a linear scale for the Horizontal PGV.

Figure 6.6-6. Hazard Curve for Seismic Scenario Class

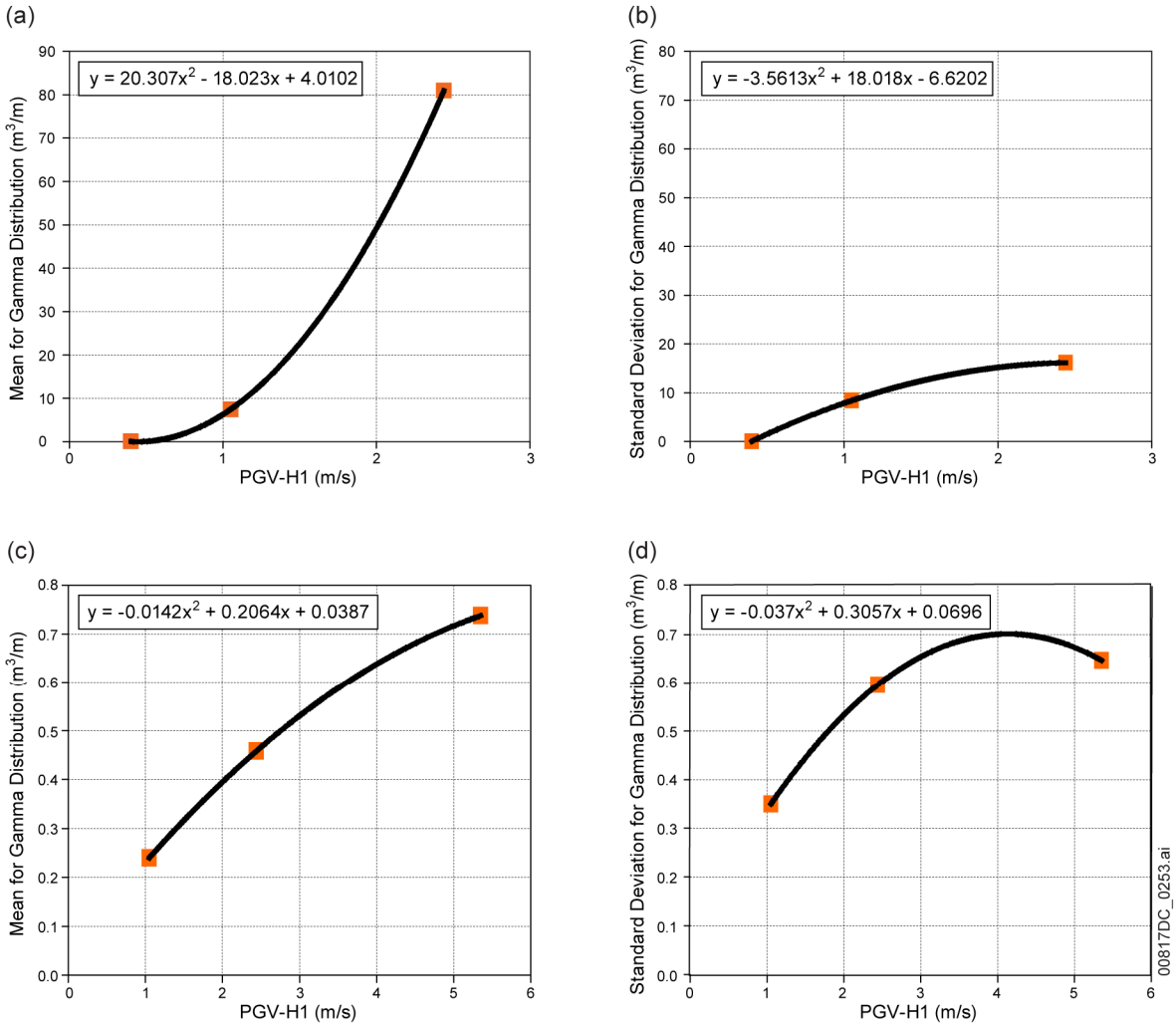

Source: DTN: MO0703PASDSTAT.001_R3 [DIRS 183148], *Lith Rubble Abstraction.xls* (a and b) and *Nonlith Rockfall Abstraction.xls* (c and d).

NOTE: The scales in plots (a) and (b) are different from those in plots (c) and (d).

Figure 6.6-7. Comparison of Mean Rockfall Volumes for Lithophysal (a and b) and Nonlithophysal (c and d) Zones

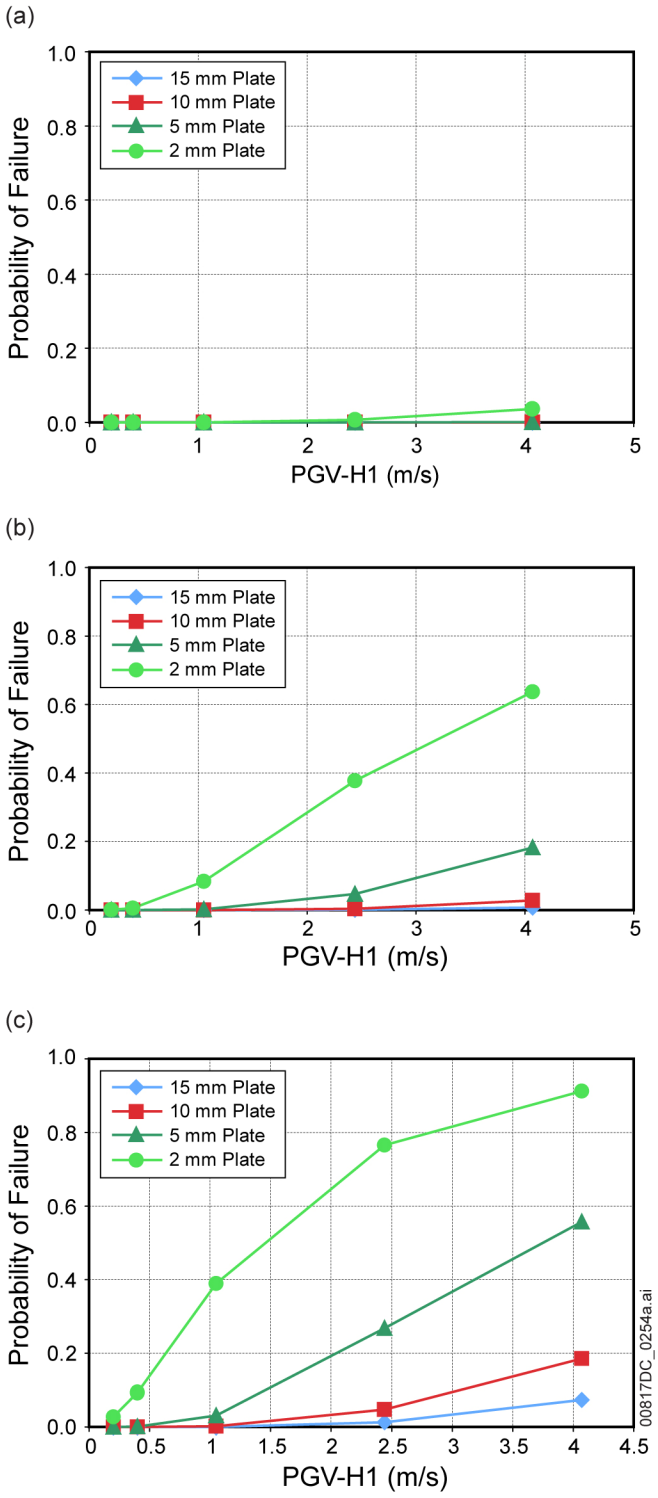

Source: DTN: MO0703PASDSTAT.001_R3 [DIRS 183148], *Plate Fragility Analysis.xls*.

Figure 6.6-8. Drip Shield Plate Fragility as a Function of Rockfall Load: (a) 10 Percent, (b) 50 Percent, and (c) 100 Percent

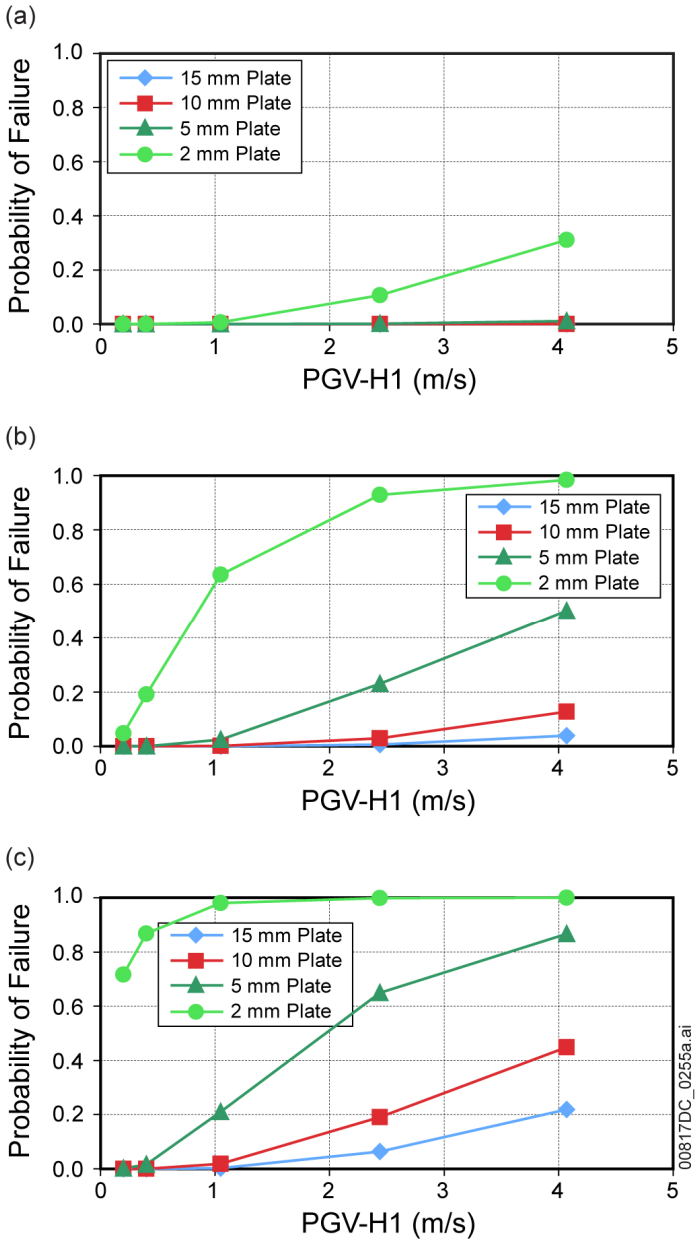

Source: DTN: MO0703PASDSTAT.001_R3 [DIRS 183148], *Frame Fragility Analysis.xls*.

Figure 6.6-9. Drip Shield Framework Fragility as a Function of Rockfall Load: (a) 10 Percent, (b) 50 Percent, and (c) 100 Percent

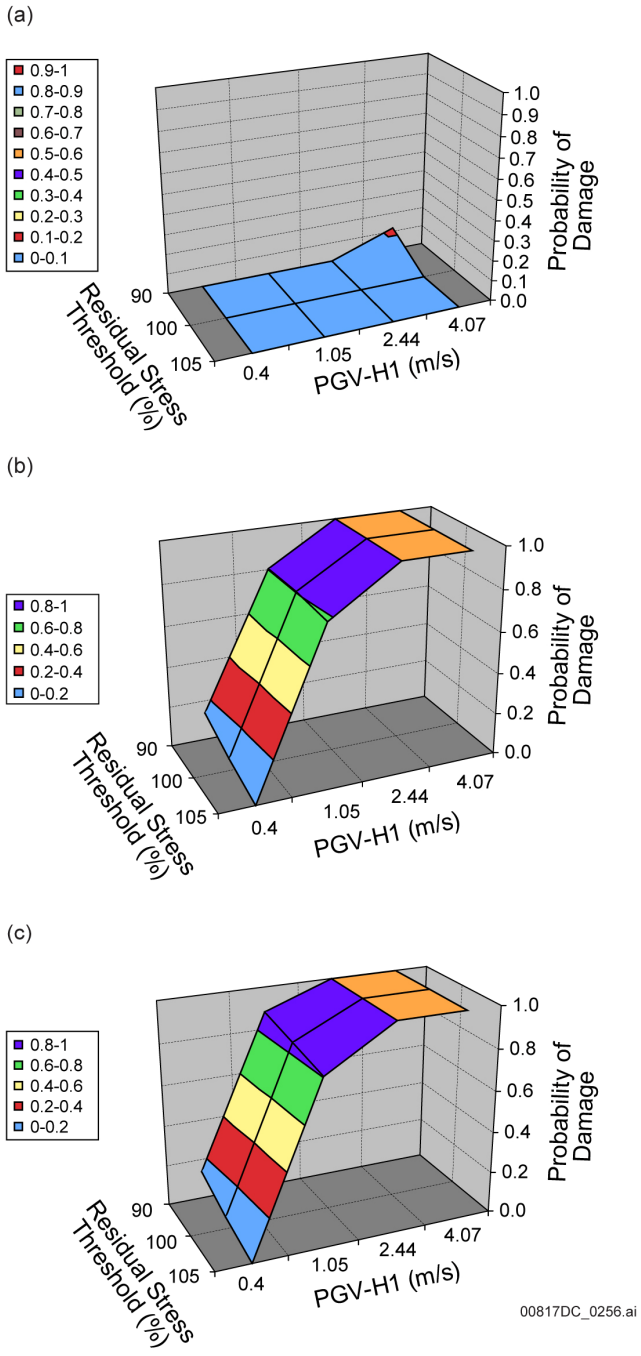

Source: DTN: MO0703PASDSTAT.001_R3 [DIRS 183148], *Kinematic Damage Abstraction 23-mm Intact.xls, Kinematic Damage Abstraction 23-mm Degraded.xls, and Kinematic Damage Abstraction 17-mm Degraded.xls*.

NOTE: Orange represents a probability of 1.0.

Figure 6.6-10. Probability of Damage for a CSNF WP under and Intact Drip Shield: (a) 23 mm OCB with Intact Internals, (b) 23 mm OCB with Degraded Internals, and (c) 17 mm OCB with Degraded Internals

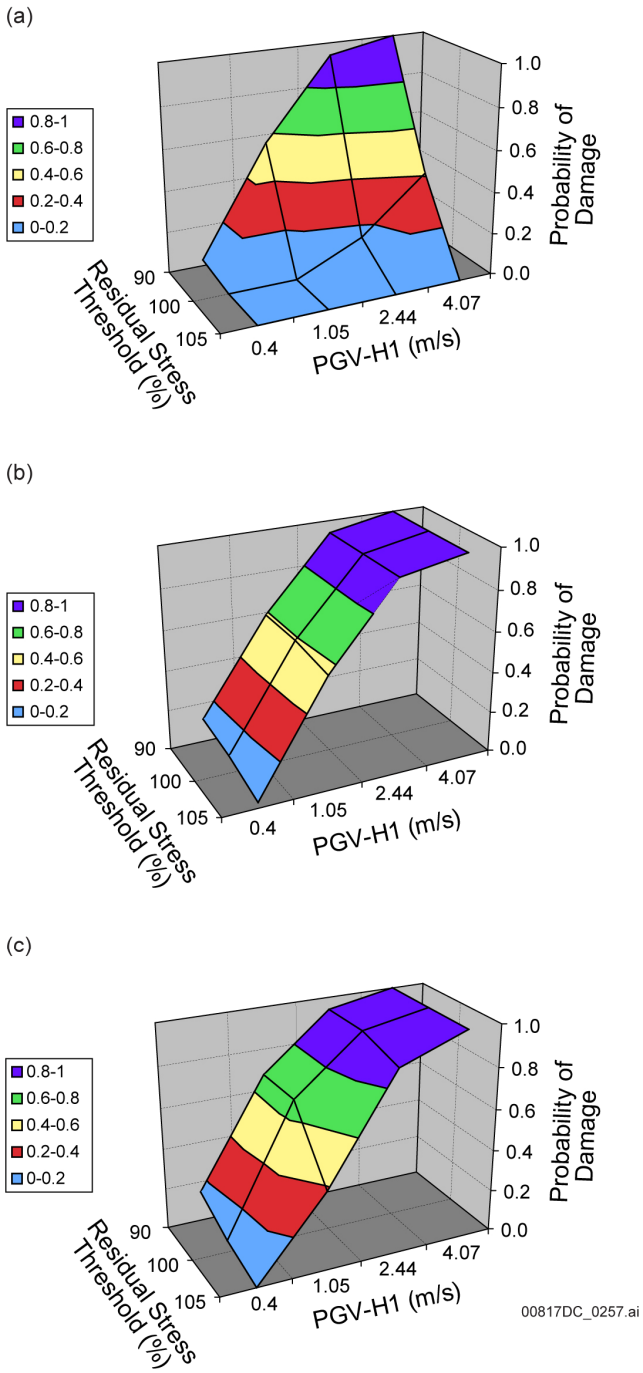

Source: DTN: MO0703PASDSTAT.001_R3 [DIRS 183148], *CDSP Kinematic Damage Abstraction 23-mm Intact.xls, CDSP Kinematic Damage Abstraction 23-mm Degraded.xls, and CDSP Kinematic Damage Abstraction 17-mm Degraded.xls*.

Figure 6.6-11. Probability of Damage for a CDSP WP under an Intact Drip Shield: (a) 23-mm OCB with Intact Internals, (b) 23-mm OCB with Degraded Internals, and (c) 17-mm OCB with Degraded Internals

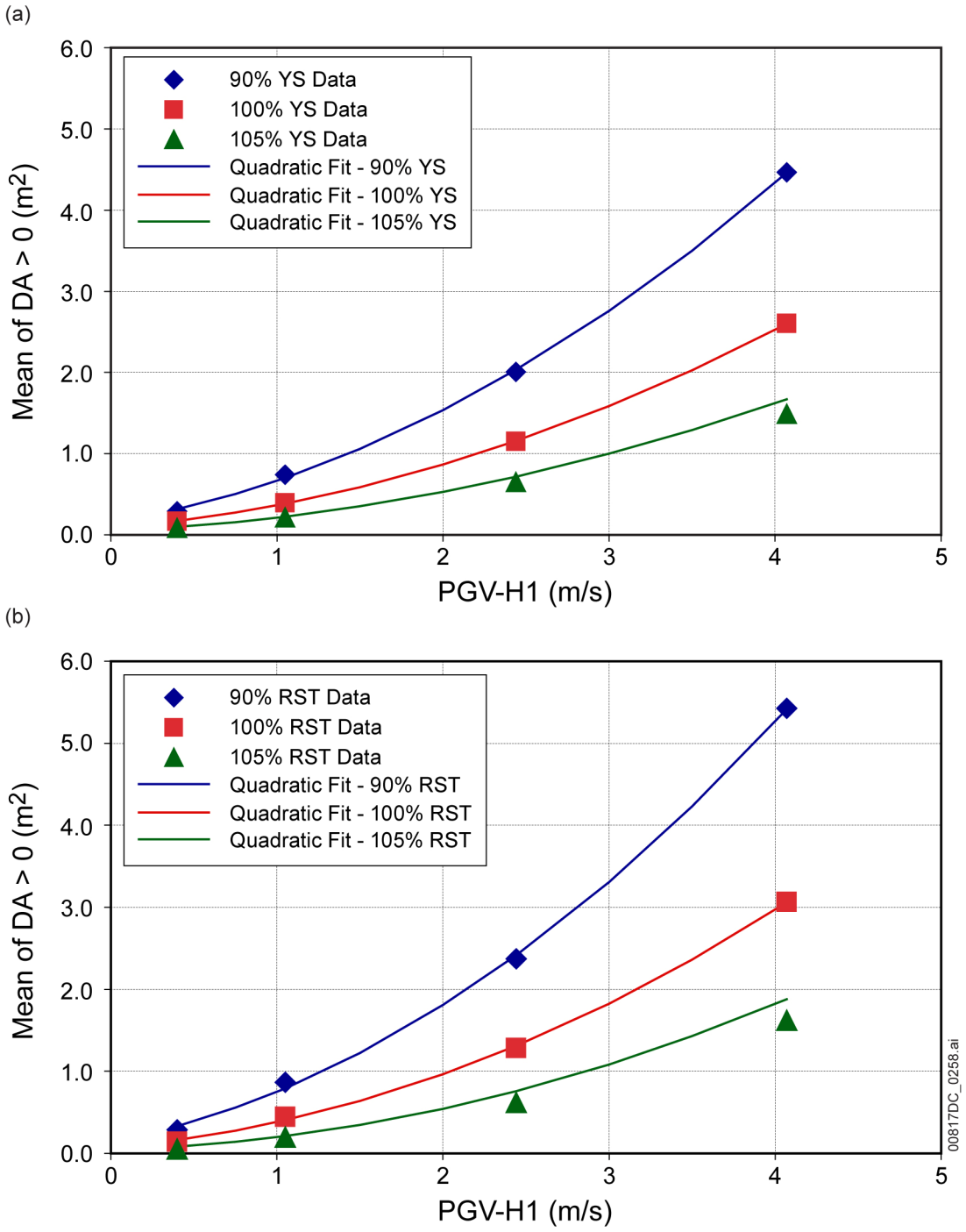

Source: DTN: MO0703PASDSTAT.001_R3 [DIRS 183148], *Kinematic Damage Abstraction 23-mm Degraded.xls* and *Kinematic Damage Abstraction 17-mm Degraded.xls*.

Figure 6.6-12. Quadratic Fit for Mean Damaged Area on a CSNF WP with Degraded Internals under an Intact Drip Shield: (a) 23-mm OCB and (b) 17-mm OCB

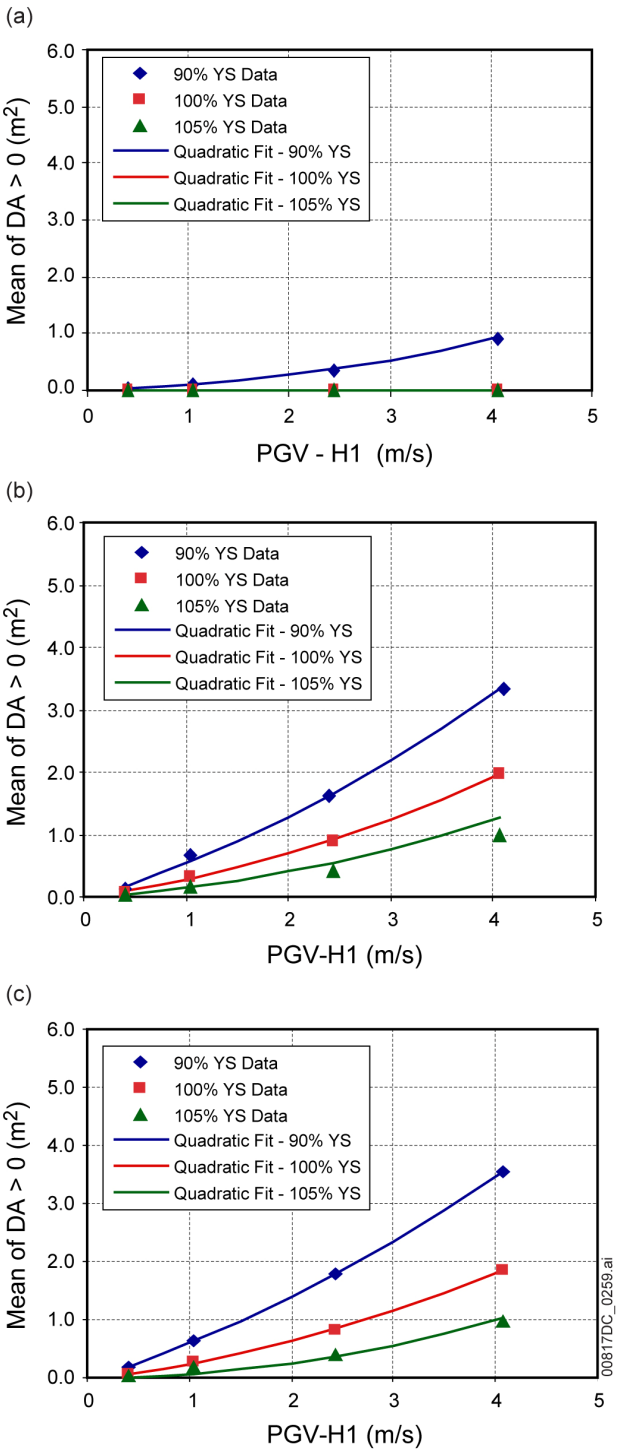

Source: DTN: MO0703PASDSTAT.001_R3 [DIRS 183148], CDSP *Kinematic Damage Abstraction 23-mm Intact.xls, CDSP Kinematic Damage Abstraction 23-mm Degraded.xls*, and *CDSP Kinematic Damage Abstraction 17-mm Degraded.xls*.

Figure 6.6-13. Quadratic Fit for Mean Damaged Area on a CDSP WP under an Intact Drip Shield: (a) 17-mm OCB with Degraded Internals, (b) 23-mm OCB with Degraded Internals, and (c) 23-mm OCB with Intact Internals

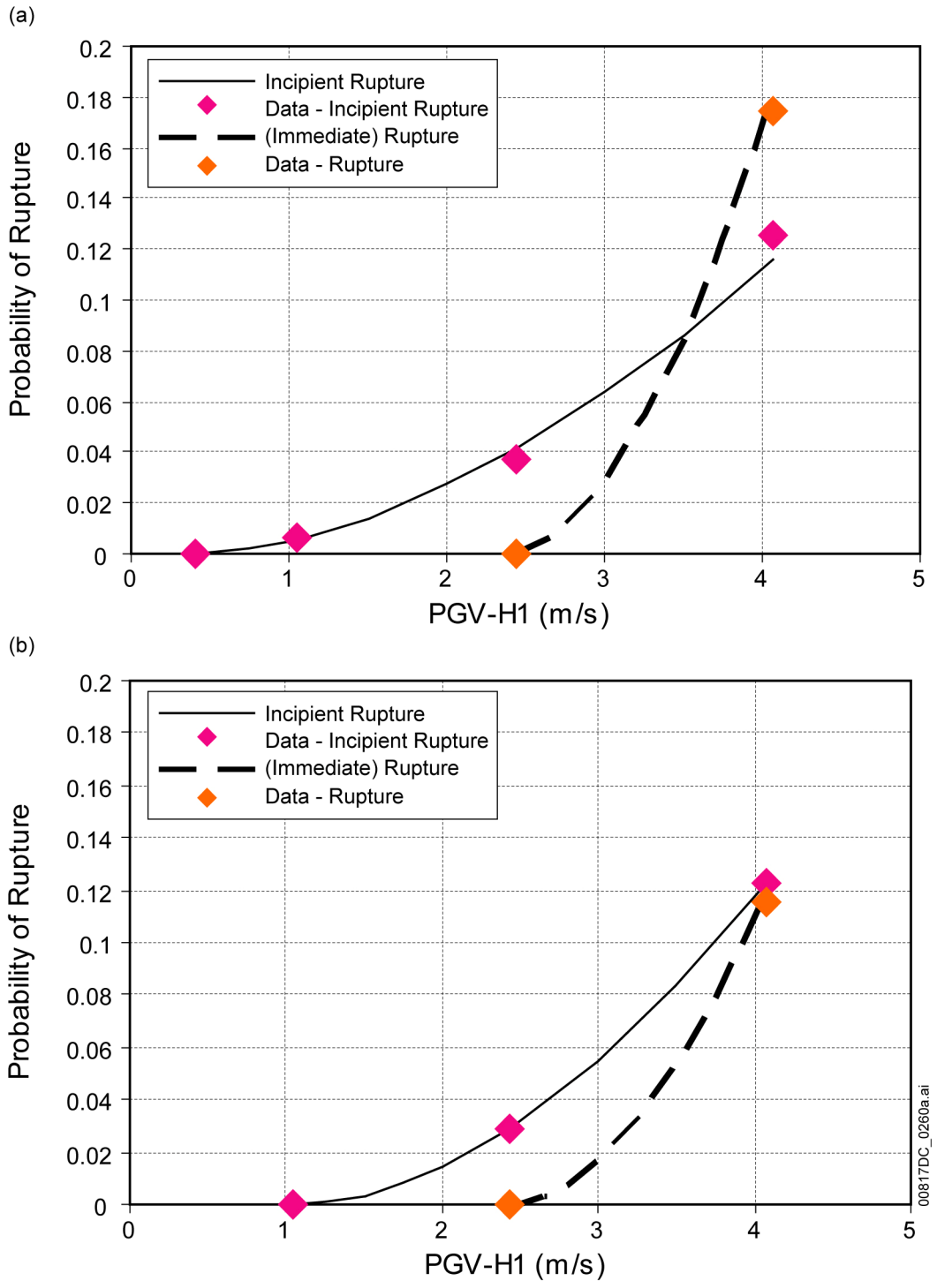

Source: DTN: MO0703PASDSTAT.001_R3 [DIRS 183148], *Rupture and Puncture Abstractions.xls*.

Figure 6.6-14. Probability of Incipient and Immediate Rupture for (a) CSNF and (b) CDSP WPs under Intact Drip Shields

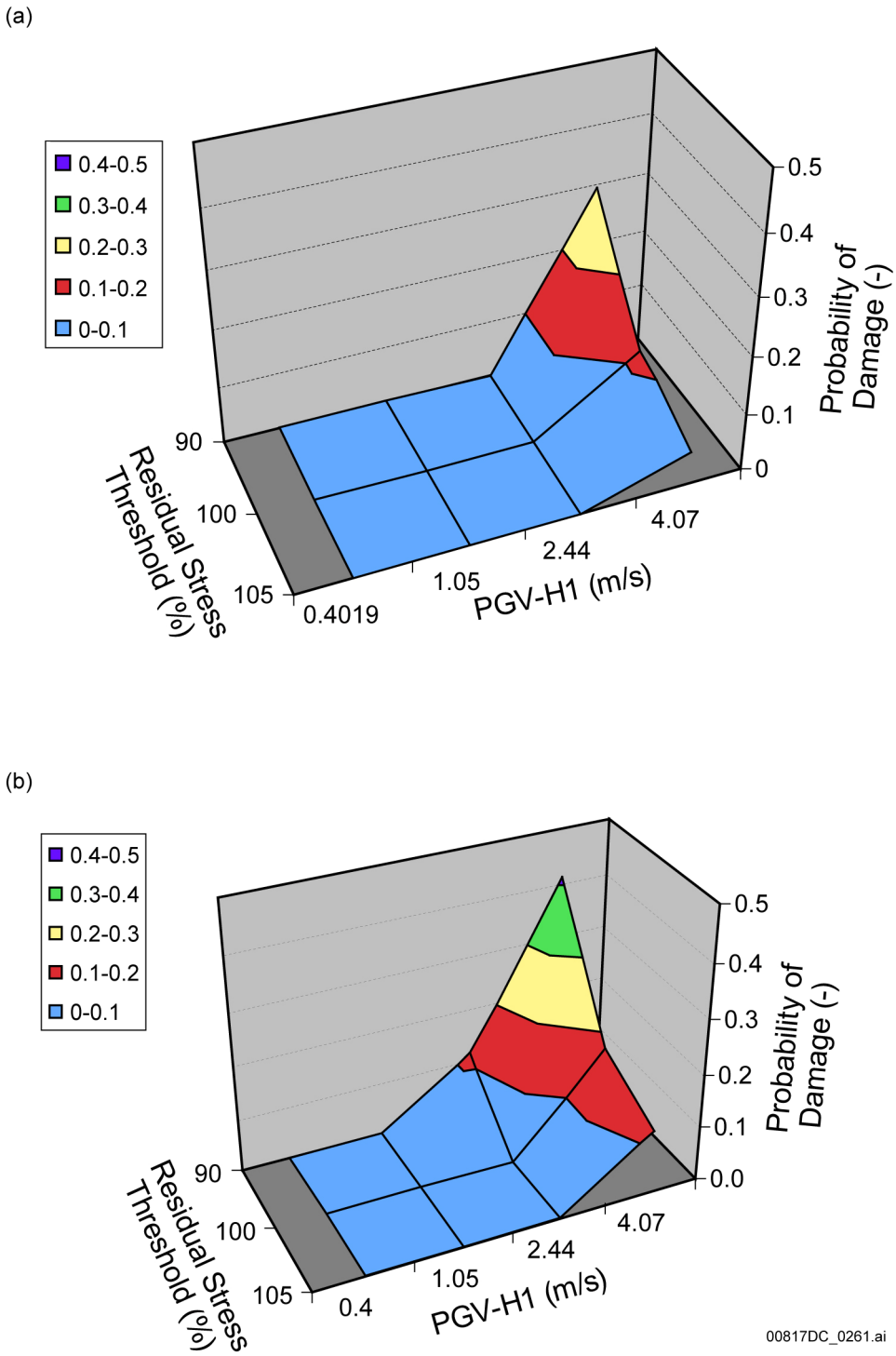

Source: DTN: MO0703PASDSTAT.001_R3 [DIRS 183148], *WP-Rubble Damage Abstraction 23-mm Degraded.xls* and *WP-Rubble Damage Abstraction 17-mm Degraded.xls*.

Figure 6.6-15. Probability of Damage for a CSNF WP Surrounded by Rubble: (a) 23-mm and (b) 17-mm

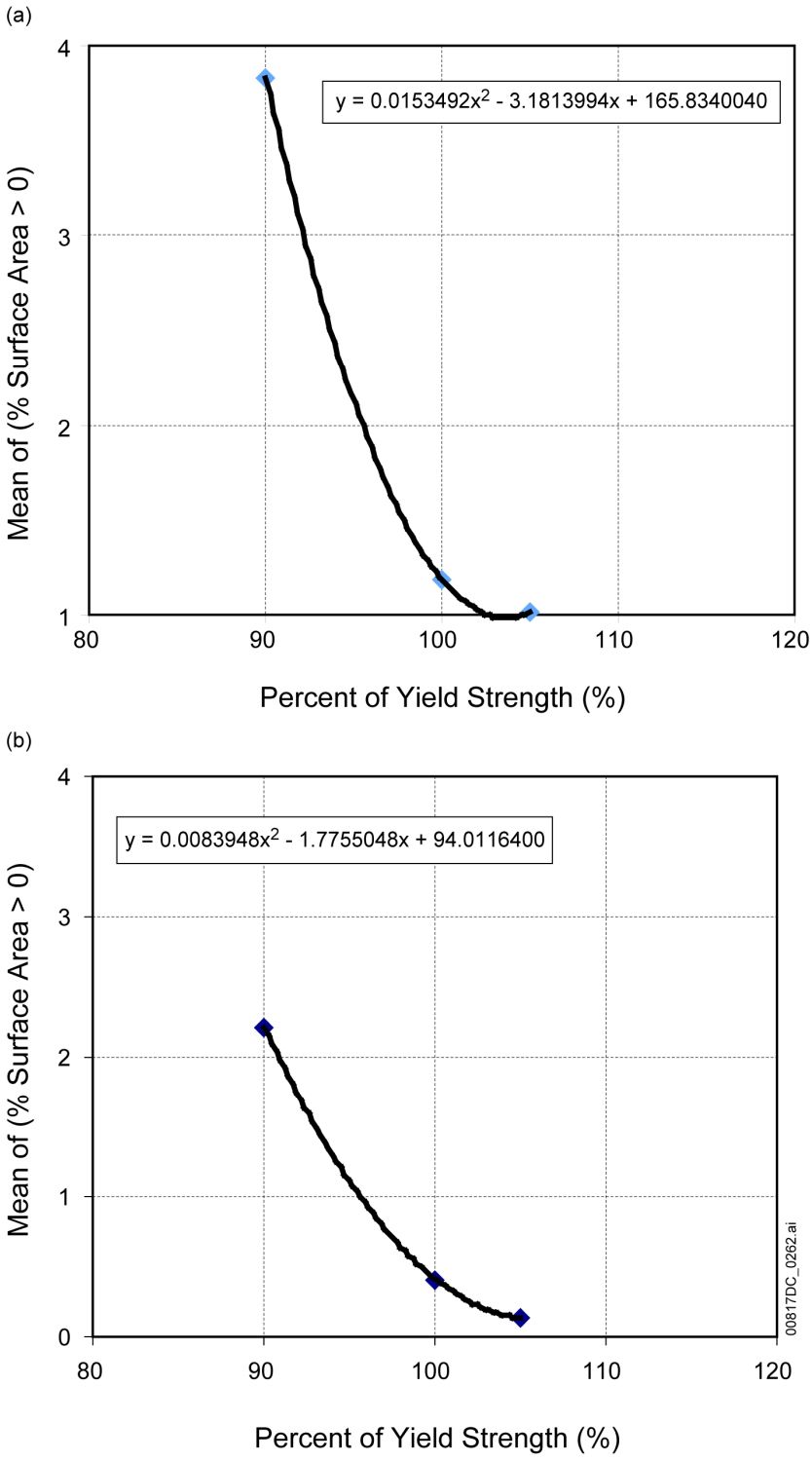

Source: DTN: MO0703PASDSTAT.001_R3 [DIRS 183148], *WP-Rubble Damage Abstraction 23-mm Degraded.xls* and *WP-Rubble Damage Abstraction 17-mm Degraded.xls*.

Figure 6.6-16. Quadratic Fit for Mean Damage Area on a CSNF WP with Degraded Internals Surrounded by Rubble: (a) 23-mm and (b) 17-mm

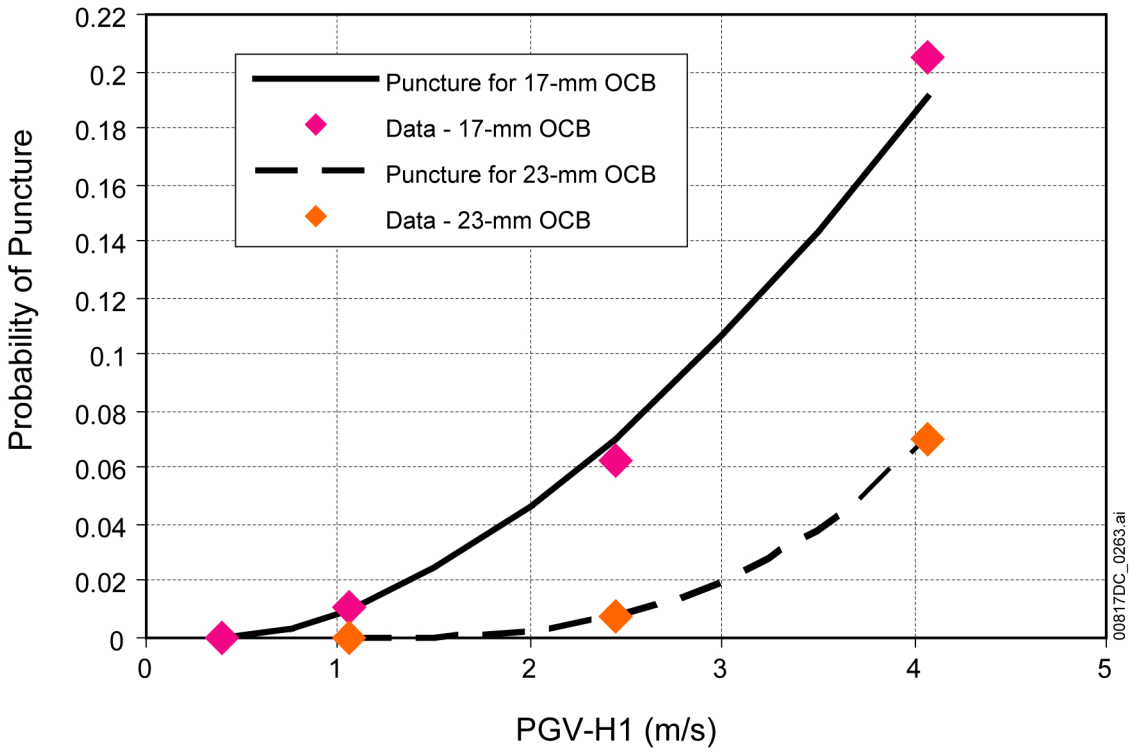

Source: DTN: MO0703PASDSTAT.001_R3 [DIRS 183148], *Rupture and Puncture Abstractions.xls*.

Figure 6.6-17. Probability of Puncture for a CSNF WP Surrounded by Rubble

INTENTIONALLY LEFT BLANK

6.7 TSPA-LA MODEL FOR THE HUMAN INTRUSION SCENARIO

The Human Intrusion Modeling Case is based on the stylized Human Intrusion Scenario as specified in NRC rule 10 CFR 63.322 [DIRS 180319], and the individual protection standard for a human intrusion of the repository in the NRC Proposed Rule 10 CFR 63.321 [DIRS 178394]. The TSPA-LA stylized Human Intrusion Scenario is based on NRC rule in 10 CFR 63.322 [DIRS 180319] as follows:

"For the purposes of the analysis of human intrusion, DOE must make the following assumptions:

(a) There is a single human intrusion as a result of exploratory drilling for ground water;

(b) The intruders drill a borehole directly through a degraded waste package into the uppermost aquifer underlying the Yucca Mountain repository;

(c) The drillers use the common techniques and practices that are currently employed in exploratory drilling for ground water in the region surrounding Yucca Mountain;

(d) Careful sealing of the borehole does not occur, instead natural degradation processes gradually modify the borehole;

(e) No particulate waste material falls into the borehole;

(f) The exposure scenario includes only those radionuclides transported to the saturated zone by water (e.g., water enters the waste package, releases radionuclides, and transports radionuclides by way of the borehole to the saturated zone); and

(g) No releases are included which are caused by unlikely natural processes and events."

In addition, NRC Proposed Rule in 10 CFR 63.321 [DIRS 178394] specifies the individual protection standard for human intrusion as follows:

"(a) DOE must determine the earliest time after disposal that the waste package would degrade sufficiently that a human intrusion (see § 63.322) could occur without recognition by the drillers.

(b) DOE must demonstrate that there is a reasonable expectation that the reasonably maximally exposed individual receives, as a result of human intrusion, no more than the following annual dose:

(1) 0.15 mSv (15 mrem) for 10,000 years following disposal; and

(2) 3.5 mSv (350 mrem) after 10,000 years, but within the period of geologic stability.

(c) DOE's analysis must include all potential environmental pathways of radionuclide transport and exposure, subject to the requirements at § 63.322."

Section 6.7 is organized as follows. Section 6.7.1 summarizes the model components and submodels of the Human Intrusion Scenario. The earliest time at which a waste package (WP) is expected to be breached by an inadvertent drilling event is discussed in Section 6.7.2. Section 6.7.2.1 describes the TSPA-LA analysis for drip shield (DS) and WP degradation. Section 6.7.2.2 discusses the unlikely events-related damage mechanisms. Section 6.7.2.3 describes the potential for WP penetration by a drilling event. Section 6.7.2.4 summarizes the findings from the analysis discussed in Sections 6.7.2.1 through 6.7.2.3. Section 6.7.2.5 discusses the treatment of likely DS and WP degradation processes considered in the Human Intrusion TSPA. Implementation and the process for estimating the mean and median annual dose for the Human Intrusion Scenario is discussed in Section 6.7.3. This section is divided into four subsections based on the treatment of radionuclide transport through the following TSPA submodels, the EBS (Section 6.7.3.1), the UZ (Section 6.7.3.2), the SZ (Section 6.7.3.3), and the Biosphere Submodel, which calculates dose (Section 6.7.3.4). The model component and submodel integration points, as well as conservatisms in submodels and abstraction models, are discussed in Section 6.7.4. The consistency of model assumptions in the Human Intrusion TSPA is discussed in Section 6.7.4.1, while Section 6.7.4.2 includes the discussion on model conservatisms. In Section 6.7.5, alternative conceptual models (ACMs) are considered.

6.7.1 TSPA-LA Model Components and Submodels for the Human Intrusion Scenario

The Human Intrusion Scenario describes performance of the repository system in the event that exploratory drilling disrupts the repository. Human intrusion disruption of the repository is addressed by a single modeling case.

The Human Intrusion Modeling Case, based upon NRC rule 10 CFR 63.322 [DIRS 180319], assumes that exploratory drilling activities intersect the repository and destroy a single DS and WP without recognition by the drillers. After penetrating a degraded DS and WP, the drillers continue to bore a conduit through to the SZ. The drillers penetrate a DS and WP with an opening the size of the drill bit and water enters the WP, mobilizing radionuclides. The released radionuclides may then be transported out of the repository (bypassing the EBS Invert Environment), moving down through the borehole to the SZ, to be transported through the SZ to the accessible environment. The TSPA-LA Model components and submodels needed to calculate total system performance for the Human Intrusion Modeling Case include the following, given that a single WP is destroyed by the intrusion:

- UZ Flow
- EBS Environment
- Waste Form Degradation and Mobilization
- EBS Flow and Transport
- SZ Flow and Transport
- Biosphere.

The model components and submodels of the TSPA-LA Model for the Human Intrusion Scenario are shown on Figure 6.7-1. Figure 6.7-2 shows the information flow within the model for the Human Intrusion Scenario in the TSPA-LA. Figure 6.7-3 indicates the major inputs and outputs of the model components and submodels included in the Human Intrusion Scenario and the foundation for confidence in the TSPA-LA Model. The TSPA-LA Model framework for the

Human Intrusion Scenario is similar to that of the Nominal Scenario Class. However, some of the submodels differ from those described in Section 6.3. These include the following:

- Mechanical damage to WPs and DSs
- Drift seepage for the Human Intrusion Scenario
- UZ Transport for the Human Intrusion Scenario
- EBS flow for the Human Intrusion Scenario.

The WP and DS Degradation Submodel is not used to calculate the corrosion failure of WPs prior to penetration time in the Human Intrusion Modeling Case. It is conservatively assumed that the WP could be penetrated without detection by the drillers. Nominal corrosion damage (either cracks or patches) subsequent to the drilling intrusion penetration releases and their dose are already included in the overall TSPA. Also, they could only serve to lower the dose attributable to release down the borehole pathway, since they would provide an avenue of escape into the UZ at spatial locations different than the borehole location (i.e., the occurrence of seismic crack damage and nominal corrosion patches and cracks would generally occur on a part of the WP surface not in contact with the borehole pathway). Thus, nominal WP breaches would not contribute in any way to increasing the possible concentration of radionuclides in the water flowing down the borehole and would rather reduce the resulting peak dose.

6.7.2 Evaluation of the Earliest Time of Waste Package Penetration by Human Intrusion

The Human Intrusion Scenario considers the effects of a single well drilled from the land surface above the repository, which penetrates the repository and passes through a single DS and WP, and into the underlying SZ. For the stylized Human Intrusion Scenario, the WP corrosion is conservatively ignored and the assumed DS failure at 200,000 years is considered to be the earliest time a driller could penetrate a WP without recognition. To determine the earliest time after disposal that a WP would degrade sufficiently that a human intrusion could occur without recognition by the drillers, the degradation mechanisms for DSs and WPs were evaluated and the earliest time at which a WP could be breached without recognition by the drillers was conservatively selected. The following discussion considers all the degradation states for a WP and DS considered for the TSPA-LA. Because degradation of WPs and DSs occurs gradually with time, the probability that a human intrusion could occur without recognition by the drillers increases with time.

6.7.2.1 General Corrosion of the Waste Package and Drip Shield

The EBS design includes Titanium Grade 7 DS supported by a Titanium Grade 29 framework, which is placed over the WPs (SNL 2007 [DIRS 179354], Section 4.1.2). As long as they remain substantially intact, the DS will divert an inadvertent drilling event (Section 6.7.2.3) away from the WP and preclude damage to a WP. The TSPA-LA Model for general corrosion is the only DS corrosion mechanism modeled. This degradation mode and abstraction model is described in Section 6.3.5. This process is modeled as being independent of temperature and relative humidity and is initiated at the time of repository closure. Because of the low corrosion rate of titanium alloy used for the DSs, the initial breaches of the DSs are not expected to occur until well after 10,000 years; more specifically, analyses predict that initial breaches of the DSs will not occur under nominal conditions until after approximately 230,000 years postclosure

(Section 6.3.5.1.3). General corrosion is modeled separately for the topside and underside surfaces of the DSs. The mean Titanium DS corrosion rates are the sum of the topside surface corrosion rate plus the underside surface corrosion rate. The corrosion rates are found in DTN: SN0704PADSGCMT.001_R2 [DIRS 182122], where the spreadsheet DS_GC_Model_Analysis_Benign Condition.xls contains the data for the underside surface, and the spreadsheet DS_GC_Model_Analysis_Agressive Condition.xls contains the data for the topside surface (used only for DSs that are exposed to dripping). The benign chemistry DS corrosion rates are applied to both the topside and underside of the DS for DSs that are not exposed to dripping water. Applying a conservative 0.9999 quantile for the DS (topside and underside) general corrosion rates over a 10,000-year period (Section 6.3.5.1.3) would reduce the original DS thickness of 15 mm (SNL 2007 [DIRS 179354], Table 4-2, Parameter Number 07-04A) by approximately 0.66 mm, to a thickness of 14.34 mm. Even applying the 0.9999 quantile titanium corrosion rate (for the topside and underside), the first DS failures due to general corrosion are not likely to occur until approximately 230,000 years after repository closure under nominal conditions.

The TSPA-LA Model for WP degradation includes four degradation modes: general corrosion, microbially influenced corrosion (MIC), stress corrosion cracking (SCC), and localized corrosion. These degradation modes and their abstractions are described in Section 6.3.5. The WPs have a dual-metal design consisting of an inner vessel and outer barrier. The inner vessel is composed of a 50.8-mm-thick layer of Stainless Steel Type 316 (material type SA-240 (UNS S31600) SNL 2007 [DIRS 179394], Table 4-3). The outer shell (i.e., outer corrosion barrier [OCB]) is a 25-mm-thick layer of Alloy 22 (material type SB-575 (UNS N06022)), a corrosion-resistant, nickel-based alloy surrounding transportation, aging, and disposal (TAD) canister made of a 300-series stainless steel such as Stainless Steel Type 316 (SNL 2007 [DIRS 179567], Tables 4-6 through 4-10). Alloy 22 protects the Stainless Steel Type 316 inner vessel from corrosion, and the Stainless Steel Type 316 inner vessel provides structural support for the thinner Alloy 22 outer shell. Because the WP outer shell is highly corrosion resistant, WPs will not be breached by corrosion processes during the 10,000-year modeling period in the absence of localized corrosion (SNL 2007 [DIRS 178519], Section 8.1). WP degradation models under nominal conditions indicate that it is unlikely that the time to initial breaching of the WPs will occur before 230,000 years postclosure (Section 6.3.5).

The WP Localized Corrosion Initiation and Propagation Analysis for the WP outer surface is based on the Localized Corrosion Initiation Abstraction developed in *General Corrosion and Localized Corrosion of Waste Package Outer Barrier* (SNL 2007 [178519], Section 6.4.4). The primary factors that determine the potential for initiating localized corrosion are sample configuration, metallurgical conditions, and exposure conditions including temperature, pH, chloride-ion concentration, and nitrate-ion concentration, which are obtained from the EBS TH Environment Submodel (Section 6.3.2) and the EBS Chemical Environment Submodel (Section 6.3.4). Localized corrosion requires the presence of seepage water on the WP surface. The potential effects of localized corrosion on the WPs during the initial 10,000-year period are, therefore, conditional on a DS failure (Section 6.3.5.2). Until a breach of the DS occurs, the WP itself is not susceptible to localized corrosion. Therefore, under nominal conditions, localized corrosion of WPs will not occur because DS failures are not expected until well after the chemical environment necessary for localized corrosion initiation has subsided (Section 6.3.5.2).

General corrosion of DSs and WPs occurs gradually over time. The general corrosion process is a surface phenomenon and the underlying metal retains its integrity and resistance to drilling until a significant amount of material has been corroded and the remaining DS or WP thickness is insufficient to prevent penetration by a drill bit. Nominal WP and DS degradation processes are insufficient to significantly degrade the titanium DS in 10,000 years. Given the slower relative degradation rates of the WPs and barring disruptive events of large magnitude, until there is a DS failure, the structural integrity of a WP is maintained and provides an additional barrier to borehole drill penetration.

6.7.2.2 Occurrence of Unlikely Events

In NRC Proposed Rule 10 CFR 63.342(b) [DIRS 178394], the NRC specifies that the human intrusion standards "…shall exclude the unlikely features, events, and processes, or sequences of events and processes, i.e., those that are estimated to have less than one chance in 10 and at least one chance in 10,000 of occurring within 10,000 years…" (i.e., an annual frequency of 10^{-5} (yr^{-1}) to 10^{-8} (yr^{-1})). Therefore, FEPs that have at least one chance in 10 of occurring within 10,000 years (i.e., a probability of occurrence greater than or equal to 1×10^{-5} per year) need to be considered for the human intrusion calculations. The following FEPs are discussed below in terms of their probability of occurrence: early failure of DSs, igneous events, and seismic events.

Early Failed Drip Shield

Although the TSPA-LA Model results show some DS failures at an early time, these failures are the result of manufacturing defects that increase susceptibility to SCC (SNL 2007 [DIRS 178765], Section 6.4). The probability of DS early failure (i.e., having an undetected defect that could cause an early failure) is determined from the DS cumulative uncertainty distribution for undetected DS defects (SNL 2007 [DIRS 178765], Table 6-10). This cumulative distribution function (CDF) gives the probability of having an undetected defect for a given DS. Considering that only a single WP and DS are penetrated during a human intrusion event, the probability of a human intrusion event intersecting a WP location that has an early failed DS can be determined by the probability of a DS defect occurring at that location. To evaluate the likelihood of this scenario, a conservative DS defect probability was chosen at the 0.95 quantile value of 6.968×10^{-6} from the DS cumulative uncertainty distribution for undetected DS defects (SNL 2007 [DIRS 178765], Table 6-10). There is no time dependency on this probability. However, it can be excluded from consideration as an unlikely event as it is an event with less than one chance in 10 in 10,000 years as defined by the NRC rule in 10 CFR 63.342 (b) [DIRS 178394]; and 10 CFR 63.322 (g) [DIRS 180319]. Even in the unlikely event that the human intrusion event were to intersect a location with an early failed DS, the likelihood of the WP being failed at the same location as a DS is even smaller. The joint probability (using the 0.9999 quantiles for DS and WP defects) for DS and WP early failure occurring at the same location is approximately 4.2×10^{-7} (SNL 2007 [DIRS 178765], Section 6.5.1, Table 6-11).

Similarly, potential effects of localized corrosion on the WPs during the initial 10,000-year period are conditional on a DS failure (Section 6.3.5.2). Given the probability of a human intrusion event at a location with an early failed DS (at a 0.95 quantile value) is 6.968×10^{-6}; a human intrusion event intersecting a WP failed by localized corrosion can be excluded as an

unlikely event (events with less than one chance in 10) per NRC rule in 10 CFR 63.342 (b) [DIRS 178394]; and 10 CFR 63.322 (g) [DIRS 180319].

Igneous Disruptive Events

Igneous disruptive events capable of causing significant damage are unlikely (i.e., igneous intrusion of the repository footprint has an annual probability of exceedance of less than 10^{-5} but greater than 10^{-8}). Therefore, further consideration of an igneous event in consort with a human intrusion stylized analysis is excluded from consideration. The exclusion is consistent with requirements of the NRC rule at 10 CFR 63.342 (b) [DIRS 178394] and 10 CFR 63.322 (g) [DIRS 180319], which exclude consideration of unlikely events (events with less than one chance in 10 in 10,000 years (i.e., an annual frequency of 10^{-5} yr^{-1}) in consort with a human intrusion event.

Seismic Disruptive Events

The analyses for seismic damage to DSs and WPs are documented in *Seismic Consequence Abstraction* (SNL 2007 [DIRS 176828]). The analyses provide a description of the damage that may occur to DSs and WPs from the mechanical response of EBS components to seismic hazards at the proposed repository horizon. The seismic induced damage to WPs and DSs includes the effects from fault displacement along faults that intersect the repository, seismic ground motion induced mechanical damage, or by rock fall, via imposed residual stresses in DSs and WPs (Section 6.6). The effect of fault displacement on the EBS is evaluated in terms of mean fault displacement hazard curves developed for faulting conditions mapped within the immediate vicinity of Yucca Mountain (SNL 2007 [DIRS 176828], Section 6.11 and Table 6-61). The Seismic FD Modeling Case includes disruption of the DSs and breach of the WPs affected by the displacement of faults, as well as nominal failures of DSs and WPs (Section 6.6.1.3). The expected number of WPs and DSs that fail from fault displacement is small because the number of WPs lying on known and generic faults is estimated to be 214, which is a small fraction of the approximately 11,000 WPs in the repository (SNL 2007 [DIRS 176828], Section 6.12.2, p. 6-255). Seismic events capable of causing significant damage from fault displacement are unlikely (i.e., WP failure due to fault displacement along faults intersecting the repository footprint has an annual probability of exceedance less than 2.2×10^{-7} [yr^{-1}] for TAD canisters and less than 2.5×10^{-7} [yr^{-1}] for co-disposed WPs (CDSP WPs) (SNL 2007 [DIRS 176828], Table 6-65). Therefore, further consideration of a seismic fault displacement event in combination with a human intrusion stylized analysis is excluded from consideration. The exclusion is consistent with requirements of the NRC rule in 10 CFR 63.342 (b) [DIRS 178394] and 10 CFR 63.322 (g) [DIRS 180319], which exclude consideration of unlikely events.

The effect of strong seismic ground motion is evaluated in terms of mean bounded ground motion hazard curve developed for Yucca Mountain (SNL 2007 [DIRS 176828], Section 6.4.3 and Table 6-3). For the seismic ground motion analysis, the threshold for considering the potential for damage to WPs and DSs is reached if the residual stress from mechanical damage exceeds the residual stress threshold (RST) for the barrier. The presence of residual stress induced by seismic events and/or related rock fall may result in local barrier degradation from accelerated SCC or rupture of the WPs and/or DSs (SNL 2007 [DIRS 176828], Sections 6.1.3

and 6.1.4). While SCC is appropriate for consideration of EBS flow and transport, it does not necessarily reflect changes to the effective material properties and may not constitute failure with respect to recognition of a change in conditions while drilling. Even with an imposed residual stress and minor amounts of corrosion and cracking, a rotating drill bit that encounters a metallic object will behave significantly different than when encountering naturally occurring geologic materials (Section 6.7.2.3). However, DS rupture, or plate fragility, is defined as the probability of rupturing or puncturing the DS plate during a seismic event (Section 6.6.1.2.2). For the evaluation of a human intrusion event, the DS rupture (plate fragility abstraction) is evaluated with respect to the earliest time a WP could be penetrated without recognition by the drillers.

The plate fragility abstraction is a function of peak ground velocity (PGV), the thickness of the DS plate, and the static load on the plates from rock fall (Section 6.6.1.2.2) (SNL 2007 [DIRS 176828], Section 6.8 and Table 6-36). Applying the maximum DS general corrosion rates over a 10,000-year period would reduce the original DS thickness of 15 mm by approximately 0.67 mm (using the 0.9999 quantiles for the underside and topside of the DS as discussed in Section 6.5.3.2.1). Given this conservative DS thickness (14.34 mm), there is a very small probability ($p<0.001$) for DS rupture to occur in a seismic event with a PGV of 1.05 (m/s). This evaluation assumes the probability of DS plate failure for a drift 100 percent filled with rubble (i.e., maximum static loading) linearly interpolated between a 10 mm and a 15 mm DS thickness (SNL 2007 [DIRS 176828], Table 6-36). A PGV of 1.05 m/s corresponds to an annual probability of exceedance of 9.955×10^{-6} (yr^{-1}) (SNL 2007 [DIRS 176828], Table 6-3). Given an annual probability of exceedance of 9.955×10^{-6} (yr^{-1}), seismic disruptive events capable of causing DS rupture are unlikely.

The other mechanism for rupture of a DS is from large rock block impacts in the nonlithophysal zones. These probabilities are given in the *Seismic Consequence Abstraction* (SNL 2007) [DIRS 176828], Table 6-54). The frequency of seismic events that result in a rupture of one or more DSs from large rock block impacts is evaluated to be 1.17×10^{-6} (yr^{-1}) (DTN: MO0712PBANLNWP.000_R0 [DIRS 184664], Nonlith LC Calculation Rev03.mxd). This again is less than the likely event cutoff of 0.1 in 10,000 years.

Consequently, with regard to the human intrusion stylized analysis in combination with a seismic event, it is concluded that seismic ground motion events are insufficient to significantly alter material properties of the DS to a sufficient degree that it would not be noticed by a driller in 10,000 years.

Finally, it should be mentioned that even in the unlikely event that a DS is damaged by a seismic event in 10,000 years, the chance of a WP being damaged by seismicity in the same time frame, in a way that it would not be recognized by the driller, is very low and below the likely/unlikely FEPs cutoff. In particular, stress corrosion cracks due to seismically-induced residual stresses in the Alloy 22 would not compromise the structural integrity of the WP; however, rupture (from the outside) or puncture (from the inside) of a WP could compromise its structural integrity. But, as demonstrated in Sections 7.3.2.6.1.3.5 and 7.3.2.6.1.3.6, both of these probabilities are less than 0.1 in 10,000 years. Thus, they are excluded from the Human Intrusion Scenario.

6.7.2.3 Potential for Waste Package Penetration by Drilling

The NRC, in the discussion regarding the timing and frequency of human intrusion (66 FR 55732 [DIRS 156671], p. 55761), states that "some evaluations of resource potential of the site suggest that Yucca Mountain (and the area immediately around it) does not represent an attractive candidate for either random or systematic exploratory drilling at this time...". A list of citations for those studies is available in the regulation. Furthermore, the elevation of the mountain, with the resultant greater depth to water compared to shallower groundwater wells that would be drilled to the south of the mountain, decreases the likelihood of groundwater exploration through the repository footprint. Regardless, the regulations specify evaluation of the timing of a human intrusion event and consideration of a stylized human intrusion assuming exploratory drilling for groundwater in the region surrounding Yucca Mountain (10 CFR 63.322(c) [DIRS 180319]). The following discussion presents several lines of evidence relevant to estimating the time when a human intrusion could occur, based upon the earliest time that current technology and practices used for groundwater exploration could lead to WP penetration without recognition by a driller.

There are a number of operational parameters that would indicate to a driller that a change in down-hole conditions would merit additional investigation, including a bit run (the removal of the bit from the hole for review and grading). These down-hole conditions could include loss of circulation, decreased penetration rate, increased drill string and bit instability, and increased drill string torque caused by differing material properties.

6.7.2.3.1 Initial Bit Selection and Drilling Principles

The bases for the following discussions are focused on typical practices used in drilling water wells in the southwestern United States. Generally speaking, the drill string assembly consists of the drill bit, drill collar, drill pipe, and in some instances, the use of stabilizers.

As described in Driscoll (1986 [DIRS 116801], pp. 278 to 286) and Bourgoyne et al. (1986 [DIRS 155233], Section 5.1), roller bits are typically used in drilling water wells due to their low cost and wide range of operational flexibility. Polycrystalline diamond cutter and diamond cutter drag bits typically are not used in water well drilling because of the high costs of these drill bits. Direct circulation down-hole hammer drills are sometimes used to drill brittle competent rock, such as welded volcanic tuff, but they typically are inefficient in unconsolidated alluvium or incompetent rock formations. This limitation reduces the use of these drills in typical water well drilling. The discussions provided herein are generally applicable to roller or hammer bits.

The initial selection of bit type is typically based on what is known about the formation characteristics. The terms usually used by drilling engineers to describe the formation characteristics are drillability and abrasiveness. The drillability of the formation is a measure of how easy the rock formation is to drill. It is inversely related to the compressive strength of the rock, although other factors are also important. The abrasiveness of the formation is a measure of how rapidly the cutting surface of a bit will wear when drilling the formation. Although there are some exceptions, the abrasiveness tends to increase as the drillability decreases (Bourgoyne et al. 1986 [DIRS 155233], Chapter 5).

The International Association of Drilling Contractors (IADC 1992 [DIRS 155232]) has developed a classification chart for selection of roller bits. Using this classification chart, roller bits with characteristics of 7-1 or 7-2 (hard semi-abrasive and abrasive formations) would be selected for drilling through the welded geologic units at Yucca Mountain, based on geomechanical properties. Roller bits are designed to take advantage of brittle failure of the rock matrix to crush, break, and remove the rock in an efficient manner. The volume of rock that is newly fractured by a tooth depends on the geometry, rock properties, and tooth penetration depth below the rock surface. The force applied to the tooth is supplied by the drill string torque and weight on the bit. The force applied to a particular situation determines the tooth penetration depth. The bit tooth penetrates into the rock until the resistant force offered back by the rock equals the force applied to the tooth. As a load is applied to a bit tooth, the pressure beneath the tooth increases until it exceeds the crushing strength of the rock and a wedge of finely powdered rock is formed beneath the tooth.

As the force of the tooth increases, the material in the wedge compresses and exerts high lateral forces on the solid rock surrounding the wedge until the shear stress exceeds the shear strength of the solid rock and the rock fractures. The rock may also exhibit ductility such that a greater tooth penetration is required to cause sufficient strain for chipping to occur (Warren 1987 [DIRS 155234]). The tooth will penetrate until the shear stress on the tooth is balanced by the shear strength of the rock.

These forces generate fractures that propagate along a maximum shear surface. As the force of the tooth increases above the threshold value, subsequent fracturing occurs in the region above the initial fracture, forming a zone of broken rock. The bit tooth moves forward until it reaches the margins of the wedge and/or fracture zone, and the process repeats (Bourgoyne et al. 1986 [DIRS 155233], Chapter 5). The crushed and broken material is then removed from the boring using circulated drilling fluids (air, water, or admixtures thereof) that also provide cooling and cleaning for the drill bit.

The drill collar is a heavy-walled length of drill pipe with a diameter less than the borehole diameter. If too much force is applied at the top of the drill stem, the drill pipe will bow and tend to cause the bit to cut off-center and, thereby, cause deviations in the borehole alignment. To compensate, drill collars are used to add weight to the lower part of the drill string assembly. This concentration of weight and the increased rigidity of the collars helps to keep the lower part of the drill assembly in alignment and provide weight to the bit to maintain appropriate penetration rate (Driscoll 1986 [DIRS 116801], p. 281). Drill collars may also be fitted with stabilizer devices that contact the borehole walls. The drill collars and stabilizers are used to maintain alignment of the drill string within the borehole and reduce vibration or wobble of the bit and drill pipe that transfers the torque from the surface to the drill bit.

6.7.2.3.2 Bit Operating Conditions and Change-in-Conditions

Bit operating conditions (i.e., drilling fluid properties and circulation rates, drill string stability, bit weight, and rotary speed) affect the rate of penetration and vibrations felt on the drill rig. These factors would be affected by the drilling assembly's entry into the emplacement drift, and the bit operating conditions would be significantly affected by the rounded geometry of the emplacement drift, DS, and WP.

The loss of drilling fluid circulation and sudden drop in weight on the bit when the drill bit breaks through the top of the emplacement drift would provide initial indications that conditions had changed significantly. The loss of circulation would occur because of the flow of drilling fluids from the borehole and into the emplacement drift which, at 5.5 m diameter and on the scale of a kilometer (km) in length, represents an essentially instantaneous increase in volume compared to the borehole volume. At that point, the driller would either try to continue drilling without compensating for the fluid loss in the hope of passing through the loss zone, would try various additives in the drilling fluid to try to seal the formation (Driscoll 1986 [DIRS 116801], p. 360), or would have to pull the drill assembly and either change drilling methods or install temporary or permanent casing to seal off the cavity. In the event of continued drilling, encountering of the DS or WP would prevent progress, and the lack of cooling from circulated fluids would eventually destroy the drilling bit and result in the drilling assembly being pulled from the hole (or otherwise cause the driller to consider alternative courses of action). Given the volume difference between the borehole and emplacement drift, it is implausible that any amount of additive would resolve the lost circulation problem, again leading the driller to some alternative course of action. Alternative courses of action, such as spot cementing through the loss zone or setting casing through the cavity, would involve pulling the drilling assembly from the borehole. In either scenario, the driller would then encounter continued volumetric problems or would encounter problems in trying to set casing due to the presence of the DS or WP within the emplacement drift.

In addition to loss of circulation, the space between the crown or sides of the emplacement drift (5.5 m) and the DS would cause the operating conditions to become unstable and would evidence themselves with a sudden increase in rotation speed as the weight on the drill bit was unloaded, followed by a sudden drop in the drill assembly (i.e., essentially free fall until the DS or invert of the drift was encountered), and/or a significant increase in the amount of vibration at the surface. Any of these conditions would cause the destabilization of the drill bit (i.e., tend to allow the bit to change direction from the original concentric alignment) and would trigger a response by the driller to address the change in conditions. This is particularly true as drilling conditions would noticeably change (due to the difference in rock and alloy material properties) if the drilling assembly came in contact with the DS material (Section 6.7.2.3.4).

The conditions described above assume that the drift has not collapsed. Rubble material in a collapsed drift could reduce the degree of these effects on drilling but would likely not eliminate them. The analysis of drift degradation (BSC 2004 [DIRS 166107]) indicates that during the regulatory period of 10,000 years, the ground support will completely lose its integrity, and drift degradation will occur due to strength decay of the rock mass within the lithophysal zone (BSC 2004 [DIRS 166107], Section 6.4.2.4). However, the collapse results in the bulking of, or increase in, the volume of the rock as the rock mass disintegrates into a number of pieces resulting in increased porosity and overall volume. The resulting bulk properties of the fill are different from that of the intact rock mass. Loss of drilling fluid circulation would still occur but perhaps could be accommodated by the driller. Additionally, the rubble pile of rocks would tend to move or shift under small loads, and the uneven loading on the drill bit would increase the lateral deviation forces (Bourgoyne et al. 1986 [DIRS 155233], Chapter 5). As such, even if the drifts collapse, the character of the rubble would be insufficient to stabilize the drill string. Severe wobbling bit action would result as the bit is rotated if the drill collars or stabilizers above the bit are not held in a concentric position in the borehole.

6.7.2.3.3 Penetration of the Drip Shield and Waste Package

To have any possibility of penetrating the DS or WP, the drilling assembly would have to contact the surfaces in an essentially perpendicular orientation. In general, deviation in alignment may be caused by the character of the subsurface material. This is because lateral deviation forces increase with relatively small changes in the contact angle between the bit and drilled material (Bourgoyne et al. 1986 [DIRS 155233], Chapter 5). Deviations may also be caused by too much or too little weight on the drill bit and differences in the pull-down force applied to the drill pipe during rotary drilling. Additionally, the varying hardness of different materials being penetrated deflects the bit from a consistent alignment.

Given that the top of the DS is curved and that most groundwater exploration holes are drilled in a near-vertical orientation (i.e., angle and directional drilling are possible but are not typically used for groundwater exploration purposes due to increased difficulty and cost), the drill bit would have to make contact at the relatively small areas that make up the apex of the DS or WP, where the surfaces are essentially perpendicular to the drill bit orientation. Only the apex of the DS or WP provides a perpendicular surface for which DS and WP geometry would not increase the lateral deviation forces.

If the drilling assembly contacts any location other than the relatively small areas that make up the apex of the DS or WP, then the relatively small drill bit diameter and high rotational speeds and the increased strength of material used for the DS and WP compared to the geologic materials (Section 6.7.2.3.4) would result in large lateral deviation forces and uneven loading on the bit. In turn, this would lead to drilling assembly instability and the bit would essentially bounce and slide on the top or side of the engineered barriers and potentially cause the drill bit to slip off of the DS or WP apex. Consequently, no penetration of the WP would occur. Furthermore, any non-slip contact with the DS or WP would be accompanied by a noticeable increase in drill string torque and reduced rate of penetration as the bit teeth contacted the metallic alloy. At the surface, the driller would recognize these conditions as a lack of drill bit penetration and excessive vibration. High levels of vibration and correspondingly low rates of penetration, such as these observed with poorly designed bits when crossing hard and abrasive formations would prompt the driller to adjust the rotary speed and weight on bit that eliminates shock. In some cases, this could include removing the drilling assembly from the borehole to inspect the bit condition (Putot et al. 2000 [DIRS 167791], p. 118), which would increase the chance for recognition of excessive bit wear and possible recognition that a metallic object had been encountered.

The ability of the drill string to penetrate a WP as a result of a sudden drop when the drill bit breaks through the top of the emplacement drift and the weight of the drill string-free falls, and potentially impacts the apex of the engineered barriers was considered. Impacts to a WP and resulting damaged area and rupture condition are determined for the OCB of the WP as documented in *Mechanical Assessment of Degraded Waste Packages and Drip Shields Subject to Vibratory Ground Motion* (SNL 2007 [DIRS 178851]).

The rupture condition of a WP is determined by comparing the maximum effective strain in the OCB (of a WP subjected to a single impact) to the ultimate tensile strain limit, which can be as low as 0.285, based on a triaxiality factor of 2.0 (SNL 2007 [DIRS 178851], Section 6.3.3, and

Appendix A). The procedure for determining the strain-based rupture condition is described in *Mechanical Assessment of Degraded Waste Packages and Drip Shields Subject to Vibratory Ground Motion* (SNL 2007 [DIRS 178851], Section 6.3.2.2.5, Figure 6-25). The maximum effective strain and rupture conditions for WP-to-pallet damage analyses, evaluated over a range of impact velocities up to 10m/s, a variety of impact locations, and a variety of impact angles, indicate that no rupture will occur for TAD-bearing and co-disposed WPs, whether intact or degraded to 17 mm with degraded internals (SNL 2007 [DIRS 178851], Tables 6-55 through 6-63 and 6-83 through 6-93).

Using Torricelli's equation (Equation 6.7-1), the upper bound estimate of impact velocity for the drill string at the WP outer barrier would be approximately 5.9 m/s for a TAD-bearing WP and 5.7 m/s for a co-disposed WP given a drop distance of 1.8 m and 1.6 m, respectively (Table 6.7-1).

$$v_f^2 = v_i^2 + 2a\Delta d \qquad \text{(Eq. 6.7-1)}$$

where

v_f = final velocity (or impact velocity of the drill string)

v_i = the initial velocity (0 m/s)

a = acceleration due to gravity (9.8 m/s)

Δd = distance from drift crown to the top of the WP (Table 6.7-1).

A 300-m long drill string assembly consisting of a drill bit, drill collar, and drill pipe, can be estimated to be approximately 14 metric tons (Table 6.7-2). Since the weight of the drill string (14 metric tons) is much less than the weight of a fully loaded WP (73.5 metric tons for a TAD-bearing WP, 58 metric tons for a co-disposed WP), and the upper bound of the impact velocity (5.9 m/s) of the lighter drill string is much less than the impact velocities used for the analyses cited above (10 m/s), no rupture of the WP will occur. The drill string velocity is an upper bound, since drilling mud and cuttings filling the borehole would create friction along the 300 m drop as well as, the likely presence of rockfall that would have accumulated in the drifts over the DSs and WPs would prevent the drill string from impacting the EBS components (i.e., a zero drop height). In addition the DS itself is another likely barrier to the drill string penetration which was not considered. The worst case location of drill string impact is at the DS crown and the DS is strongest at that point. A more probable scenario would be that the drill string would bend the DS into contact with the WP which would result in a very distributed load to the WP, further reducing the impact velocity. If the drill string could penetrate the DS, much of the impact energy to the WP would be reduced by the penetration (or crushing) of the DS.

6.7.2.3.4 Comparative Material Strength

Assuming that the drilling assembly does not slide off the apex of the DS, then a significant change in down-hole conditions would also be recognized because the failure mechanisms of brittle rock (such as that present at the repository host horizon) and ductile alloys (such as the materials used for the DS and WPs) differ significantly. These changes in failure mechanisms are so significant that specialized down-hole techniques and tools are used to drill through metal.

Milling (a technique used for drilling through metal) produces a different failure mechanism than brittle failure that roller bits and hammer bits typically produce. Bits designed for drilling rock would not be efficient for drilling through metal and would likely be seriously damaged, and the milling techniques needed to bore metals (Avallone 1987 [DIRS 103508], pp. 13-63 to 13-64) are not used in rock drilling unless required for specialized applications (i.e., Driscoll 1986 [DIRS 116801], pp. 316 to 319, Figure 10.10 and Figure 10.54).

Brittle materials are characterized by the fact that rupture occurs without any noticeable prior change in the rate of elongation. Thus, for brittle materials under tension, there is no difference between the ultimate strength and breaking strength. Also, under tension, the strain at the time of rupture is much smaller for brittle than for ductile materials (Beer and Johnston 1981 [DIRS 166708], p. 36). In general, brittle materials are weaker in tension than in shear (Beer and Johnston 1981 [DIRS 166708], p. 101), and brittle materials are significantly stronger in compression than in tension (i.e., the tensile strength of concrete is about 10 to 20 percent of its compressive strength; also see Table 6.7-3 for a comparison of rock strength in compression and tension). For brittle materials, strength is typically reported as compressive strength rather than tensile strength, while ductile material strengths are typically determined in tension.

The ductility of a material, such as the alloys used for the DSs and WPs, is usually measured as the percent reduction in area (or the elongation that occurs during a tensile test). Ductile materials, with a minimum elongation in tensile testing, will not fail in service through brittle fracture (Boyer and Gall 1984 [DIRS 155318]), which is the failure mode exhibited by the repository host horizon materials. Also, for ductile metals, the compression strength is generally assumed equal to the tensile strength (Beer and Johnson 1981 [DIRS 166708], p. 584). Generally speaking, values obtained for the yield strength and ultimate strength of a given material are only about half as large in shear as they are in tension, and the shear modulus is generally less than one-half, but more than one-third, of the modulus of elasticity of that material (Beer and Johnston 1981 [DIRS 166708], pp. 68 and 69).

Therefore, if the differences between milling and rotary drilling tools are ignored and rotary bits could be used to penetrate the engineered barriers, a measure for comparing strength properties between brittle and ductile materials is needed. One such parameter is a comparison of the modulus of elasticity of these differing materials. Because of the lack of elongation, the stress-strain diagram for brittle materials is generally linear, and the modulus of elasticity provides a convenient method for comparing material properties between brittle and ductile materials. This also suggests that comparison of tensile strength of brittle materials to yield strength of ductile materials may also be appropriate. Comparison of the compressive strength of rock materials and tensile strength of alloy is also appropriate. Furthermore, the reported shear modulus could be compared (if available) or a value of twice to three times the shear modulus could be compared to the modulus of elasticity.

Various rock properties for materials at Yucca Mountain are shown on Figure 6.7-4 and in Table 6.7-3, including uniaxial compressive strength, tensile strength, and modulus of elasticity (Young's modulus). Based on the design drawings and data tracking numbers (DTNs) cited, the yield strength, tensile strength, and modulus of elasticity for the DS and WP materials are shown in Table 6.7-4.

Studies that have been conducted to correlate operational parameters to the rate of penetration of the drill bit indicate that the rate of penetration may range from inversely proportional to the square of the strength of the material being drilled to inversely proportional to the strength of the material, all other factors being equal (Bourgoyne et al. 1986 [DIRS 155233], Equation 5-19; Kahraman 2000 [DIRS 167761], Equations 8, 12, and 14). Putot et al. 2000 [DIRS 167791], p. 123) suggests, at least for balling tendencies in shales and for a given weight on the bit, that drilling performance collapses upon a doubling of the rotary speed. Assuming that a change in the penetration rate by a factor of 1.5 or greater (increase) or 0.66 or less (decrease) (i.e., some condition occurring before performance collapse) would be sufficient to be noticed by a driller, a change in compressive strength of materials by a factor of 1.5 (or possibly less if one assumes the inverse square relationship presented by Bourgoyne et al. 1986 [DIRS 155233]) would cause a significant change in drilling conditions that would be recognized by the driller.

Table 6.7-3 indicates that the mean compressive strength of the rock material ranges from 19.3 MPa to 188.8 MPa. At room temperature, the tensile strength of the DS materials ranges from 345 MPa to 895 MPa (Table 6.7-4). Thus, the factor of compressive strengths ranges from about 1.8 (345/188.8) to as great as 46 (895/19.3). The tensile strength of the WP material at room temperature ranges from 550 MPa to 802 MPa (Table 6.7-4). This represents factors of 2.9 (550/188.8) to as great as 42 (802/19.3). If one conservatively assumes the yield strength of the engineered barrier materials is comparable to rock compressive strength, the factors decrease. For the DS material at room temperature, the factor ranges from 1.5 (275/188.8) to 23 (450/19.3). For the WP material at room temperature, the factors range from 1.3 (240/188.8) to as great as 21 (403/19.3). However, given that all WPs include Alloy 22 material in the outer barrier, the lower end of the range is bounded at a factor of 1.9 (358/188.8). Therefore, at room temperature, there is a minimum factor of 1.9 for the WPs and 1.5 for the DSs. If one assumes an inverse proportionality of rock strength to rate of penetration, the penetration rates would decrease to less than 67 percent of the rock penetration rate when intersecting a DS and to less than 53 percent of the rock penetration rate when intersecting a WP and, therefore, be recognizable, as previously discussed.

At elevated temperatures, such as those during the thermal period (i.e., 200^{o}C), the strength properties of the DS material are reduced (DTN: MO0003RIB00073.000_R0 [DIRS 152926]) for Titanium Grades 7 and 16. The factor reduces in range from 1.1 (207/188.8) to as great as 12 (228/19.3), based on compressive strength. However, the properties of the Alloy 22 outer barrier are not as significantly reduced. The factor for compressive strengths for the elevated temperature ranges from 3.5 (662/188.8) to 36 (701/19.3). The minimum factor of 1.1 for the DS and rock strength comparison at elevated temperature would not by itself produce a sufficient change in penetration rate to be noticed by a driller. However, further penetration to a WP, with a larger compressive strength change, would produce a sufficiently reduced penetration rate.

Furthermore, the mean tensile strength of the brittle rock units is reported to range from 7.9 MPa to 10.9 MPa (or approximately 6 percent of the corresponding mean compressive strength). These rock tensile strengths are at least a factor of 19 less than those of the ductile engineered barrier materials, even at elevated temperatures. Even conservatively assuming an equivalence of the yield strength of a ductile material to tensile strength of brittle material generates a difference of a factor of 13.

Similarly, the mean modulus of elasticity for the rock materials is on the order of 6.9 to 33.6 GPa. By contrast, for the ductile alloys, the modulus of elasticity ranges from 107 to 206 GPa, representing a minimum factor of 3.2 different from the rock properties. These differences in tensile strength and modulus of elasticity between the brittle rock and ductile engineered barrier materials would further contribute to lack of drill bit penetration and excessive vibration.

Finally, the recognizable differences in penetration rate or vibrations are only applicable in the improbable situation of a rock drill bit hitting sufficiently near the engineered barrier apex to avoid bouncing or sliding (such as by impacting a metal crack) to initiate penetration into the engineered barrier. It is more likely that rotary bits for rock, which are not designed for drilling in metal, would simply bounce and slip off either the DS or WP.

The discussion provided above would be applicable even if the DS or one of the materials used in the WP were degraded to the point where structural integrity were lost or, in the case of the DS, the interlock mechanism were bent and penetrated by the drilling assembly.

Summary of Waste Package Penetration by Drilling Analysis

Selection of a bit for drilling involves knowledge of the characteristics of the rock. As indicated in Tables 6.7-1 and 6.7-2, there are significant differences between the tensile strengths and other material properties of the geologic units at Yucca Mountain and the materials for the DS and WP. Because the materials used in the DSs and WPs have high tensile strengths, yield strengths, and increased modulus of elasticity compared to the host rock properties, the tooth of a roller bit cannot penetrate enough to cause sufficient strain for chipping to occur. Rather, if contact with the DS occurs, the rotation of the bit would result in a tearing or shearing action with associated and recognizable high torque values. Consequently, the ductility of the metals makes them nearly impenetrable by techniques used in drilling rock. Boring in metals typically utilizes a milling technique. The down-hole milling tools needed to penetrate the DS and WP are not typically used in groundwater exploration, and use of such tools would be a clear indicator of recognition of penetration of some type of metallic, anthropogenic structure.

6.7.2.4 Earliest Time of Waste Package Penetration by Human Intrusion

Conclusions based on information presented above suggest that a human intrusion event, if it were to occur before the WPs and DSs had sufficiently degraded, would not happen without recognition by the drillers. General corrosion of the DS is not expected to thin the DS plates significantly before 230,000 years (Section 6.7.2.1) and seismic ground motion cracks are not expected to affect a rotating drill bit because the failure mode and drill bit interaction are significantly different for rock and metals, as discussed in Section 6.7.2.3. In general, until a breach of the DS occurs, the structural integrity of the WP is maintained, providing an additional barrier to drill-bit penetration. The analysis provided in this section indicates that an unrecognized intrusion will not occur prior to 10,000 years following closure of the repository and that several possible modes of DS and WP damage that might contribute to drilling penetration of the DS or WP can be screened out as unlikely (per 10 CFR 63.342(b) [DIRS 178394]), such as early failure and all damage modes related to seismicity. For the TSPA-LA Human Intrusion Scenario, the WP degradation is conservatively ignored and the human intrusion event time, based on DS corrosion and observable effect on the drilling system

is taken to be no less than 200,000 years. Although some uncertainty exists about the timing of when penetrating a WP would not be detected, an assumption of penetration at 200,000 years is appropriate. This is a conservative estimate since there is less than a 0.0001 chance of DS general corrosion failure prior to 230,000 years (based upon the 0.9999 percentile corrosion rates) and because WP degradation (formation of open breaches) takes significantly longer than this. Thus, until some time after 200,000 years, there is a double barrier to drilling penetration of the waste forms. Therefore, for the stylized Human Intrusion Scenario, 200,000 years is conservatively assumed to be the earliest time a driller could penetrate a WP without recognition. The dose results described below use this conservative intrusion time without uncertainty.

6.7.2.5 Treatment of Likely Waste Package Degradation Processes

Section 6.7.2.2 described the screening of unlikely DS degradation FEPs from the analysis of the occurrence time of the earliest unrecognizable drilling penetration, since this earliest time is conservatively based on DS degradation rather than actual WP penetration. It also indicated that seismic rupture or puncture damage of a WP, even in the unlikely event of a DS failure, is unlikely, too. However, 10 CFR 63.322(g) [DIRS 180319] does imply that all likely FEPs must be included. For DS degradation only, the general corrosion process is considered to be a likely FEP, while for WP degradation, both nominal corrosion processes and seismic degradation of co-disposal WPs are likely FEPs. However, the effects of these likely WP degradation FEPs are treated conservatively in this human intrusion analysis by effectively screening out their effects. In particular, as implied by 10 CFR 63.322 [DIRS 180319], it would appear that the main focus of the Human Intrusion Scenario is on the incremental dose possible due to drilling penetration. Dose to the RMEI arising from general corrosion or likely seismic degradation FEPs is already part of the overall TSPA. Therefore, the only reason for including these FEPs in the human intrusion TSPA would be if they could increase the dose due to a drilling penetration of a single WP. However, the opposite is true, as explained below.

It is highly probable, for example, based on the results of the Seismic Ground Motion Modeling Case (Section 6.6), that co-disposal packages will fail by seismically-induced stress corrosion cracks before the occurrence of the postulated human intrusion event at 200,000 years, even for smaller ground motions that occur at annual frequencies greater than 10^{-5} per year (the likely/unlikely FEP cutoff). For example, as described in Section 7.3.2.6.1.3.7, the maximum frequency of events that causes SCC damage to a co-disposal WP is estimated to be 2.181×10^{-5} per year. For a Poisson process at this occurrence frequency, this implies a 98.7% chance of one or more damaging seismic events within 200,000 years $[= 1 - \exp\{(-2.181 \times 10^{-5}\ \text{yr}^{-1})(2 \times 10^{-5}\ \text{yrs})\}]$. Ignoring diffusive radionuclide releases through these cracks prior to the time of the drilling intrusion is conservative; however, because accounting for these diffusive releases would reduce the radionuclide content of the WP for nuclides that are not solubility limited, such as ^{99}Tc and ^{129}I including minor, but conservative, effects on the actinide releases. The same logic applies to possible WP damage prior to 200,000 years due to nominal SCC processes.

Regarding likely seismic crack damage and nominal corrosion damage (either cracks or patches) subsequent to the drilling intrusion penetration, these releases and their dose are already included in the overall TSPA. Also, inclusion of these releases could only serve to lower the dose attributable to release down the borehole pathway, since the cracks and patches would provide an

avenue of escape into the UZ at spatial locations different than the borehole location (i.e., the occurrence of seismic crack damage and nominal corrosion patches and cracks would generally occur on a part of the WP surface not in contact with the borehole pathway). Thus, these seismic or nominal WP breaches would not contribute in any way to increasing the possible concentration of radionuclides in the water flowing down the borehole. In fact, if included, the releases associated with these patches and cracks would lower the concentration of radionuclides flowing down the borehole for nuclides that are not solubility limited, such as ^{99}Tc and ^{129}I.

In summary, general corrosion and likely seismic degradation of the WP can be conservatively omitted from the human intrusion TSPA.

6.7.3 TSPA-LA Model Implementation

The stylized Human Intrusion Scenario is based on the human intrusion scenario in NRC rule 10 CFR 63.322 [DIRS 180319], and the individual protection standard for a human intrusion of the repository in 10 CFR 63.321 [DIRS 178394].

6.7.3.1 EBS Transport for Human Intrusion

Conceptual Model—The human intrusion borehole is assumed to be drilled from the ground surface (at a random location within the footprint of the repository), through the DS and a single WP (top and bottom) to the water table. All cladding, either CSNF or DSNF, is assumed destroyed when drilling intersects a WP. The initial fraction of failed cladding and the fraction of fuel available for corrosion are set to one. The WP type is randomly selected, either CDSP WP or CSNF WP. The location of the intrusion is also unknown and is therefore randomly placed in one of the five repository percolation subregions. After penetration of the WP via a drilling event, water will flow into the WP and the waste form degradation and mobilization will occur. Nominal Scenario Class submodels for Waste Form Degradation and Mobilization (Section 6.3.7) and EBS TH Environment (Section 6.3.2) were applied in the Human Intrusion Scenario. Radionuclide mass is released from the intruded WP to the EBS Transport Submodel (described in Section 6.3.8). Nominal Scenario Class submodels for transport of mass from the UZ to the SZ (described in Section 6.3.9) were modified for the Human Intrusion Scenario calculation to simulate mass transport through a borehole pathway.

Implementation—For a human intrusion event, the WP type (CSNF or CDSP) and WP location within the repository footprint need to be characterized. These properties, WP type and WP location, are treated as aleatory uncertainties and randomly selected from assigned probability weights:

1. The probability of a human intrusion event impacting a CSNF type WP is set equal to the fraction of CSNF WPs relative to the total number of WPs in the repository (combined CSNF and CDSP WPs). The probability of impacting a CDSP WP is assigned the remaining percentage. The number of WPs projected to be emplaced in the repository is 11,629 (Section 6.3.7, Table 6.3.7-1). There are 8,213 CSNF WPs (including 417 Naval SNF WPs) and 3,416 CDSP WPs (Section 6.3.7, Table 6.3.7-1). Thus, there is about 70 percent probability the intruded WP is a CSNF WP and about 30 percent probability the intruded WP is a CDSP WP.

2. The location of the WP intersected by a Human Intrusion drilling event can be randomly selected based upon the areal distribution of the five percolation subregions that have been defined over the repository horizon as defined by the EBS TH Environment Model Component described in Section 6.3.1. The mean infiltration, glacial-transition climate percolation flux values at the base of the PTn for each of the 3,264 MSTHM Process Model subdomains are used to group each of the subdomains into one of five repository percolation subregions (Section 6.3.2). The probability of an event (i.e., Human Intrusion failed WP) occurring in any of the five percolation subregions is the same as the distribution used to define the percolation subregions (i.e., 5 percent, 25 percent, 40 percent, 25 percent, and 5 percent) (Section 6.3.2.2.1).

Once the WP type and percolation subregion are selected, the representative temperature and relative humidity time histories are applied for calculating the waste form degradation rate, in-package chemistry, and transport properties in the EBS. The seepage flux through the intruded WP is applied by taking the percolation flux at the base of the PTn (supplied by the MSTHM; Section 6.3.2) for the selected percolation subregion. The Seepage DLL, used to compute the drift-scale seepage, is exercised using the same method as the Igneous Intrusion Modeling Case to get the percolation flux without flow focusing effects at the drift boundary (Section 6.5.1).

The percolation flux (a Darcy flux) is converted into a volumetric flux by multiplying it with the borehole cross-sectional area, 0.0324 m^2, which is calculated using an 8 in. (20.3 cm) borehole diameter. The borehole diameter is a fixed value based on the range of outer drill pipe diameters used in direct rotary drilling, or 2 3/8 to 6 in. (0.60 to 15.2 cm) (Driscoll 1986 [DIRS 116801], p. 282). It is assumed that the diameter of the borehole would be slightly larger than the outer drill pipe diameter; therefore, 8 in. (20.3 cm) is adopted.

The entire calculated volumetric flux is used as the flow through the WP for the advective transport calculation through the WP. For the diffusive transport calculation through the WP, the diffusive area is set equal to the cross-sectional area of the borehole, and the downstream boundary concentration is effectively set to zero concentration to maximize diffusion out of the WP. This is done by giving the invert cell pathway a very large water volume. The borehole water flux is assumed to flow directly into the penetrated WP without any diversion of the water by the DS or WP. The advective and diffusive mass flux out of the WP is summed and then passed to the UZ borehole below the WP.

6.7.3.2 UZ Transport for Human Intrusion

Conceptual Model—The radionuclide mass (both dissolved and colloidal) released from the WP penetrated by the human intrusion borehole is assumed to be vertically transported down the borehole to the water table. The borehole transport pathway is conceptualized to be an originally uncased borehole that undergoes degradation shortly after it was drilled from wall collapse. For the purposes of modeling transport through this degraded borehole, the matrix and fracture properties of the UZ rock types comprising the repository horizon are utilized. The rubble fill in the borehole is considered to have properties similar to the undisturbed repository host rock matrix while any preferential pathways within the rubble fill are given fracture properties of the host rock. As a result, the collapsed matrix blocks are expected to occupy about 99 percent of

the borehole volume while about 1 percent of the borehole volume is occupied by the fracture (consistent with the fracture porosity of the undisturbed rock). Although the preferential pathways may be tortuous and may not remain continuous throughout the length of the borehole and over the simulated time periods, the assumption of a continuous vertical fracture pathway over the entire length of the borehole is considered to simplify the modeling. When a human intrusion occurs, the three-dimensional TSPA-LA UZ Transport Submodel (Section 6.3.9) is replaced with a one-dimensional Human Intrusion Borehole Transport Submodel. The three-dimensional submodel calculates UZ transport using FEHM (V2.24-01, STN: 10086-2.24-01-00 [DIRS 179419]), whereas the Human Intrusion one-dimensional submodel calculates mass transport from the base of the WP to the water table using a single GoldSim pipe element.

The mass released from the intruded WP is passed to the one-dimensional pipe that simulates the borehole effects in the UZ beneath the WP. The properties that define the borehole fill are chosen to be consistent with the near-drift rock properties used in the UZ Transport Submodel (described in Section 6.3.9). The transport path length through the borehole is determined to be the vertical path length between the repository and the future water table. Because the repository host rock and water table elevations change over the UZ and SZ transport domains, the shortest possible transport path length is conservatively chosen. The volumetric water flux that is passed through the WP for computing advective transport is maintained throughout the borehole – there are no additional sources or sinks for water in the borehole.

Implementation—A schematic cross-section of a borehole bisecting the repository system and intruding through the underlying UZ to the water table is shown on Figure 6.7-5. The borehole is conceptualized to be filled with the rubble of collapsed matrix blocks that have preferential pathways similar to the fractures in the undisturbed host rock near the drift (Figure 6.7-6). The volume fraction occupied by the preferential pathways is assumed to be the same as the fracture porosity of the undisturbed host rock. Figure 6.7-7 is a schematic illustration of the key parameters used to calculate flow and transport through the UZ borehole pipe to the saturated zone and on to the biosphere. The fracture properties such as fracture aperture, porosity, and frequency (Table 6.7-5) are assumed to be the same as that for the undisturbed rock type in the vicinity of the repository horizon (such as the TSw unit). To be consistent with the UZ Transport Submodel, the property sets grouped for rock units TSw34, 35, 36, 37, and 38 are used to define the borehole properties (see property set associated with Group 8 given in Table 1 of DTN: LA0701PANS02BR.003_R2 [DIRS 180497]). For model simplification, these values do not vary with depth, although the borehole may cut across other lithologic units. Table 6.7-6 shows the calculated fracture properties associated with the borehole pathway. The number of vertical fractures within the diameter of the borehole is determined by considering the fracture frequency (calculated to be about four fractures per meter) and comparing it to the diameter of the borehole (approximately 0.2 m) calculated from a borehole cross-sectional area of 0.0324 m^2. This results in less than one fracture per borehole diameter, which is rounded up to be one fracture for the borehole. Assumption of vertical orientation of the fractures is consistent with the conceptualization of fractures in the UZ Transport Submodel (Section 6.3.9). The vertical fracture geometry is assumed to be like parallel plates without any infill material throughout the length of the borehole. The rubble filling the borehole surrounds the fracture. The fracture aperture and fracture porosity (fraction of the borehole volume occupied by the fracture) are considered fixed at 0.00264 m and 0.0105, respectively, which are average values for Group 8 rock type of the UZ Transport Submodel (DTN: LA0701PANS02BR.003_R2 [DIRS 180497]).

No uncertainty is applied to these parameters as it is not currently known how the uncertainty range would be affected by a borehole that cuts across several lithologic units of varying thicknesses. In order to compute the plan area of the fracture, the fracture width is needed in addition to the fracture aperture. Since the width of the cross-cutting fracture could vary in the circular borehole based on the fracture orientation, the average width, calculated by dividing the borehole cross-sectional area by its diameter, giving a value of about 0.16 m, is used.

Both advective and diffusive transport of radionuclides in the borehole are modeled by using the pipe pathway in GoldSim. A dual-porosity approach is adopted by modeling a discrete fracture that is surrounded by the matrix. The cross-sectional area of the pipe pathway is defined to be equal to the plan area of the fracture (a discrete fracture with no infill) while the matrix diffusion zones in the pipe pathway are used to define the rubble material that fills up the borehole around the fracture. The radionuclide mass flux from the WP is passed into the fracture, where it advects vertically downwards and diffuses into the surrounding matrix normal to the flow. The maximum diffusive distance into the matrix is set equal to half the distance between two fractures (about 0.125 m), and the entire surface of the fracture wall within the borehole is assumed to be wetted for diffusive transfer to the matrix (Figure 6.7-6). The diffusion of radionuclides irreversibly associated with colloids is not modeled between fracture and matrix, consistent with the UZ Transport Submodel implemented using FEHM DLL. All of the water flowing through the borehole is passed through the vertical fracture, which is the most conductive zone in the borehole. The fractures are assumed to be free flowing with no infill or obstructions. No retardation of the radionuclides (dissolved or colloidal) is modeled on the fracture surface. A fracture longitudinal dispersivity value of 10 m is assumed in the fracture that is consistent with the values used in the UZ Transport Submodel (SNL 2008 [DIRS 184748], Section 4.1.6).

The saturation values for the fracture and matrix along with the matrix density and porosity are taken from the EBS-UZ Interface Model described in Section 6.3.8, while the matrix tortuosity for diffusion calculations are taken from DTN: LB0702PAUZMTDF.001_R1 [DIRS 180776], for Rock Group 3, which includes values for rock unit TSw. Within the matrix media, the radionuclides are assigned the sampled K_d values for devitrified units used in the UZ Transport Submodel, for the entire pathway.

A flat lying water table beneath the repository is estimated to be located at an elevation of about 850 m, based on the water table rise estimated to occur during the glacial-transition climate period (SNL 2008 [DIRS 184748], Section 6.4.8). For the repository elevation, a value of 1,040 m is assumed which is consistent with present design documents where all repository drifts are at elevations of 1,039 m or higher (SNL 2007 [DIRS 179466], parameter 01-02). Thus, the path length of the borehole from the repository to the SZ is set at 190 m.

6.7.3.3 SZ Transport for Human Intrusion

Conceptual Model— The transport of radionuclides through the SZ in the Human Intrusion Scenario is identical to the Nominal Scenario Modeling Case, with the exception of the selection of the mass entry point to the SZ Source Region. From the borehole, the radionuclides are passed to one of the four SZ source regions (SZ region). The SZ source region is selected in such a way that it spatially corresponds to the EBS percolation subregion intersected during the

human intrusion event. Additionally, mass irreversibly associated with colloids are partitioned to fast and slow fractions in the SZ.

Implementation—In order to apply spatial correlation between the EBS percolation subregions (where the radionuclides enter the borehole) and SZ source regions (where the radionuclides exit the borehole), the five EBS percolation subregions are mapped to the four SZ source regions. The relative areal fraction of the five EBS percolation subregions within the four SZ source regions is determined first and then converted into the probability of each SZ source region to accept the radionuclides released from a given EBS percolation subregion through the borehole. A more detailed description of the four SZ source regions (quadrants) can be found in *Particle Tracking Model and Abstraction of Transport Processes* (SNL 2008 [DIRS 184748], Section 6.5.16).

The spreadsheet *fehm_repo_nodes_GT10%.xls* (DTN: LA0702PANS02BR.001_R1 [DIRS 180322]) provides the mapping of the UZ nodes at the repository horizon with the five EBS percolation subregions. There are 560 UZ nodes included in the five percolation subregions, along with their geographic locations in UTM coordinates. The 560 UZ node locations sorted by percolation subregion are mapped to the SZ quadrants in the spreadsheet *PS_EBSmaptoSZ.x*ls (output DTN: MO0708TSPAGENT.000 [DIRS 183000]) and the fraction of each of the five percolation subregions to the four SZ regions is calculated (Table 6.7-7).

6.7.3.4 Mean Annual Dose Submodel for the Human Intrusion Scenario

The TSPA-LA Model calculates the mean or median annual dose for the Human Intrusion Scenario using a two-step process. First, the TSPA-LA Model generates a set of 9,000 realizations, i.e., 9,000 annual dose histories, by using a LHS sample of 30 over the three aleatory parameters (WP type, percolation subregion, and SZ source region) and an LHS sample of 300 over the epistemically uncertain parameters in all the submodels. For each realization, the single human intrusion time is fixed at 200,000 years after the closure of the repository. The resulting 9,000 annual dose histories are then averaged in groups of 30, corresponding to the 30 aleatory samples for each epistemic sample thus producing 300 expected dose histories (Equation 6.1.2-26). These 300 expected dose histories are then averaged at each time to produce the overall mean annual dose history or their 50th percentile values are computed at each time to produce the median annual dose history. Note that the 300 epistemic samples for this modeling case match the 300 epistemic samples used for the overall performance assessment calculations.

6.7.4 Model Component Consistency and Conservatism in Assumptions and Parameters

To enhance understanding of the complex interactions within the TSPA-LA Model, a discussion of consistency among model components and submodels and identification of conservative assumptions in abstractions, process models, and parameter sets supporting the Human Intrusion Scenario are discussed below. Many of the nominal abstractions, process models, and parameter sets are used in the Human Intrusion Scenario and, therefore, many of the discussions of the implementation provisions in Section 6.3 apply to the Human Intrusion Scenario.

6.7.4.1 Consistency of Assumptions

WP and DS Material Corrosion in the Human Intrusion Scenario—General corrosion and SCC of the WP and DS materials are not applied to the WP/DS pair penetrated by a human intrusion event. The WP/DS general corrosion and SCC submodels are turned off for the Human Intrusion Modeling Case.

Effect on the TSPA-LA Model—The early penetration time of a WP/DS pair of 200,000 years postclosure during a Human Intrusion Scenario event is a conservative assumption. After the WP is penetrated, the entire waste form is exposed to the water flux through the WP. Applying the general corrosion model would not result in an earlier failure time (as demonstrated in Section 6.7.2). The radionuclide releases will be predominately via advective transport. Additional SCC cracks or general corrosion patches would not increase the volumetric water flux or mass flux of radionuclides released from the WP. This assumption will have no effect on the results of the Human Intrusion Scenario.

6.7.4.2 Identification of Conservatisms in Submodels and Abstractions

Human Intrusion Event Time—The probability associated with a human intrusion event time of 200,000 years postclosure assumes a WP would be degraded sufficiently to be undetected by drillers using the common techniques and practices that are currently employed in exploratory drilling for ground water in the region surrounding Yucca Mountain (NRC Rule 10 CFR 63.322(c) [DIRS 180319]). Assuming an early event time is conservative in respect to the probability of WP failure.

UZ Borehole as a Fracture Pathway—This fracture is conceived to be a highly conductive zone with elevated flow velocities through the fracture void space. Matrix diffusion into the host rock occurs and depends on fracture frequency. Using the fracture frequency for the UZ host rock (~ 4 per meter) yields only one fracture, given the diameter of the borehole. Matrix diffusion over the length is calculated as half the distance from the nearest fracture. Therefore, a limited amount of matrix medium is used to define the matrix diffusion zone between fractures in the pipe pathway.

Fewer fractures result in less surface area in the pipe pathway. A smaller surface area results in less sorption into the UZ rock matrix as the radionuclides travel through the UZ pipe pathway.

UZ Borehole Pathway Length—The Human Intrusion Scenario assumes the shortest possible transport path length. The conservative estimate for future water table rise places a flat water table at an 850 m elevation, reached during the glacial transition climate period (SNL 2008 [DIRS 184748], Section 6.4.8). Based on elevations reported in *TSPA Data Input Package for Requirements Analysis for Subsurface Facilities* (SNL 2007 [DIRS 179466], parameter number 01-02), a value of 1,040 m is assumed for the repository drift elevation (all repository drifts are at elevations of 1,039 m or higher).

A conservative length of the borehole from the repository to the SZ is set at 190 m. This conservatism tends to shorten radionuclide transport times.

6.7.5 Alternative Conceptual Model(s) for the Human Intrusion Scenario for TSPA-LA

Section 6.2.1 outlines the general consideration and treatment of ACMs used to support the TSPA-LA Model. ACMs related to individual submodels used in the Human Intrusion Scenario calculations are discussed in relevant Section 6.3 sections. There are no ACMs specific to the stylized Human Intrusion Scenario.

INTENTIONALLY LEFT BLANK

Table 6.7-1. Waste Package Specification and Design Dimensions

Parameter		Source	Description
Drop Height (TAD-bearing)	1.80 m	SNL 2007 [DIRS 179354], Figure 4-1, *In-Drift Configuration*.	Distance from drift crown to top of DS plus the distance from the DS to the top of WP.
Drop Height (CDSP WP)	1.63 m		
Nominal loaded mass for TAD-bearing waste package	162,055 lbm (73.5 mT)	SNL 2007 [DIRS 179394], Table 4-3	NA

Table 6.7-2. Specifications of Drilling Components

Parameter		Source	Description
Length of Drill String	300 m	SNL 2007 [DIRS 179466], Table 4-1	Assumed depth from the surface to the repository horizon. Based upon design information for minimum standoff distance from repository to water table.
Weight of Drill Steel	20 lb/ft (29.8 kg/m)	American Petroleum Institute 1992. Specification for Drill Pipe. API Spec. 5D, 3rd Edition, Table 6-1, 4.5-in drill pipe.	Drill pipe weight for standard 4.5 inch OD well pipe.
Length of Drill Collar	30 ft (9.1 m)	Grant Prideco 2003 [DIRS 183165], p. 99, drill collar number NC 44-62	Typical drill collar length for 6.25 inch OD drill collar.
Number of Drill Collars	4	NA	Assumed 100 ft of drill collar (10% of depth), based on common drilling practices.
Weight of Drill Collar	90.52 lbs (41.0 kg)	Grant Prideco 2003 [DIRS 183165], p. 99, drill collar number NC 44-62	Typical weight for 6.5 inch OD drill collar.
Weight of Drill Bit	38 kg (83 lb)	Varel International 2006 [DIRS 183166], Bit Weights Table, p.27, 8.5 “ bit	Assumed approximately 8” (20.3 cm) borehole diameter, based on current drilling practices for a typical water well with an outer pipe diameter less than 6 in (15.2 cm) (Driscoll 1986 [DIRS 116801], p.282).
Total Weight of Drill String Assembly	13.8 mT	NA	(Length of Drill Sting × Weight of Drill Steel) + (Length of Drill Collar × Number of Drill Collars × Weight of Drill Collar)+ Weight of Drill Bit

Table 6.7-3. Uniaxial Compressive Strength and Young's Moduli by Rock Unit

Rock Unit	Uniaxial Compressive Strength Mean (MPa)	Tensile Strength Mean; Range (MPa)	Shear Modulus (GPa)	Elasticity (Young's Modulus) Mean; Range (GPa)
Topopah Springs Tuff – upper lithophysal zone (Tptpul)	19.3	–	–	13.0; 5.0–21.5
Topopah Springs Tuff – lower lithophysal zone (Tptpll)	23.8	8.3; 3.2–14.3	0.80–8.21	6.9; 5.0–9.2
Topopah Springs Tuff – middle nonlithophysal zone (Tptpmn)	188.8	10.9; 4.3–16.8	–	33.6; 13.4–47.3
Topopah Springs Tuff – lower nonlithophysal zone (Tptpln)	129.9	7.9; 4.8–13.7	–	33.6; 13.4–47.3

Sources: Mean Uniaxial Compressive Strength data (also referred to as Ultimate Strength) for the Tptpul and Tptpll are calculated as the mean of the strength data from *Drift Degradation Analysis* (SNL 2007 [DIRS 166107], Table E-9). The Mean Uniaxial Compressive Strength of the Tptpmn unit is from *Drift Degradation Analysis* (SNL 2007 [DIRS 166107], Table E-14). The Mean Uniaxial Compressive Strength of the Tptpln is calculated as the mean of the strength data from DTN: MO0408MWDDDMIO.002 [DIRS 171483], *Calculation Files\Material property\rock mass strength v2.xls*, worksheet Intact Strength (using Ultimate Differential Strength data with a Confining Pressure of either 0 or 0.1 MPa).

Tensile Strength (SNL 2007 [DIRS 166107], Table E-70).

Shear Modulus estimated for rock mass qualities 1 through 5 (SNL 2007 [DIRS 166107], Table E-10).

Mean for Elastic Modulus (Young's Modulus) (SNL 2007 [DIRS 166107], Tables E-6 and E-9).

Table 6.7-4. Material Properties for Drip Shield and Waste Package Fabrication

Engineered Barrier Material	Use	Yield Strength at 0.2% Offset (MPa)	Tensile Strength (MPa)	Modulus of Elasticity (GPa)
Titanium Grade 7[a] and Grade 16 (at room temperature)	Drip Shield	275–450	345	106.87
Titanium Grade 7[a] and Grade 16 (at 400°F/204°C)	Drip Shield	138–152	207–228	–
Titanium Grade 24	Drip Shield	–	895[b]	113.8[c]
Alloy 22 (UNS N06022) (at room temperature)[d]	Waste Package	358–403	765–802	206
Alloy 22 (UNS N06022) (at 400°F/204°C)[d]	Waste Package	262–303	662–701	196
Type 316 N Grade Stainless Steel (minimum properties)[e]	Waste Package	240	550	196

[a]DTN: MO0003RIB00073.000_R0 [DIRS 152926] for Titanium Grades 7 and 16.
[b]Tensile strength for Titanium Grade 24 (ASME 1998 [DIRS 145103], Section II, Table 1).
[c]Modulus of Elasticity for Titanium Grade 24 (ASM International 1990 [DIRS 141615], p. 621).
[d]DTN: MO0003RIB00071.000_R0 [DIRS 148850] for Alloy 22 (UNS N06022).
[e]DTN: MO0003RIB00076.000_R0 [DIRS 153044] for Type 316N.

Table 6.7-5. Borehole Properties used in UZ Flow and Transport Calculations

Parameter Name	Description	Parameter Value	Reference
HI_UZ_Borehole_Length	Distance between the repository horizon elevation and the estimated maximum water table elevation during the Glacial-Transition Climate.	190 m	(SNL 2008 [DIRS 184748], Section 6.4.8) and (BSC 2003 [DIRS 161727])
HI_UZ_Borehole_Disp	UZ borehole fracture dispersivity.	10 m	(SNL 2008 [DIRS 184748], Section 4.1.6)
HI_UZ_Fracture_Aperture	Distance between fracture openings in UZ borehole. Aperture, 2b (m), is calculated using fracture porosity and frequency distribution for rock units closest to the repository horizon (Group 8 or tswF[4,5]).	0.00264 m	(SNL 2008 [DIRS 184748], Table 6-15)
HI_Drill_Patch_Area	Borehole cross-sectional (circular) area. Also referred to as the drill patch area which is the area assumed to be affected by the intruding drill bit. This value is calculated using an 8 in (20.3 cm) borehole diameter. The borehole diameter is assumed to be slightly larger than the commonly used 2 3/8 to 6 in (0.60 to 15.2 cm) outer drill pipe diameters used in current drilling practices.	0.0324 m^2 (based on 8 in (20.3 cm) borehole diameter)	(Driscoll 1986 [DIRS 116801], p. 282)
HI_UZ_Fracture_Porosity	Fraction of the borehole area occupied by the fracture	0.0105	(SNL 2008 [DIRS 184748], Table 6-15)

Table 6.7-6. Borehole Fracture Properties used in UZ Flow and Transport Calculations

Parameter Name	Description	Parameter Value
Hl_UZ_Frac_Freq	The number of fractures per meter in host rock. Value is used as estimate of fractures in borehole and is calculated as fracture porosity divided by fracture aperture.	~4 1/m
Diff_Distance_To_Matrix	The distance between the fracture and matrix set equal to half the distance between two fractures.	~0.125 m
Radius_Drill_Patch	Radius of the borehole equal to the square root of the circular borehole cross-sectional area (drill patch area) divided by pi.	~0.101 m
Avg_Width_Fracture	Assuming the fracture is vertical in orientation and is cross-cutting the borehole, the fracture width is a function of the bisecting location relative to borehole center (Figure 6.7-6). This width can vary from a minimum value approaching zero to a maximum value equal to the borehole diameter (~0.2 m). Therefore, an average width is calculated by dividing the drill patch area by the borehole diameter.	~ 0.160 m
Fracture_Plan_Area	Cross-sectional (rectangular) area of the fracture. Equal to the product of the fracture aperture and average fracture width.	~0.0004 m^2
Fracture_Perimeter	The length of all sides of the rectangle created by fracture aperture and fracture width.	~0.324 m

Source: UZ Transport model parameters used to calculate the values listed in the table taken from DTN: LA0701PANS02BR.003_R2 [DIRS 180497].

Table 6.7-7. Fraction of SZ Source Region Nodes in each Percolation Subregion Bin

Fraction of SZ Source Region Nodes in each Percolation Subregion Bin					
	B1	**B2**	**B3**	**B4**	**B5**
SZ1	0.1071	0.3786	0.3973	0.4929	0.6071
SZ2	0.8929	0.4571	0.2857	0.1000	0.0000
SZ3	0.0000	0.1357	0.3125	0.4071	0.3929
SZ4	0.0000	0.0286	0.0045	0.0000	0.0000
Total	1	1	1	1	1

Source: Output DTN: MO0708TSPAGENT.000 [DIRS 183000], file *PS_EBSmaptoSZ.xls* .

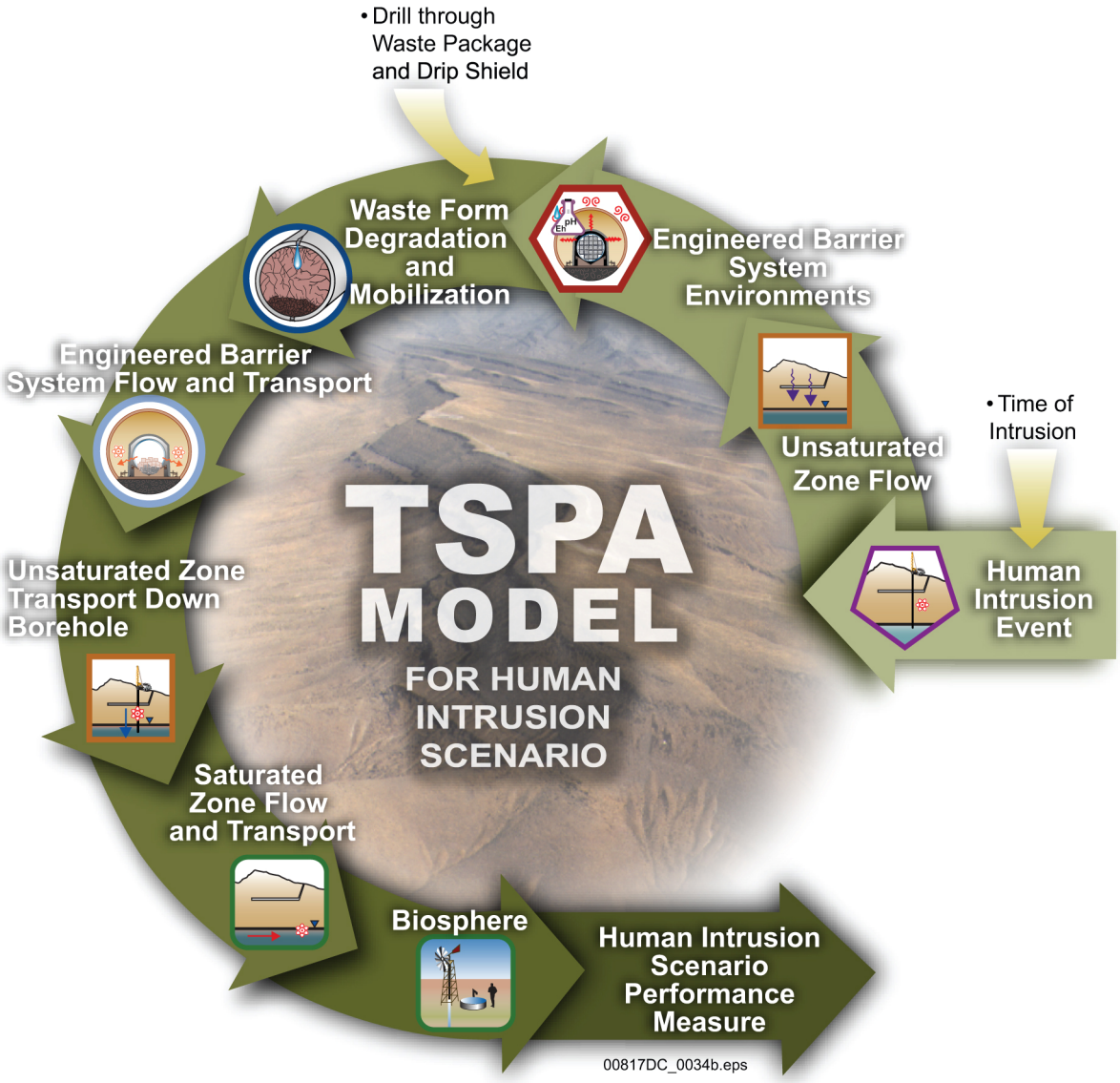

Figure 6.7-1. Schematic Representation of the TSPA-LA Model Components for the Human Intrusion Scenario

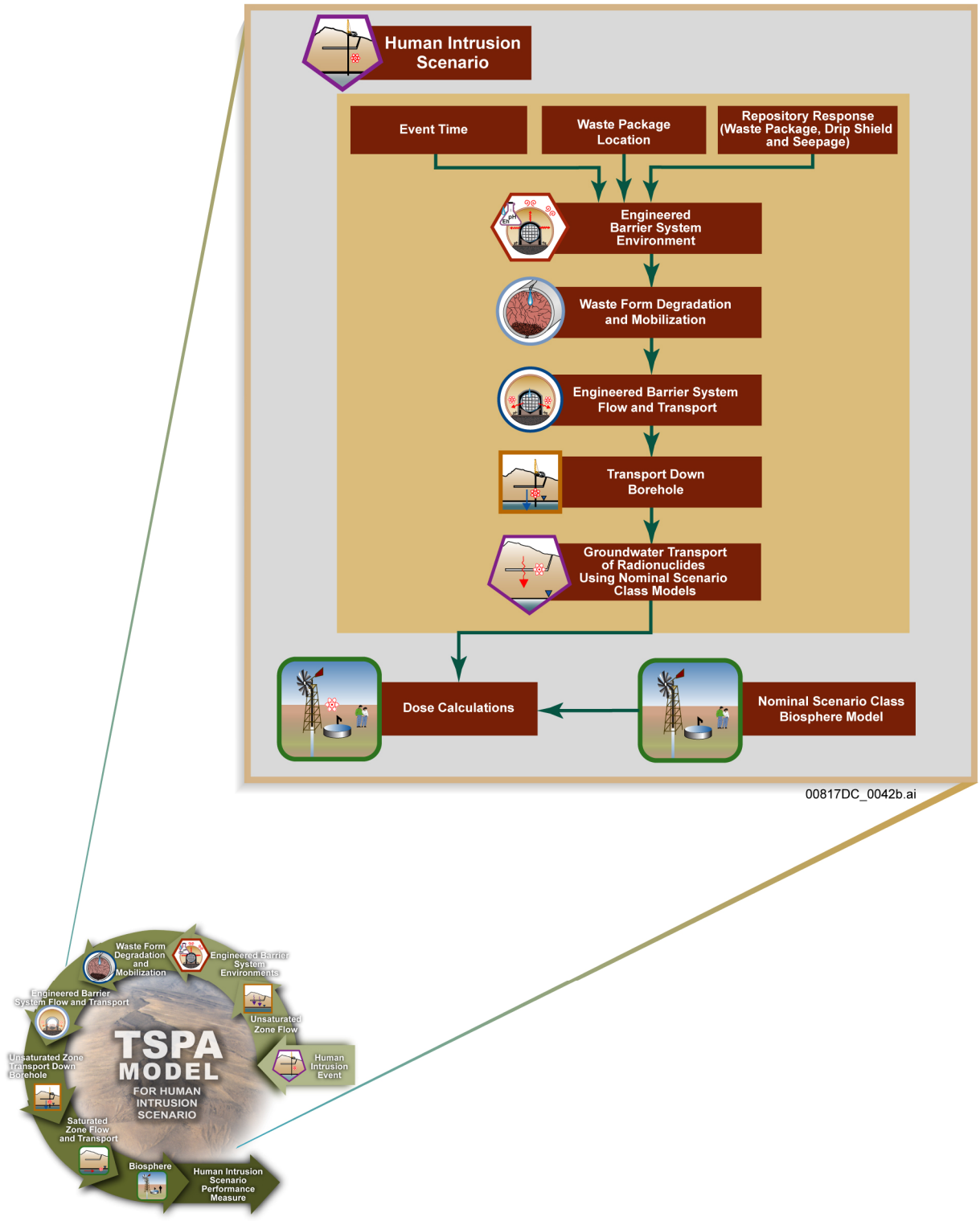

Figure 6.7-2. Information Flow Diagram for the Human Intrusion Scenario in the TSPA-LA Model

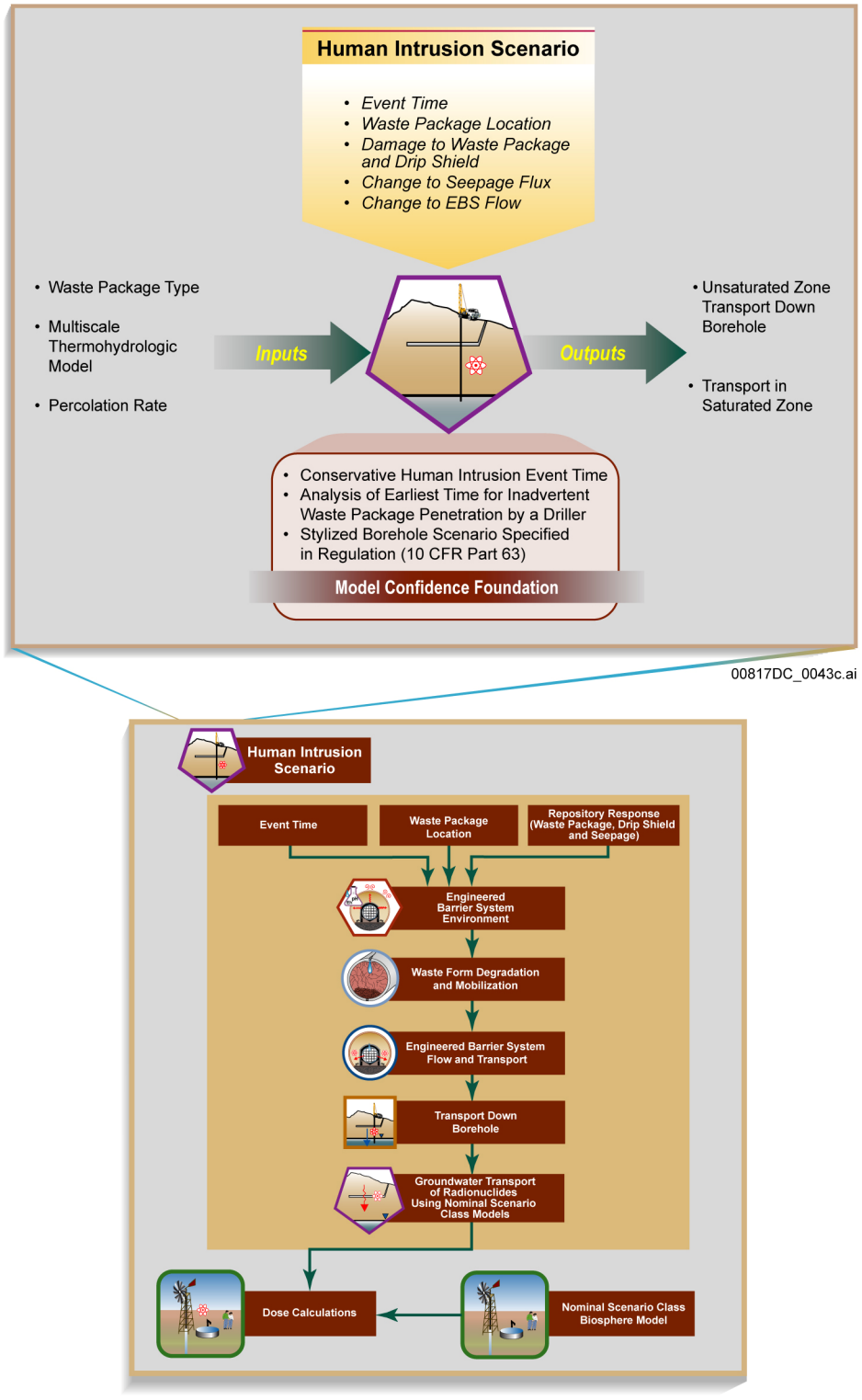

Figure 6.7-3. Inputs, Outputs, and Basis for Model Confidence for the Human Intrusion Scenario

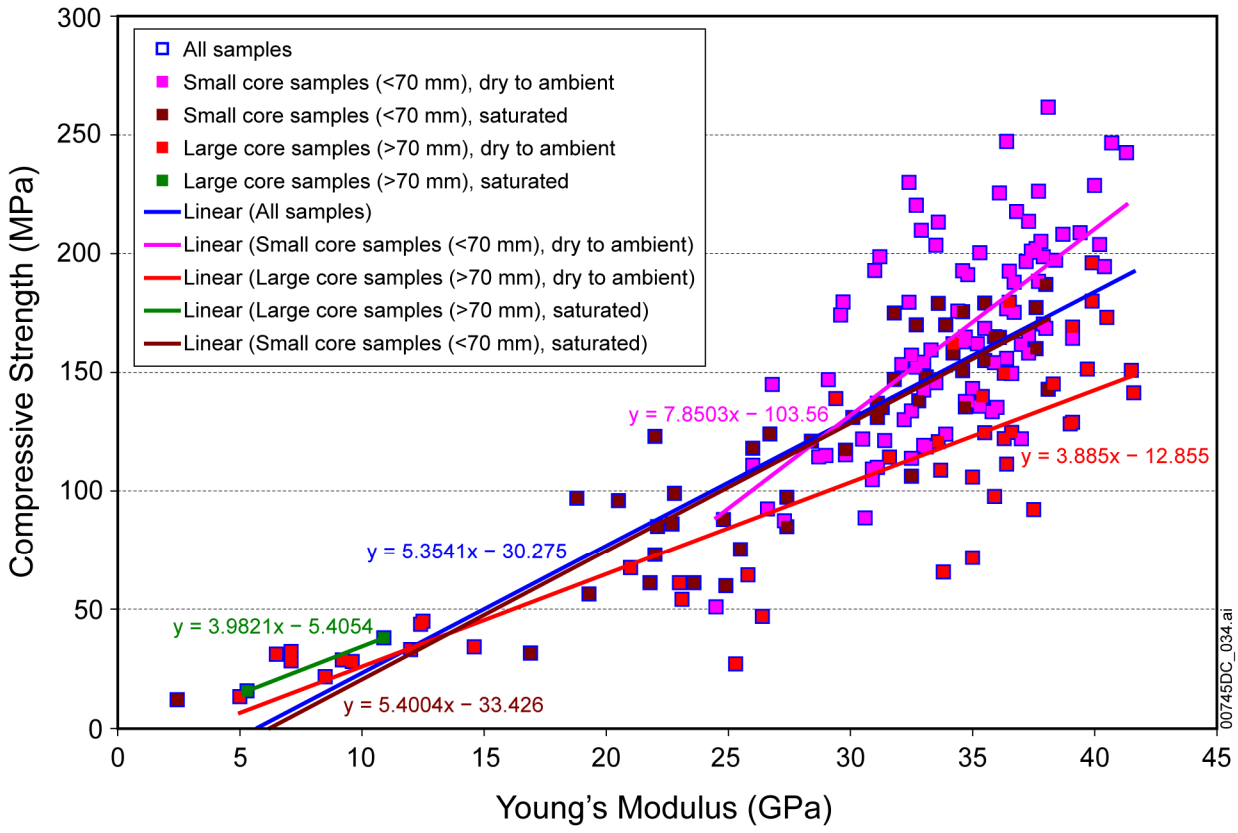

Source: BSC 2007 [DIRS 178693], Figure 6-37.

Figure 6.7-4. Unconfined Compressive Strength versus Young's Modulus in Tptpll Zone

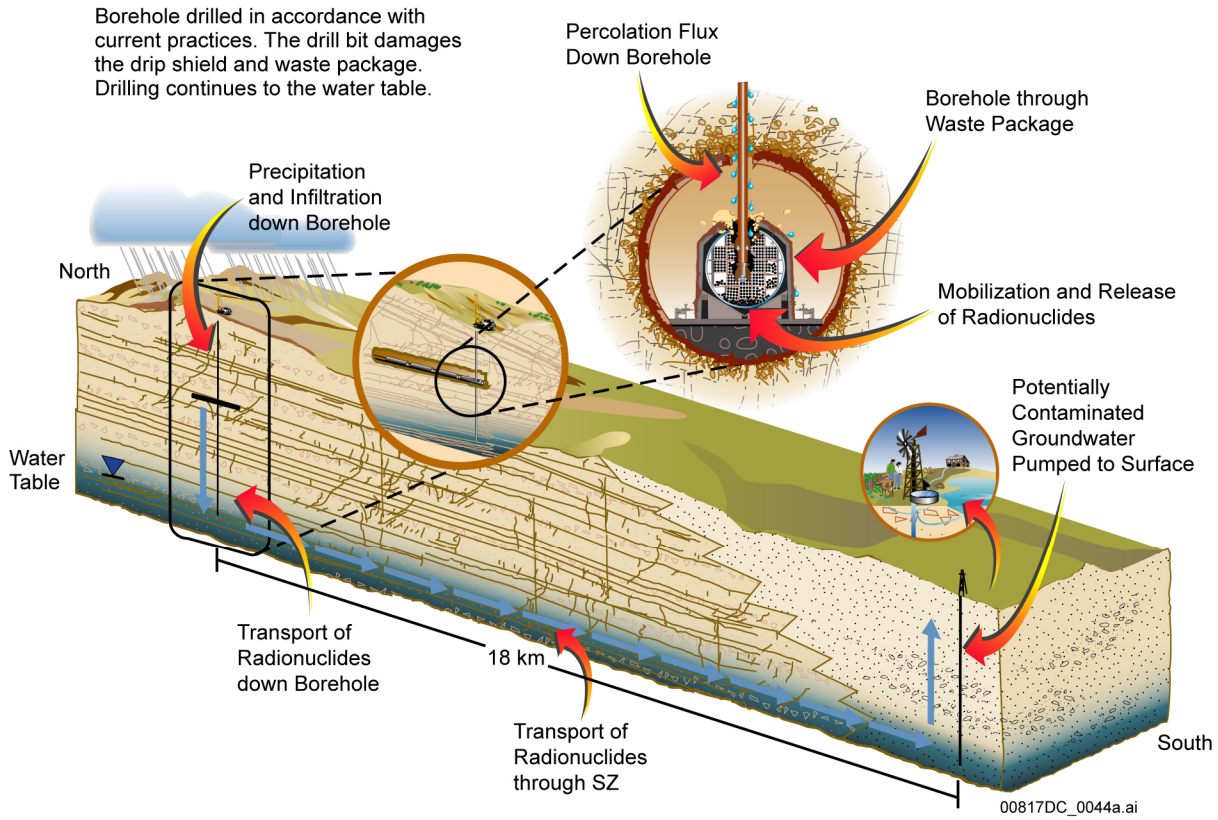

Figure 6.7-5. Conceptualization of the Human Intrusion Scenario for the TSPA-LA and Subsequent Radionuclide Releases to the Accessible Environment

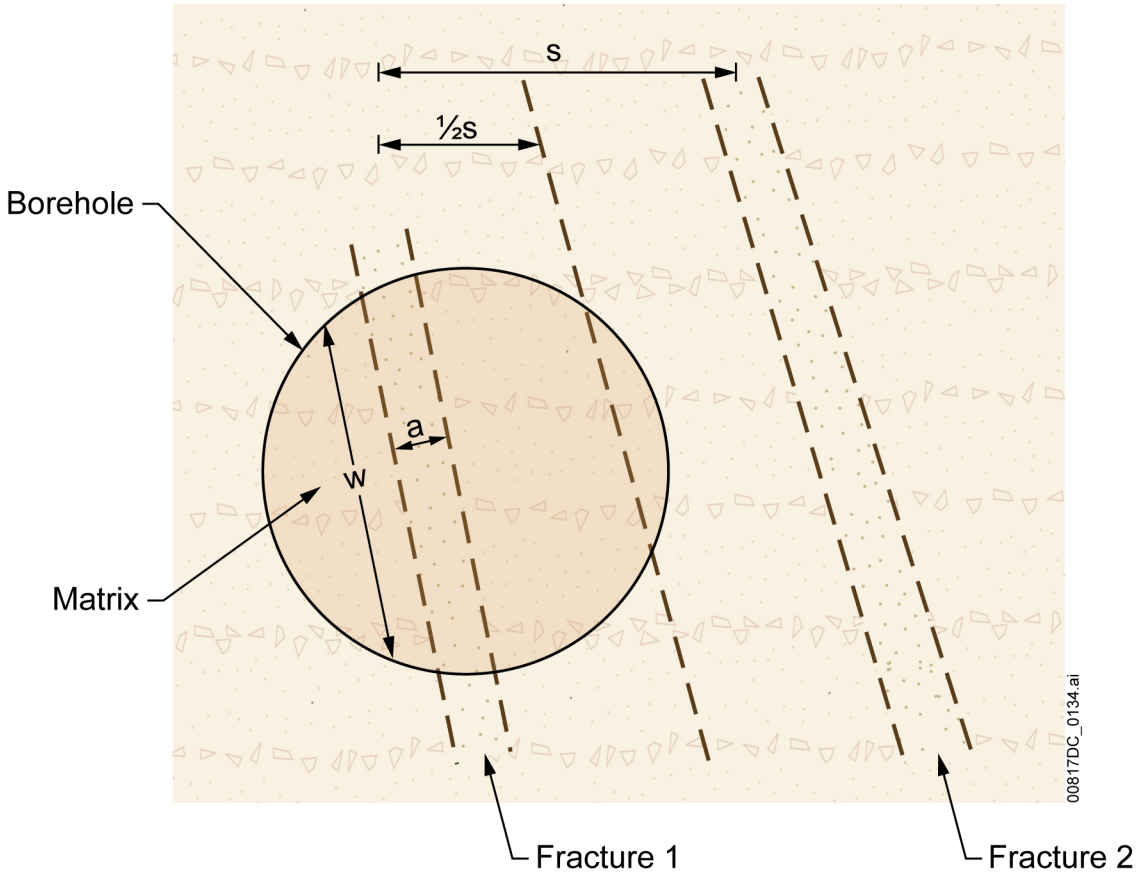

w = fracture width
s = fracture spacing
a = fracture aperture
½s = diffusion length between fracture and matrix
Borehole = Drill Patch Area = 0.0324 m^2

Figure 6.7-6. Schematic Depiction of Borehole (map view) with a Bisecting Fracture

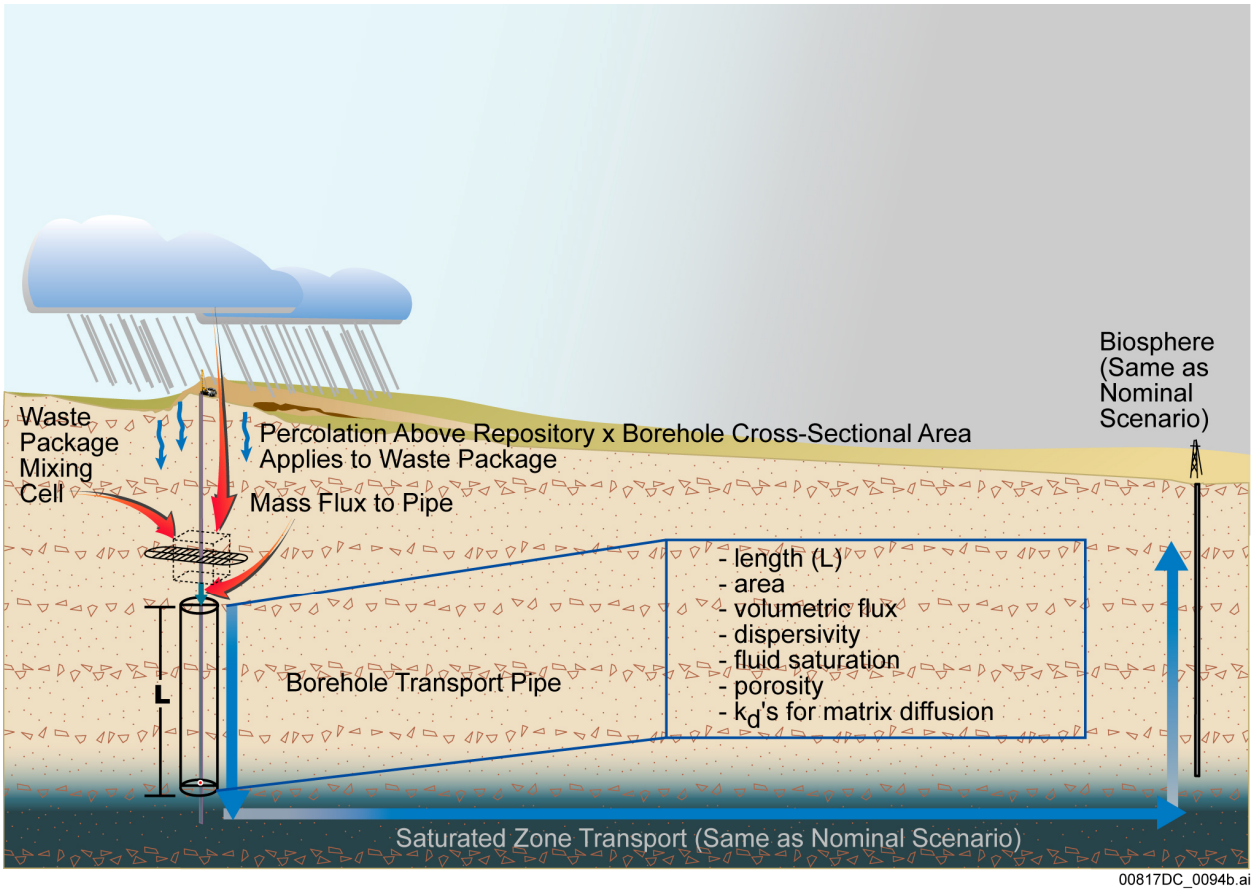

Figure 6.7-7. Schematic Illustration of the Implementation of Human Intrusion in TSPA-LA

INTENTIONALLY LEFT BLANK